The linkage between serial cyclone clustering and weather regimes

Master thesis
by

Sebastian Müller

June 2021

INSTITUTE FOR METEOROLOGY AND CLIMATE RESEARCH
KARLSRUHE INSTITUTE OF TECHNOLOGY (KIT)

Advisor:	Dr. Christian Grams
Second Advisor:	Prof. Dr. Joaquim Pinto

Contents

1 Introduction

Strong extra-tropical cyclones, which are synoptic-scale low pressure systems, in the North-Atlantic European region are a major cause for economic losses in Europe. Strong winds associated to the cyclones, can damage buildings severely, especially by untiling their roofs (Swiss Re, 2000). This allows damage to the interior by heavy rainfall accompanying the cyclones, which adds further to the economic losses. Hawcroft et al. (2012) showed that extra-tropical cyclones are the main contributor to the total precipitation, with severe ones being responsible for over 20% of the total yielded amount and are therefore often accompanied by flooding (e.g. Fink et al., 2009; Pfahl and Wernli, 2012).

Cumulative losses for the insurance industry over small time periods are however the largest when multiple cyclones occur in quick succession in the same area - a so-called serial cyclone clustering (SCC) (Vitolo et al., 2009). Previous studies found that such events appear not completely by chance but instead are connected to dynamical processes (e.g. rossby wave breaking, secondary cyclogenesis) and large-scale conditions (Mailier et al., 2006; Pinto et al., 2014; Priestley et al., 2017, 2020). On sub-seasonal time scales from multiple days to a few weeks, quasi-stationary and persistent patterns of the large-scale conditions, so-called weather regimes (WRs) (Vautard, 1990; Michelangeli et al., 1995), are especially important for cyclone occurrence and their paths and thus also influence the occurrence of serial cyclone clustering (Mailier et al., 2006; Vitolo et al., 2009; Dacre and Pinto, 2020). A study from Grams et al. (2017) for the North-Atlantic European region, using a more recent definition of seven year-round weather regime types, has shown an important shift of the cyclonic activity depending on the weather regime type, however a thorough analysis of the linkage between serial cyclone clustering and different weather regime types is still missing.

Additionally, it was shown that the strength of the winter stratospheric polar vortex (SPV) modulates the probability density function of the North Atlantic Oscillation (NAO) index (Baldwin and Dunkerton, 2001). Similarly, Domeisen et al. (2020) found a change in frequency of some of the seven year-round weather regimes in cases of sudden stratospheric warmings (SSW), which represent a severely weakened stratospheric polar vortex.

Therefore, we examine the interaction between serial cyclone clustering at three different latitudes (45°N, 55°N, 65°N) and the prevailing weather regimes types. We also aim to understand if serial cyclone clustering in some of those latitudes is dependant on an especially weak or strong stratospheric polar vortex and discern the role of the weather regimes. This is achieved by addressing following research questions:

1. Do specific weather regimes modulate the cyclone occurrence in the North-Atlantic European region in a similar matter as serial cyclone clustering?

2. What are the predominant weather regimes during serial cyclone clustering and is there a lead-lag interaction between the occurrence?

3. When does serial cyclone clustering occur in respect to the stage of a regime life cycle and do regime transitions play a vital role for the occurrence of serial cyclone clustering

4. In what manner does the stratospheric polar vortex influence serial cyclone clustering and what is the role of the weather regimes?

The remainder of the thesis is structured as follows. Chapter 2 provides background information on the general circulation in the North-Atlantic European region and covers some results of previous studies regarding serial cyclone clustering and weather regimes. Afterwards, in chapter 3, the data and methods used for this study are described. Chapter 4 encompasses all results regarding the linkage between weather regimes and serial cyclone clustering and the stratospheric influence. Lastly, in chapter 5 the results are summarized and possibilities for further research are given.

2 Background information

This chapter provides some background information about the general circulation, especially in the mid-latitudes. It also covers previous findings of serial cyclone clustering and weather regimes analysis.

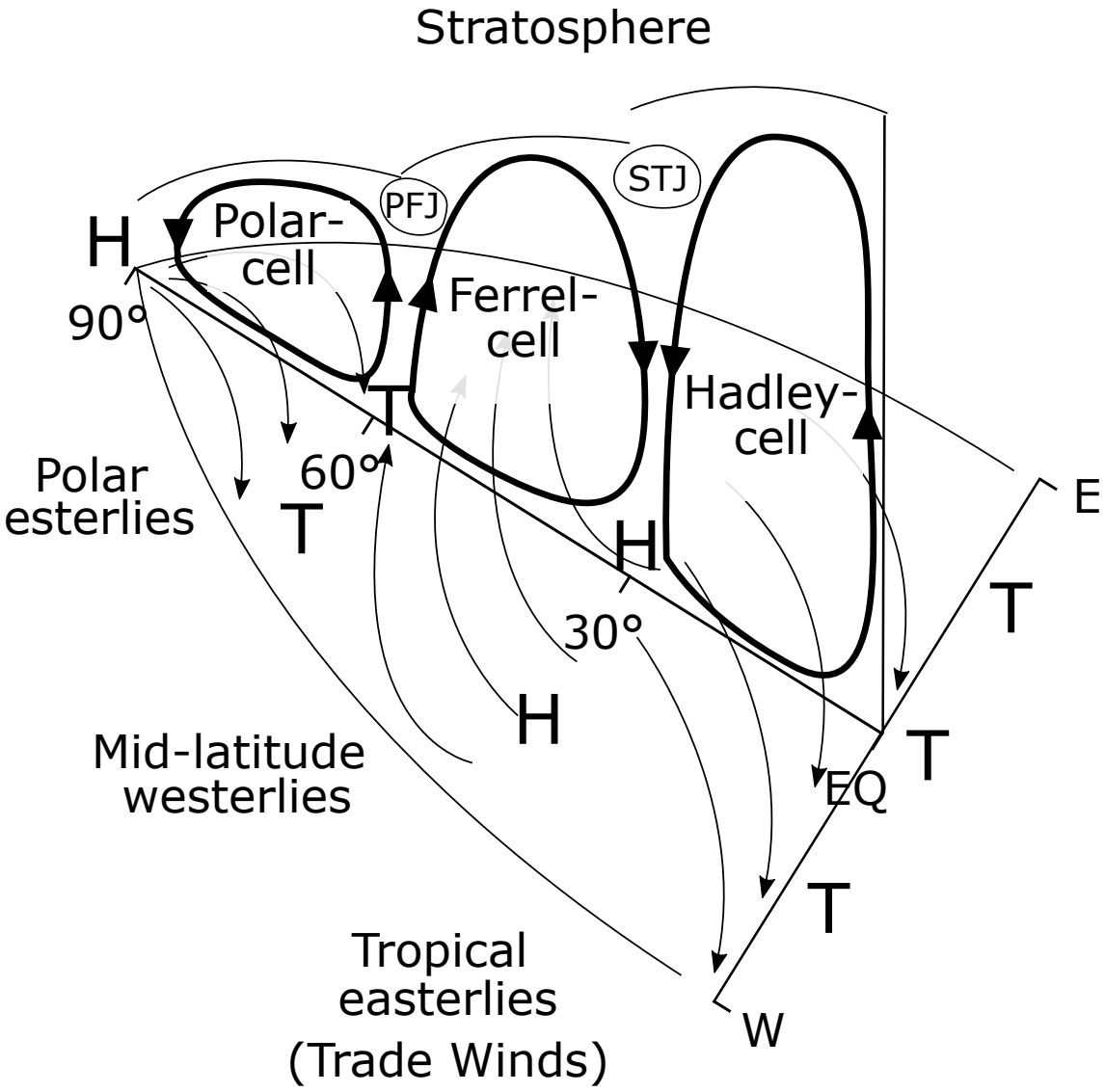

Figure 2.1: Sketch of the three-cell-model representing a simplified version of the general circulation for one hemisphere assuming a uniform composition of the Earth's surface.

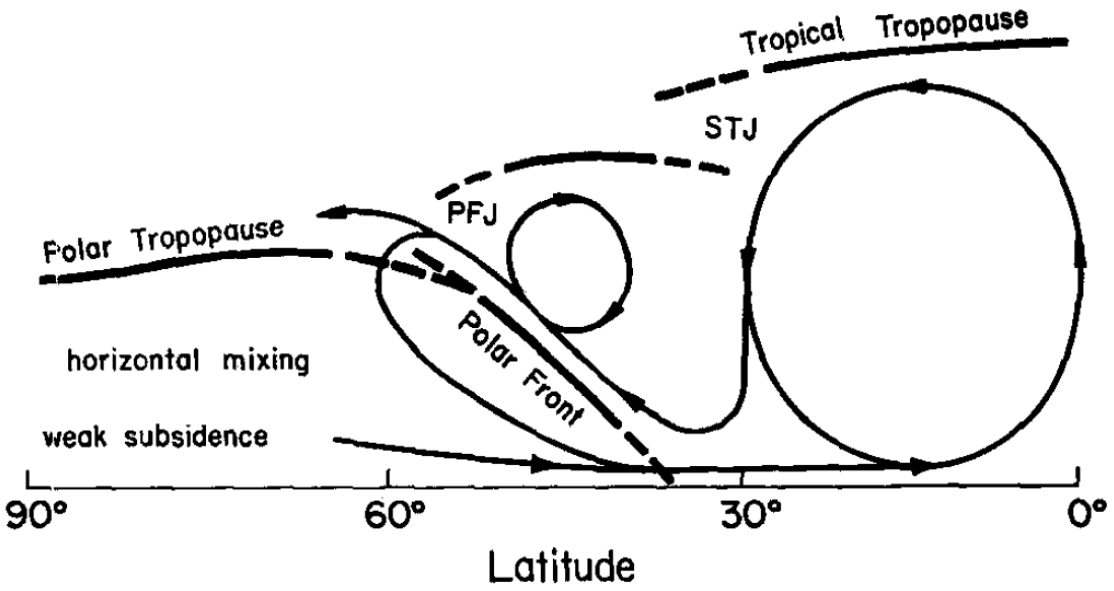

Figure 2.2: Sketch of the mean meridional circulation during the northern hemisphere winter (from Reiter (1969)).

2.1 Atmospheric flow in the northern mid-latitudes

Earth is a highly complex system and its general atmospheric circulation is strongly influenced by its characteristics. Especially many inequalities, e.g. sea-land distribution, sea surface temperature distribution or orography, make a comprehensive description very difficult (Kraus, 2004). In a simplified model, however, assuming a uniform composition of the Earth's surface, the general circulation is driven by its own rotation and the large temperature gradient between the equatorial and polar regions due to the difference in incoming solar energy (Kraus, 2004; Spiridonov and Ćurić, 2021). In such a case, the general circulation can be described with the three-cell-model, consisting of the Hadley, Ferrel and Polar-cell (cf. Fig. 2.1). Strong warming near the equator in the Intertropical Convergence Zone (ITCZ) leads to rising air and low surface pressure. The rising air is forced to move polewards after reaching the tropical Tropopause, cools on its way to the poles and descends at around 30°N causing a zone of high pressure in the subtropics. While the air moves polewards in the upper atmosphere it converges since the circumference decreases. Due to the conservation of angular momentum, the wind speed increases with latitude and forms the subtropical jet (STJ) at about 200 hPa at approximately 30°N (Riehl, 1962; Seman, 2020). The surface pressure difference induces northerly winds which are deflected westwards due to the Coriolis force, resulting in the trade winds. In the polar region strong cooling occurs which increases the density, inducing a sinking motion which leads to high surface pressure and a southward motion. Due to the Coriolis force the wind is again deflected and the results are the polar easterlies connected to the Polar-cell. The non-thermally driven Ferrel-cell in the mid-latitudes connects the Hadley- and Polar-cell.

The transition between the Ferrel and Polar-cell is however more complex than depicted in Figure 2.1. Cold air from the polar regions is undercutting the warm air originating from the tropics (Fig.

2.2) resulting in an area with a strong temperature gradient, the polar front (Spiridonov and Ćurić, 2021). Following the thermal wind relation, the strong latitudinal temperature gradient results in a strong increase of wind speed with height forming the polar front jet (PFJ) above the polar front (Reiter, 1969; Seman, 2020; Spiridonov and Ćurić, 2021) which is an important characteristic of the mid-latitudes.

Following the geostrophic balance, the upper level westerlies would be only zonally oriented. In fact, inequalities in e.g. the sea-land-distribution, the sea surface temperature or the orography add a meridional component and therefore a displacement from the globally zonal state (Kraus, 2004). The resulting latitudinal change is equivalent to an increase or decrease of the coriolis parameter and consequently the planetary vorticity. Since the vertical component of the absolute vorticity is conserved in an inviscid barotropic fluid in which the divergence of the horizontal velocity equals zero, relative vorticity is generated to counteract the displacement bending the zonal flow and eventually leading to the meandering of the jet (Reiter, 1969; Kraus, 2004; Spiridonov and Ćurić, 2021).

On the global scale these waves are known as planetary Rossby-waves. Since they move slowly to the east, they tend to be stationary within the westerly background flow and therefore can be seen in monthly or seasonal means of the upper level geopotential or wind fields (Reiter, 1969). During the northern hemisphere winter, the planetary wave number is three and the flow is characterized by three troughs with a weaker one over Europe and stronger ones over North America and East Asia (Fig. 2.3). The importance of the sea-land distribution and orography for the waviness becomes apparent when comparing the geopotential height fields of both hemispheres. In the southern hemisphere winter the mean geopotential shows less waviness and a more zonally oriented flow (cf. Fig. 2.3).

Peculiar to the mid-latitudes are however not only the large planetary Rossby waves but also shorter and faster moving ones embedded into the large-scale flow, which develop into the well-known extra-tropical cyclones/anticyclones forming the mid-latitude storm tracks. These transient eddies are substantial for the heat transfer between the lower and higher latitudes and have its origin in the strong baroclinity alongside the polar front (Kraus, 2004).

Another import role for the mid-latitude circulation, especially the location of the storm tracks, in the winter season can be attributed to the Stratosphere (Baldwin and Dunkerton, 2001). During the winter season a westerly jet forms in the extra-tropical Stratosphere due to the strong radiative cooling in the absence of sunlight, the so-called polar night jet or stratospheric polar vortex (SPV), which naturally breaks down after the polar night. A strong SPV tends to shift the storm tracks northwards while a weak SPV results in a more southward shift (Baldwin and Dunkerton, 2001). Due to the very stable conditions in the stratosphere, the troposphere mainly interacts with the SPV through vertically propagating waves, which is enhanced during the winter season because of the strong baroclinity in the troposphere (Furtado, 2005). Breaking of those waves at the level of the SPV adds westwards acceleration and therefore can weaken the jet substantially. Continuous wave breaking can lead to a complete breakdown of the SPV and an easterly flow which as a result warms the stratosphere substantially, also known as a sudden stratospheric warming.

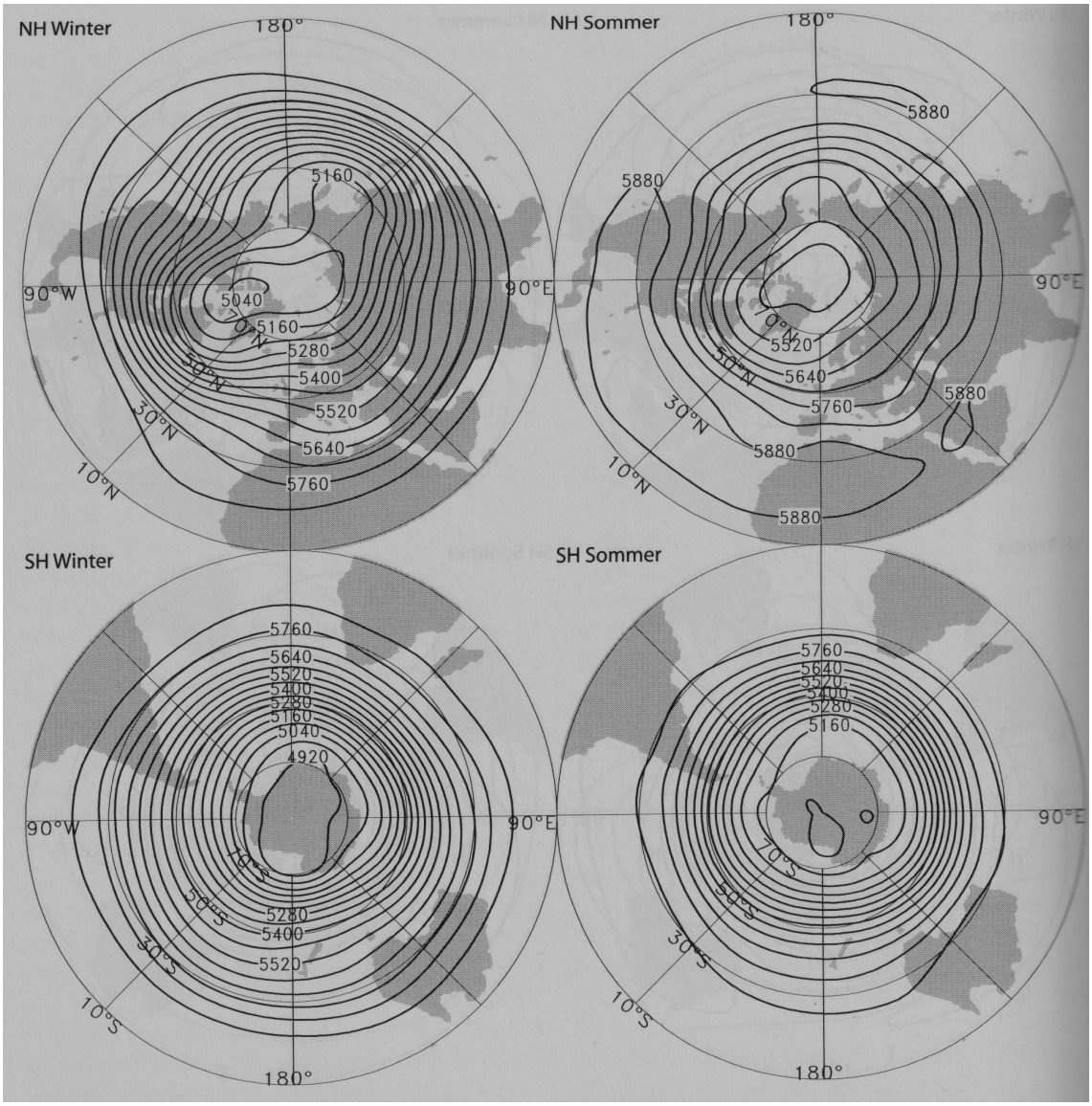

Figure 2.3: Time mean of 500 hPa geopotential height for northern and southern hemisphere winter/summer in gpm (from Kraus (2004)).

2.2 Serial cyclone clustering

In the scope of this study serial cyclone clustering describes an extreme event where multiple severe extra-tropical cyclones cross a similar area in quick succession following previous studies from e.g. Pinto et al. (2014) or Priestley et al. (2017). From a statistical viewpoint, clustering in general is a means to build groups, however these are not confined to one definition. In fact, cyclones can be clustered by various criteria, with the three basic ones being clustering by locality, clustering by similarity and clustering by seriality (Dacre and Pinto, 2020).

Clustering by locality can be used to determine regions where many cyclones gather, independent of their strength and the time in between them. An example of clustering by locality are the storm tracks, since they describe paths of high cyclone occurrence independent of their strength and without any temporal information (Dacre and Pinto, 2020).

On the other hand, clustering by similarity focuses the attention on the cyclone characteristics instead. This is particularly helpful when comparing the socio-economic impacts of different cyclones since these are heavily coupled to characteristics like precipitation or wind speed (Catto, 2016; Dacre and Pinto, 2020). Similarly, cyclones could also be clustered by their development rate, to analyse for example only the behaviour of explosive cyclones (Catto, 2016).
Lastly, clustering by seriality concentrates on finding groups with high occurrence frequencies within in a certain time period. However if no further constraints are made, cyclone strength or other characteristics are disregarded. This clustering type is the basis for the definition we use, but is further refined by incorporating some of the other clustering types. By limiting an analysis on only severe cyclones, clustering by similarity is used while defining a specific area for an analysis is an example for clustering by locality (Dacre and Pinto, 2020).
In addition to the different clustering approaches, seriality can be determined differently, by either setting an absolute frequency threshold (Pinto et al., 2014; Priestley et al., 2017) or using relative frequency metrics (Mailier et al., 2006; Vitolo et al., 2009), which take the spatially varying cyclone frequency climatologies into account.
Extensive research about serial cyclone clustering has already highlighted many connections between serial cyclone clustering and other atmospheric processes. Serial cyclone clustering at 55°N in the United Kingdom tends to occur alongside a prolonged, stable and intensified jet extending into Western Europe. Cyclonic/anticyclonic Rossby-wave breaking to the north/south of the jet has been found to play an important role in upholding those conditions, by transferring easterly movement into the jet (Pinto et al., 2014). This is also verified by Priestley et al. (2017), however it was also shown that the behaviour clearly changes with SCC at different latitudes. Rossby-wave breaking mainly occurs north of the jet in case of SCC at 45°N and south of the jet for SCC at 65°N. Furthermore, the SCC period length increases with enhanced Rossby-wave breaking activity and the jet exit strength. Pinto et al. (2014) and Priestley et al. (2020) have also shown that cyclone families and secondary cyclones are important for the occurrence of SCC. Primary cyclones tend to create environmental conditions that favour the development of secondary cyclones by increasing Rossby-wave breaking activity at the flanks of the jet. Less dynamically, but more statistically oriented studies have shown that in general the likelihood for clustering depends on its region and strength. Clustering is most likely to occur in the exit region of the storm tracks for intense cyclones and less likely in the entrance region east of North America (Mailier et al., 2006; Vitolo et al., 2009; Dacre and Pinto, 2020).

2.3 Weather regimes

Day to day weather is strongly dependent on the presence or absence of an extra-tropical cyclone or anticyclone. However these weather systems act only on synoptic time-scales from a day to a week and cover lengths of 1000 km to 6000 km (Kraus, 2004; Lackmann, 2011). Forecasting on longer time scales but similar spatial resolution faces the challenge of atmosphere's chaotic nature, which can lead to rapidly developing initial errors in predictions (Vautard, 1990; Ferranti et al., 2015). On larger spatial scales or longer time scales ranging from about five days to a few weeks, statistical analysis revealed that a finite number of quasi-stationary patterns recur for prolonged time periods, the so-called weather regimes, which can explain a large amount of the large-scale

flow variability (Vautard, 1990; Michelangeli et al., 1995; Grams et al., 2017). Even though transient waves modulate the day to day weather, weather regimes have been found to be connected to extreme events on sub-seasonal time scales, such as cold and heat waves or extreme precipitation leading to flooding (Cassou et al., 2005; Cattiaux et al., 2010; Neiman et al., 2004; Matsueda, 2011). Therefore, as a means to increase sub-seasonal forecast skill, weather regimes can find applications in many sectors such as agriculture, water management, disaster risk reduction and public health (White et al., 2017). Especially the energy sector, with a growing investment into renewable energies, benefits not only from more accurate sub-seasonal predictions, but also from statistical analysis which show the uneven energy generation during different regime types (White et al., 2017; Grams et al., 2017).

While the importance of weather regimes has been shown quite clearly throughout different studies (e.g. Cassou et al., 2005; Cattiaux et al., 2010; White et al., 2017; Grams et al., 2017), a precise universal definition of weather regimes is missing. Since weather regimes take a statistical approach, the number of patterns as well as their location can vary depending on the analysis method (Michelangeli et al., 1995). In their study of the probability density distribution of planetary waves, Hansen and Sutera (1986) found two regime types. On the other hand, using a clustering approach, Mo and Ghil (1988) found six to seven relevant regimes. Despite the differences it was shown by many studies that four regimes tend to represent the winter/summer large-scale variability quite well and is therefore used for many present studies (Vautard, 1990; Michelangeli et al., 1995; Yiou and Nogaj, 2004; Ferranti et al., 2015; Matsueda and Palmer, 2018). These patterns include two regime types representing the positive/negative phase of the North Atlantic Oscillation (NAO) also referred to as zonal regime/Greenland anticyclone, which feature a northerly/southerly shift the jet, a blocking type also referred to as European-blocking due to its dipole structure with a positive geopotential anomaly over Scandinavia and the British Isles and a negative one south of Greenland and lastly, the Atlantic ridge regime featuring a strong ridge over the whole eastern Atlantic (e.g. Vautard, 1990; Ferranti et al., 2015; Matsueda and Palmer, 2018). Despite the good representation in general, studies from e.g. Jerez and Trigo (2013) or Zubiate et al. (2017) have shown that the four regimes present good results on monthly time scales but are not detailed enough on daily to weekly time scales. A more recent approach, also utilized in this study (more details in chapter 3), is to use seven regime types for a year-round variability description (Grams et al., 2017; Beerli and Grams, 2019).

3 Data and methods

This chapter contains a description of the data sets and methods used in this study. The first section gives an overview over reanalysis data in general and introduces the two data sets ERA-Interim and ERA-5. The second part provides the necessary mathematical background and covers the methods for determining the weather regimes and serial cyclone clustering.

3.1 Data

3.1.1 Reanalysis data

Retrospective analysis data, short reanalysis data, are long-term climate data sets which are globally complete. The main reason for their development was to do climate research and determining long-term trends (Compo et al., 2011). Even though observational data depict the past atmospheric state based on measurements, they alone are not sufficient to accurately represent the state of the Earth system, hence modelled data is necessary. Numerical weather prediction systems and their data assimilation methods are however rapidly developing to ensure the best possible real-time forecast (Compo et al., 2011). This makes it difficult to compare archived data over long-term periods, since inconsistencies arise from the difference in data assimilation and forecasting systems, eventually leading to false results. In contrast, reanalysis data are computed with consistent methods throughout the whole reanalysis period and thus are free of those inconsistencies. To ensure the correct representation of the past atmospheric state, they combine earlier observations and short-term forecasts, to recreate past synoptic analysis with a single consistent modern computing and data assimilation method (Compo et al., 2011; Jeppesen, 2020). Others than climate research and analysis of long-term trends, reanalysis data are nowadays found in a wide range of applications. For example they are also used in education, policy making or business, especially regarding the renewable energy sector.

3.1.2 ERA-Interim

Contemporary, there is a wide range of reanalysis data from different institutions available. This study mainly uses the ERA-Interim reanalysis data set from the European Center of Medium-Range Weather Forecasts (ECMWF). ERA-Interim features global data from 1979 to August 2019 with a temporal resolution of six hours for a wide range of upper-air and surface variables. The atmospheric model uses ECMWF's Integrated Forecasting System (IFS) cycle 31r2 with 60 vertical hybrid sigma-pressure levels up to 0.1 hPa. Its dynamical core uses a spectral grid for the basic dynamical fields with a horizontal resolution of T255. For surface and other grid-point fields a reduced Gaussian grid is used instead, with a horizontal resolution of 79 km (Dee et al., 2011; Berrisford et al., 2011). However, this study only uses the time period from 1979 to 2015. See Dee

et al. (2011) for a more detailed explanation of the forecast model and data assimilation method of ERA-Interim

3.1.3 ERA-5

ERA-5 represents ECMWF's newest reanalysis data set following ERA-Interim. One of its main strengths is the improved temporal and spatial resolution and therefore being able to represent the atmospheric state in more detail. It uses IFS cycle 41r2 with 137 vertical hybrid sigma-pressure levels up to 0.01 hPa. Its horizontal resolution was increased to T639 resulting in a 31 km resolution on a reduced Gaussian grid. Other strengths are the assimilation of larger numbers of reprocessed data sets and the availability of ensembles for uncertainty estimates. See Hersbach et al. (2020) for a more detailed description.
We use ERA-Interim for the determination of weather regimes and serial cyclone clustering, but ERA-5 for the synoptic fields in the case studies analysis. The stratospheric analysis also uses ERA-5 due to the better representation of the stratospheric polar vortex. For the stratospheric analysis, we replace the years 2000 to 2006 with ERA-5.1 data, which is essentially a remake for this period, to combat the stratospheric and upper-tropospheric cold bias (Simmons et al., 2020).

3.2 Methods

3.2.1 Mathematical basics

This part features a description of the mathematical methods used for further calculations and statistical analysis.

Principal component analysis and empirical orthogonal functions

The principal component analysis (PCA) is commonly used to analyse complex variability patterns of meteorological fields or to compress large data sets. With the PCA, the complex structure is fractionalised into a set of functions which are uncorrelated in the spatial dimension (Preisendorfer and Mobley, 1988). These functions, known as empirical orthogonal functions (EOFs), are orthogonal and normed (length of one) and therefore build a orthonormal basis in the vector space for the variability pattern. Therefore the complex structure can be displayed as a sum of more simplified EOFs together with their respective amplitudes, known as the principal components (orthogonal and uncorrelated in the temporal dimension). For example the time evolution of a 500 hPa geopotential height field $z(t,x)$, $t = 1,...,n$; $x = 1,...,p$ can be displayed as followed

$$z(t,x) = \sum_{j=1}^{p} a_j(t) e_j(x), \tag{3.1}$$

with $a_j(t)$ being the principal components and $e_j(x)$ the EOFs (Preisendorfer and Mobley, 1988). Another common depiction of the PCA is by interpreting the time evolution of a field as a matrix $\boldsymbol{Z}$, with columns representing the time evolution and rows representing the spatial distribution

(Björnsson and Venegas, 1997). In this form the PCA is denoted as a matrix multiplication of the principal components matrix and the EOF matrix:

$$\boldsymbol{Z} = \boldsymbol{AE}. \tag{3.2}$$

Data compression by means of PCA can then be achieved by only taking all the EOFs up to a fixed number, instead of all. Even though the data reduction is large, the information loss is comparatively small, because the EOFs are ordered in a way that first few tend to dominate the others (Björnsson and Venegas, 1997).

k-means and agglomerative clustering

Clustering describes the process of partitioning data sets by forming groups that share different attributes such as e.g. occurrence in time, geographical position or intensity. Since categorizing or grouping is such an important task, it finds utilization in many different branches, e.g. data mining, machine learning, geophysical research, psychological studies, to name only a few (Estivill-Castro, 2002; Hamerly and Elkan, 2002; Hart et al., 2015; Cattell, 1943). Since there is no universal definition for clustering, many types of clustering algorithms have been developed (Estivill-Castro, 2002). In this study two types are used, k-means clustering and a special agglomerative hierarchical clustering.

K-means clustering is a partitioning method that tries to form k groups based on minimizing the deviation of each cluster member from the cluster centroid. The number of groups are predefined and objects are assigned one after another towards the closest cluster centroid which is continuously adjusted based on all cluster members (Chen et al., 2002).

Agglomerative hierarchical clustering algorithms assign an individual cluster to each data point or vector. Then nearest clusters are merged and a new centroid is calculated. This process is iterated until a certain cut-off criteria is reached (Chen et al., 2002). In this study we use the algorithm after Hart et al. (2015), which uses the euclidean distance to determine the nearest clusters. Following the iterative process, smaller clusters are successively incorporated into bigger clusters, gradually increasing the distance between each cluster centroid. The total number of clusters is derived from the agglomeration step, where the second derivation of the distance according to the agglomeration step reaches its peak (Hart et al., 2015).

Monte Carlo simulation and bootstrapping

Monte Carlo simulation is in general a computational generation of random objects. Often those objects are represented by samples from probability distributions. Monte Carlo simulations are mostly used to get information about a complex system if analytical studies are difficult or not possible (Kroese et al., 2014; Brown, 2016). Due to the loose definition, a wide variety of applications with different objectives for Monte Carlo methods exist. Possible use cases are e.g. sampling, estimation or optimization. However, they all share the basic principle of repeating an experiment multiple times (Kroese et al., 2014). This is essential for using the law of large numbers. It states that the average result of multiple repeats of the same probabilistic experiment (independent and identically distributed) approaches (weak law of large numbers) or is equal to

(strong law of large numbers) the expected result if the experiment is repeated infinitely. The cheap computational power nowadays also allows to solve easier problems quickly without using an analytical approach. An example of a Monte Carlo simulation would be the computation of the median distribution of normally distributed samples e.g. of size 100. Repeating the sampling process e.g. 1000 times would give an accurate representation of the median distribution, which is then also normally distributed (Chen, 2017).

The boostrap is a variation of a Monte Carlo simulation. In this case the samples are taken from a given data set instead of a probabilistic distribution. It is used to estimate the uncertainty of different statistics e.g. percentiles, averages, minimum, maximum without the need to know the underlying distribution of the data set (Brown, 2016). However, the data set is not ensured to be independent and identically distributed (i.i.d.), therefore to replicate a data set that is i.i.d. , sampling with replacement must be used. Computationally the sampling is done by randomly choosing elements of the data set until the sample size is equal to the data set size. Mathematically the samples are drawn from the empirical cumulative distribution function (CDF) derived from the data set, which for an ordered data set $x_1 ... x_n$ of size n is defined as

$$F_n(x) = \begin{cases} 0, & x < x_1 \\ \frac{k}{n}, & x_k \leq x < x_{k+1} \\ 1, & x_n < x \end{cases} \tag{3.3}$$

It is a step function that increases equally for each element in the data set and estimates the unknown underlying CDF which the data set is taken from. Similar to the law of large numbers, the Glivenko-Cantelli Lemma states that $F_n(x)$ converges towards the true CDF $F(x)$ for n approaching infinity (Brown, 2016).

Percentiles and statistical significance

Percentiles are used to compare values within a data set or to represent uncertainties. They are especially useful for their inherent robustness by definition and for determining extremes within a data set. They are also useful in determining if results, following a normal distribution, are skewed. Percentiles describe how many elements of an ordered data set are below a certain threshold, without consideration of the actual values of the data, thus leading to inherent robustness. For example, the 95th percentile, commonly written as $p_{0.95}$ or p_{95}, corresponds to the element or value for which 95% of all elements are smaller.

Comparing results of samples to climatological values to find correlations often raises the problem that anomalies might only inhere from statistical errors due to a reduced sample size. Therefore testing for statistical significance becomes important in finding true correlations between a given criteria and changes in the results. A useful parameter for the comparison of two data sets or for statistical testing is the percentile rank. The percentile rank gives the percentage of scores within a data set that are smaller or equal to the given score.

While there are many possibilities to test for statistical significance, the following provides an example of two methods that we utilise in this study. By using bootstrapping we can retrieve a climatological frequency distribution from random samples and a resampled frequency distribu-

tion. With those, the percentile rank of the resampled distribution within the climatology can be calculated. We can then test for statistical significance on the 10% level. Frequencies that have a percentile rank of more than 95% or less than 5% are statistically significant. The second method uses a similar idea, but without explicitly calculating the percentile rank. Instead the overlap between the two distributions is decisive (cf. Fig. 1 of Büeler et al., 2020). Statistical significance on the 10% level is achieved if, for positive anomalies, the $p_{0.1}$ value of the resampled distribution is larger than the $p_{0.9}$ of the climatological distribution. For negative anomalies the $p_{0.9}$ value has to be smaller than the $p_{0.1}$ value of the climatological distribution (Büeler et al., 2020).

3.2.2 Weather regimes

This section introduces the technical background of weather regimes including the definition and calculation methods of the weather regime index and weather regime life cycles.

Weather regime types

This study uses the seven year-round weather regime types for the Atlantic-European region following Grams et al. (2017). Weather regimes are based on 10-day low pass filtered normalised 500 hPa geopotential height anomalies using a 90 day running mean as a climatology and k-means clustering in the phase space spanned by the leading seven EOFs (Charlton-Perez et al., 2019; Mohr et al., 2020). For the 500 hPa geopotential height fields, ERA-Interim data with a six hourly temporal and 1° horizontal resolution are used in the time period from 11 January 1979 to 31 December 2015 and the region from 80°W to 40°E, 30°N to 90°N. Firstly, a 90 day running mean at the respective time is subtracted from the 500 hPa fields. Secondly, the anomalies are 10-day low pass filtered to exclude short lived transient circulation patterns. Thirdly, the filtered anomalies are normalised to remove the seasonality and allow for year-round weather regime types. Normalisation is done by dividing the filtered geopotential height anomalies by the spatial mean of a 30 day standard deviation. Lastly the seven leading EOFs which explain about 76.7% of the variance are clustered year-round using k-means clustering with seven clusters (Grams et al., 2017). The no-regime contains all those cases which cannot be attributed to either of the seven regime types
The resulting geopotential height anomalies of the seven weather regimes are shown in Fig. 3.1. Three regimes are called cyclonic regimes, encompassing the Atlantic trough (AT), the Zonal regime (ZO) and the Scandinavian trough (ScTr), and feature an especially strong negative geopotential height anomaly leading to enhanced cyclonic activity. Four regimes, namely Atlantic ridge (AT), European blocking (EuBl), Scandinavian blocking (ScBl) and Greenland blocking (GL), are considered blocking regimes and are dominated by an especially large positive geopotential height anomaly.
Cyclonic regime types lead to more zonally oriented geopotential contours over central and northern Europe (cf. figure 3.1). Therefore, the jet is more zonally oriented and cyclones are able to reach into central and northern Europe more easily. Strong winds and mild surface conditions in winter are further attributes of cyclonic regimes. Blocking regimes lead to rather cold and foggy conditions, due to prolonged high pressure over central and northern Europe. Contrary to the cyclonic regimes, blocking regimes share that cyclones are either deflected to the south or north of central Europe. Greenland blocking, and to a slight extent Scandinavian blocking, feature a

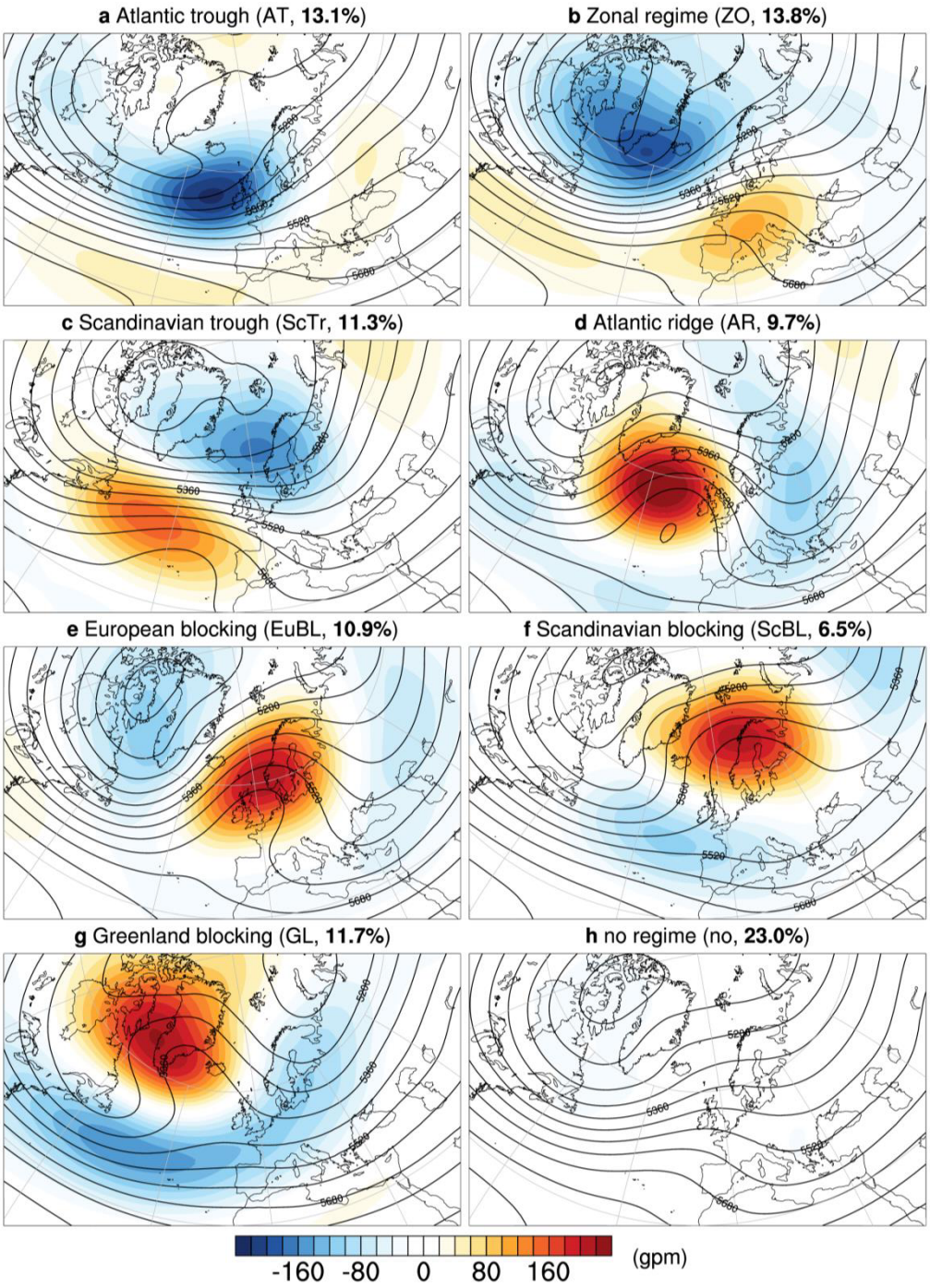

Figure 3.1: Mean low-pass filtered (10 days) geopotential height anomalies of all seven weather regime types (shading) in geopotential meter (gpm) as well as geopotential (contours) for the weather regimes and no regime condition (winter mean) in the winter season (DJF). The weather regime abbreviations are as followed: AT – Atlantic trough, ZO – Zonal regime, ScTr – Scandinavian trough, AR – Atlantic ridge, EuBl – European blocking, ScBl – Scandinavian blocking, GA – Greenland blocking, no – no regime. Percentages in the title besides the abbreviations represent the occurrence frequency during the winter season (supp. Fig. 1 of Grams et al. (2017)).

general shift of the jet to the south while Atlantic ridge and European blocking are connected with a more wave-like jet.

Weather regime index

The weather regime index is used to quantify how much a weather regime type projects on to the current synoptic situation (Michel and Rivière, 2011; Grams et al., 2017). The projection of the synoptic situation on to a weather regime $P_{\mathrm{WR}}(t)$ is calculated as the mean of $\phi^L \cdot \phi^L_{\mathrm{WR}}$ over all grid points. ϕ^L is the low-frequency geopotential anomaly and ϕ^L_{WR} is the low-frequency geopotential anomaly for days attributed to a certain weather regime. The complete equation for the projection is as follows:

$$P_{\mathrm{WR}}(t) = \frac{1}{\sum_{(\lambda,\varphi)\in \mathrm{NH}} \cos\varphi} \sum_{(\lambda,\varphi)\in \mathrm{NH}} \phi^L \phi^L_{\mathrm{WR}} \cos\varphi. \tag{3.4}$$

The weather regime index is the standardised projection anomaly from the climatological projection $\overline{P}_{\mathrm{WR}}$:

$$I_{\mathrm{WR}} = \frac{P_{\mathrm{WR}}(t) - \overline{P}_{\mathrm{WR}}}{\sqrt{\frac{1}{NT}\sum_{t=1}^{NT}[P_{\mathrm{WR}}(t) - \overline{P}_{\mathrm{WR}}]^2}}, \tag{3.5}$$

where NT denotes the total number of days.

Weather regime life cycles

Weather regime life cycles represent time periods in which the atmospheric circulation over the North-Atlantic European region resembles the pattern of a certain weather regime. The objective determination of weather regime life cycles is based on the weather regime index that needs be larger than the standard deviation of the weather regime index ($I_{\mathrm{WR}} > \sigma(I_{\mathrm{WR}})$), which is equal to 1 since the weather regime index is standardised. This criteria must be met for at least five days. During the life cycle period the weather regime index has to reach a local maximum and there must be a five day period of monotonic increase/decrease before/afterwards (see details in Grams et al., 2017).

3.2.3 Serial cyclone clustering

Identifying and tracking cyclones automatically for research purposes, especially climatological studies, is a difficult task and multiple methods has been developed to do so. This is due to the many characteristics of an extra-tropical cyclone and the non universally agreed definition for its precise location (Walker et al., 2020). This leads to a multitude of tracking algorithms using different meteorological criteria, e.g. meridional winds (Booth et al., 2017), eddy kinetic energy (Wang et al., 2017) or geopotential height (Raible et al., 2008). However, two variables are used most frequently, these are the minima of mean sea level pressure (Hoskins and Hodges, 2002; Wernli and Schwierz, 2006) and the relative vorticity at 850 hPa (Hodges, 1994, 1995).

Although a variety of tracking methods exits, the comparison from Pinto et al. (2016) demonstrates that results from different tracking methods qualitatively match each other.

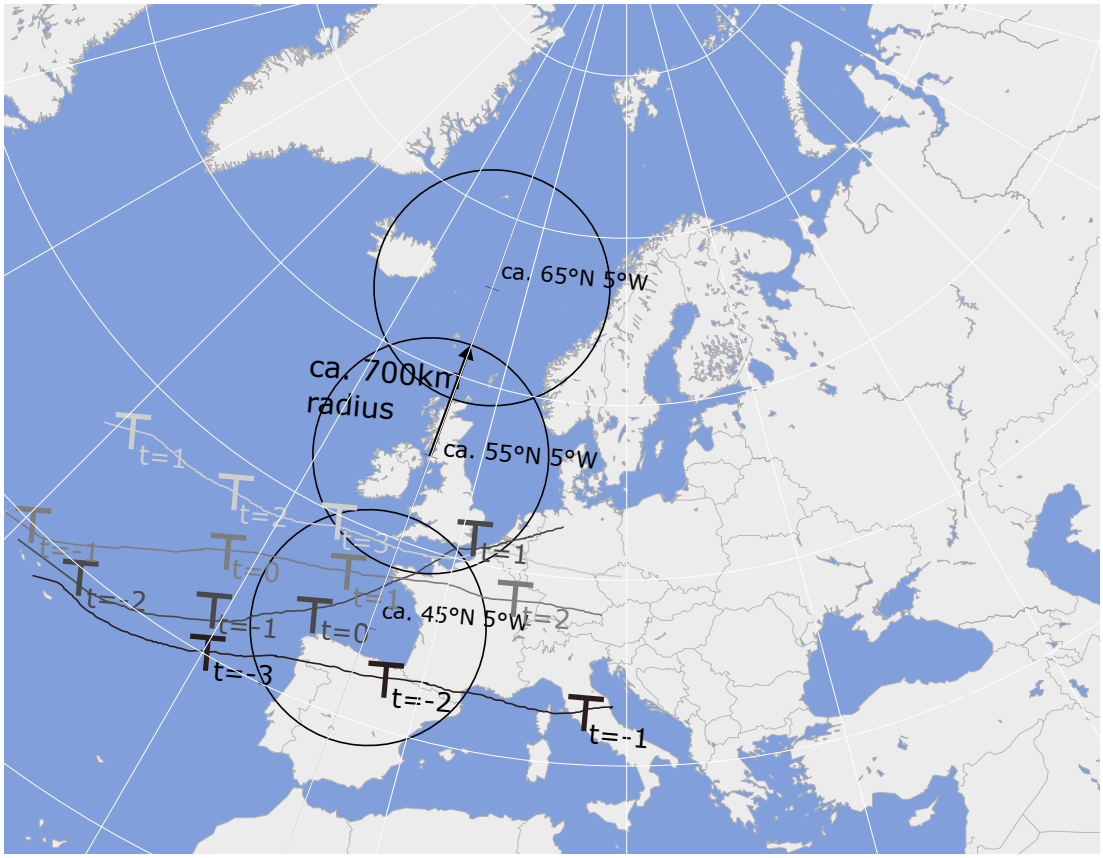

Figure 3.2: Serial cyclone clustering boundary conditions, showing the used locations, radius and an example for SCC at 45°N. The Ts represent the position of a cyclone for a specific time step, indicated by its index, throughout a seven day period. Different grey shadings refer to different cyclones. Four cyclones pass the area around 45°N within seven days and therefore fulfil the requirements for counting as a SCC period.

Cyclone identification and tracking

This study uses the cyclone identification and tracking described by Hodges (1994, 1995), using the 850 hPa relative vorticity fields. Within a vorticity field, vorticity maxima are determined for regions which surpass a relative vorticity of $1 \cdot 10^{-5}\,\mathrm{s}^{-1}$. Tracks are formed by using a nearest neighbour distance approach for each time step with consideration that some signals might vanish from one frame to another but appear again in frames afterwards. Lastly, smooth tracks are achieved by minimizing a cost function. See Hodges (1994) for more details. The results in determining serial cyclone clustering with this tracking method are consistent (Priestley et al., 2017) with the results in Pinto et al. (2014), using mean sea level pressure as the main variable for identifying and tracking cyclones instead.

Cyclone clustering

For the computation of serial cyclone clustering periods, this study follows the approach of Priestley et al. (2017). Three locations are set as base points at different latitudes (45°N, 55°N, 65°N) and 5°W. The area which cyclones have to pass through is then determined by a circle around the base points with a 700 km radius. To ensure only strong cyclones are counted for cyclone clus-

tering, the mean sea level pressure of the cyclone core has to be smaller than the fifth percentile of the climatological mean sea level pressure at the respective coordinate. Since lower pressure correlates to stronger cyclones, the cyclones counted for cyclone clustering must belong to the strongest five percent.
Lastly, the number of cyclones passing through the respective area within seven days has to be equal or greater than a certain threshold that is discussed in the following. For 45°N the average daily cyclone count in the winter period from 1979 to 2015 is about 0.13 cyclones per day. At 55°N and 65°N the average daily cyclone count is higher with 0.42 and 0.63 cyclones per day. Following the definition from Pinto et al. (2014); Priestley et al. (2017) we use a threshold of more than three cyclones ($n \geq 4$) for 55°N and 65°N, but lower it for 45°N due to the large discrepancy in the average daily cyclone count to more than two ($n \geq 3$). Figure 3.2 illustrates the set up used for determining serial cyclone clustering, as well as fictional cyclone tracks for a seven day period to show the definition of serial cyclone clustering in an exemplary way.

3.2.4 State of stratospheric polar vortex

This study uses the strength of the stratospheric polar vortex (SPV) as a measurement for the stratospheric state to analyse the influence of the stratosphere on serial cyclone clustering and the possible link to weather regimes. For quantification of the strength of the stratospheric polar vortex, we use the 10 hPa zonally averaged zonal wind at 60°N $u10$ which is on average between $25\,\mathrm{m\,s^{-1}}$ and $35\,\mathrm{m\,s^{-1}}$ in the winter (see. Fig A.1 in appendix). Of particular interest are cases which feature a weak stratospheric polar vortex or even a minor/major sudden stratospheric warming (SSW), when the westerly winds are weakened to only about $u10 = 10\,\mathrm{m\,s^{-1}}$ or even reversed (Shi et al., 2020). The classification of SCC periods into cases with a similar stratospheric polar vortex strength is based on an agglomerative hierarchical clustering method (see chap. 3.2.1.

4 Results

4.1 Link between the weather regimes and SCC

4.1.1 Modulation of cyclone frequency due to weather regimes and SCC

During serial cyclone clustering there are an anomalous high amount of cyclones in the respective regions. Therefore the cyclone frequency during SCC periods is modulated compared to the climatological mean frequency. Likewise weather regimes describe the most common large scale circulation patterns, which are reflected in anomalies from the climatological mean. Thus, also cyclone tracks and preferred regions of cyclone occurrence are likely modulated during regimes. Therefore an analysis of the mean cyclone frequency during SCC periods, as well as during different weather regimes in winter is carried out (Fig. 4.1, 4.2). Anomalies are calculated by subtracting a winter (DJF) climatology from 1979 to 2015. Contrary to the SCC identification, this analysis uses the cyclone tracking from Wernli and Schwierz (2006), which is based on enclosed contours

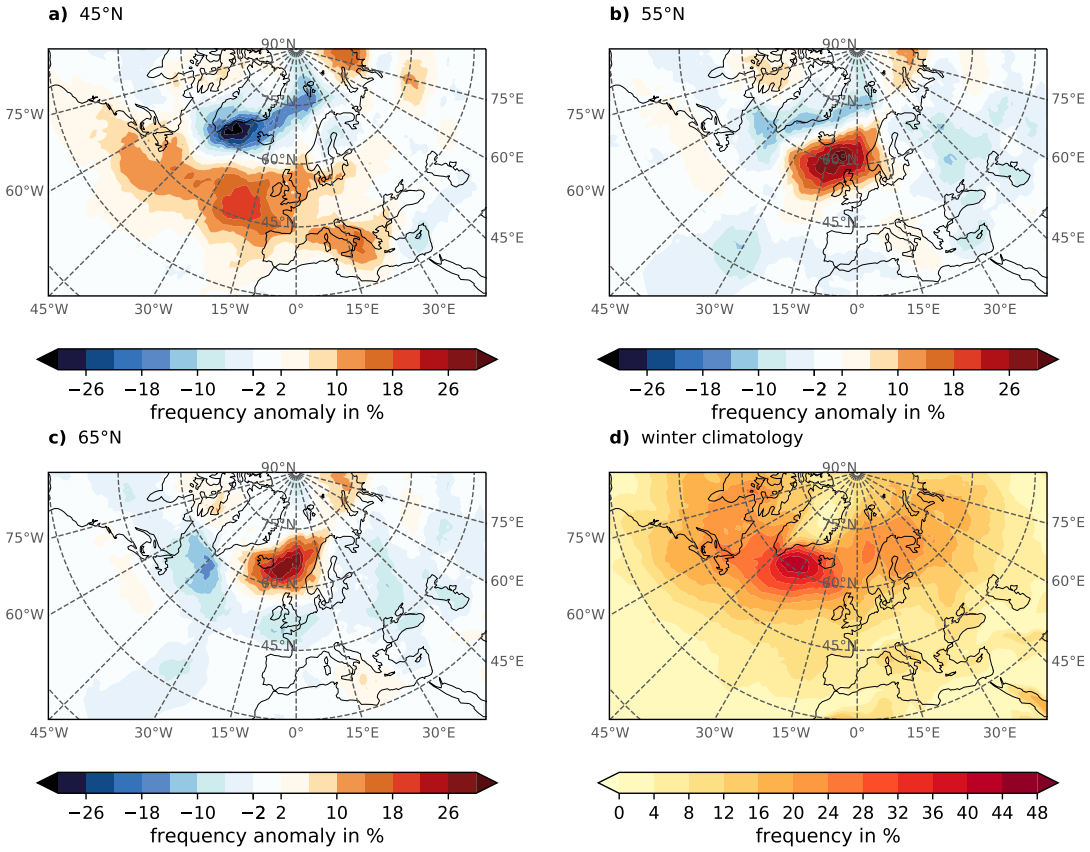

Figure 4.1: Cyclone frequency anomalies for SCC at 45°N 5°W (top left), 55°N 5°W (top right) and 65°N 5°W (bottom left) in winter (DJF). Anomalies are calculated with respect to the winter climatology 1979 - 2015. Here cyclone identification of Wernli and Schwierz (2006) is used.

of mean sea level pressure. During SCC at 45°N there is a strong decrease in cyclone activity near Greenland. An increase in cyclone frequency can be seen over Europe as well as the Mediterranean region around Italy and the Atlantic, mainly between 40°N and 55°N, with a maximum west of France. For SCC at 55°N the region of enhanced cyclone activity is shifted northwards in between Iceland and Great Britain. The area of enhanced frequency is also focused on a smaller region yielding in larger frequency anomalies in this region. Contrary to the strong negative anomaly for SCC at 45°N, SCC at 55°N shows widespread regions with rather weak decreased cyclonic activity. Lastly, the cyclone anomaly field for SCC at 65°N exhibits a strong positive anomaly further north, east of Iceland and a weakening south of Greenland. For all latitudes regions of enhanced cyclonic activity match with the regions used in determining SCC quite well (cf. Fig. 3.2) which is also expected since at least three/four cyclones are forced to cross these regions within seven days.

The modulation of cyclone occurrence due to different weather regime types can be seen in Figure 4.2. The Atlantic trough regime features an increase of cyclones in the North-Atlantic Ocean close to the Norwegian Sea, mainly between Iceland and Great Britain at latitudes from 50°N to 70°N. While the cyclone frequency is enhanced by more than 34% in this regions, other areas in the North-Atlantic European region, show a slight decrease of about -10% to -6%. The Zonal regime shifts the jet further north, so that more cyclones occur near Iceland and alongside Scandinavia with a maximum of about 30%. Elsewhere, cyclones occur less often, resulting in a decreased frequency of about -10% to -6%. In case of the Scandinavian trough, cyclone occurrence is enhanced over the Norwegian Sea and Scandinavia with an increase up to 26% at the expense of cyclones in Southern Europe with a decrease of about -6% and a large area in the North-Atlantic Ocean south of Greenland. In this region the decrease is even larger with up -20% to -14%. During the Atlantic ridge regime the cyclonic activity south of Iceland is greatly reduced by up to -26%, while all around the cyclone frequency is increased, e.g. over Eastern Europe or the Mediterranean Sea. The European blocking modulates the cyclone occurrence so that in most of central and northern Europe, the cyclone frequency is decreased. This decline ranges from -10% to -6% over central Europe to -26% to -22% over Northern Europe. However cyclone frequency is slightly enhanced over southern Europe and strongly increased with up to 22% over Greenland and the Arctic Sea. In case of Scandinavian Blocking, more cyclones occur in a large area over the North-Atlantic Ocean south of Greenland with an increase up to 18% which extends south-eastwards and lessens alongside Great Britain and France. The cyclonic activity is also enhanced over the Mediterranean Sea, while it is greatly reduced over Scandinavia by up to 26%. Lastly, Greenland blocking features an enhanced cyclone occurrence over the central parts of the North-Atlantic Ocean between 40°N and 55°N with an increase up to 26%. This lessens but extends to large parts of Europe with an increase in cyclone frequency of about 10%. The cyclonic activity over Greenland and Iceland is however severely decreased by more than -30%.

Comparing the cyclone frequency of the weather regimes (Fig. 4.2) and the cyclone anomalies of SCC at different latitudes (Fig. 4.1) already yields possible links between weather regimes and SCC. Four weather regime types are especially prominent in this comparison, the Atlantic trough, the Zonal regime, the Scandinavian trough and the Greenland blocking. Cyclone frequency anomalies for SCC at 55°N share a similar region of enhanced cyclonic activity with the Atlantic trough regime, in between Iceland and Great Britain. The Zonal regime and the Scandinavian

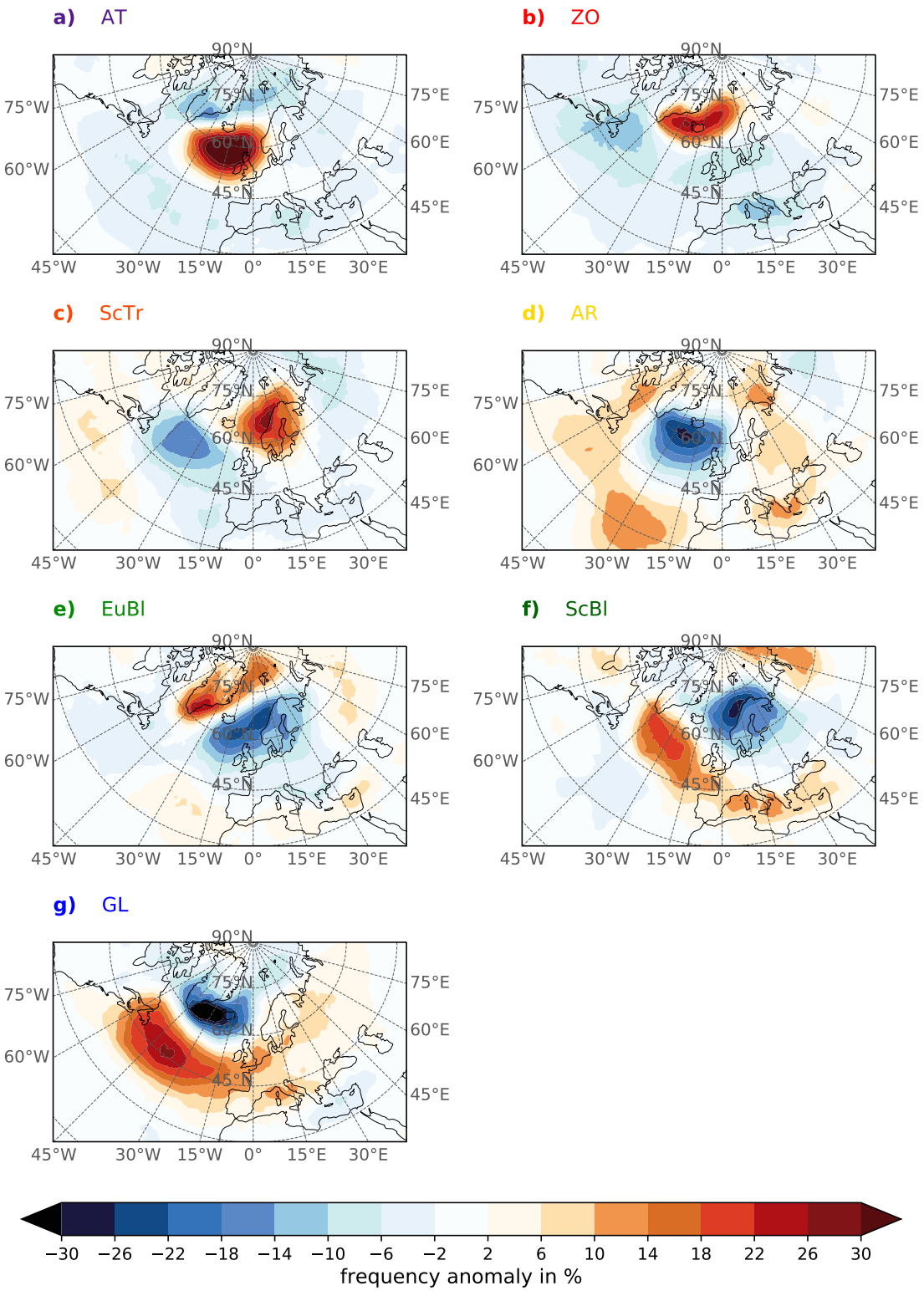

Figure 4.2: Cyclone frequency anomalies for the seven weather regime types based on an extended winter (NDJFMA) climatology from 1980 to 2015. Weather regime abbreviations are as followed: AT – Atlantic trough, ZO – Zonal regime, ScTr – Scandinavian trough, AR – Atlantic ridge, EuBl – European blocking, ScBl – Scandinavian blocking, GL – Greenland blocking. Here the cyclone identification algorithm of Wernli and Schwierz (2006) is used.

trough, however, show enhanced cyclonic activity around Iceland matching the anomalies for SCC at 65°N. Lastly, a region of marked cyclonic activity over the Atlantic between 40°N and 55°N is shared between both Greenland blocking and SCC at 45°N, with the maximum slightly shifted closer to Europe in case of SCC at 45°N.

(a)

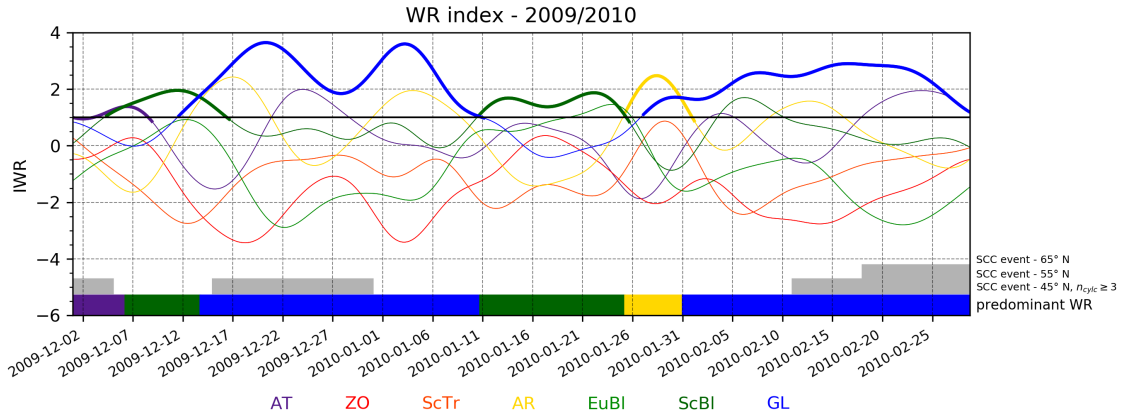

(b)

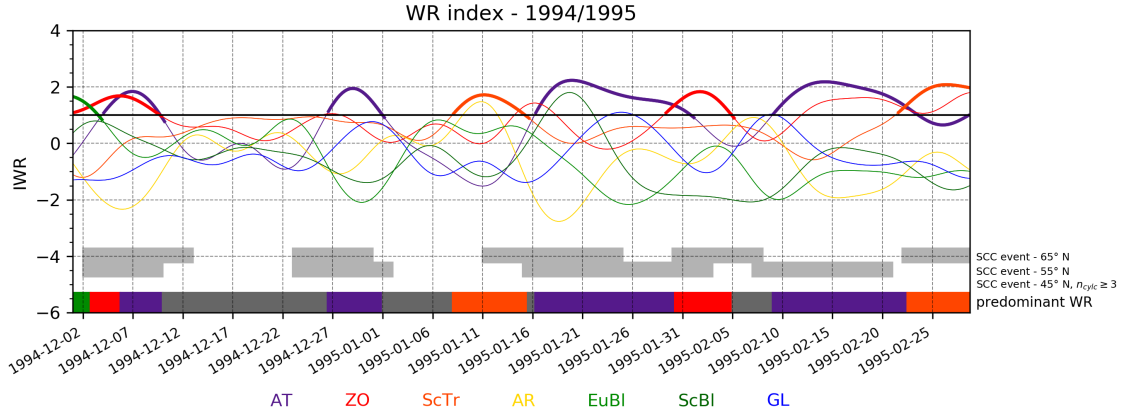

Figure 4.3: Weather regime index time (IWR) series for the winters 2009/2010 (a) and 1994/1995 (b). Colours represent the different weather regime types, abbreviation as followed: AT – Atlantic trough, ZO – Zonal regime, ScTr – Scandinavian trough, AR – Atlantic ridge, EuBl – European blocking, ScBl – Scandinavian blocking and GL – Greenland blocking. The thick bottom bar shows the regime life cycle type that has the strongest projection; grey means no active life cycles. Light grey bars denote SCC periods at different latitudes. SCC periods encompass all days with for the period relevant cyclones. This means all days ± 3 with $n_{\text{cycl}} \geq 4$ or $n_{\text{cycl}} \geq 3$ in case of 45°N within 7 days.

4.1.2 Modulation of weather regimes during SCC - case studies

While the cyclone frequency comparison already yielded some interesting results, further research is carried out by analysing individual case studies. In these case studies, the link between SCC occurrence and the weather regime index is examined, by making yearly winter time series from 1979 to 2015 of the weather regime index and denote SCC periods for each latitude. Figure 4.3 shows two of the 36 winter periods, which best represent the observed coherence. Each different coloured line depicts the time series of the weather regime index for one of the seven weather regimes. The thick coloured bar at the bottom of the figure illustrates which weather regime type has an active life cycle and the strongest projection for each time step. If no weather regime type has an active life cycle, the bar is coloured dark grey to express that none of the seven regime types dominate the current circulation pattern. The black line at $I_{\text{WR}} = 1$ is the threshold used in

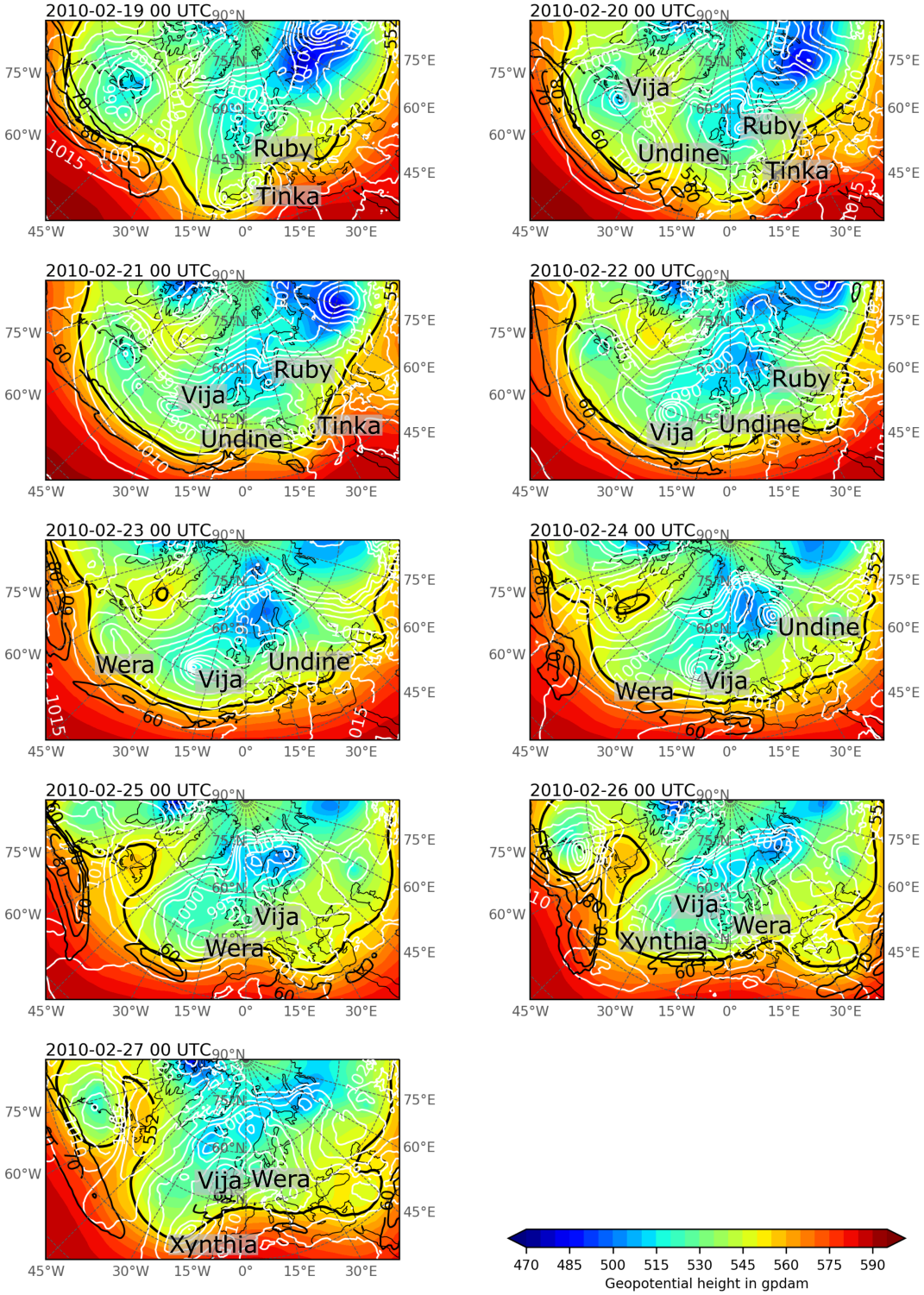

Figure 4.4: Evolution of the synoptic situation during a 9 day period from 19/02/2010 to 27/02/2010 where SCC occurs at 45°N and 55°N. The shading represents the geopotential height at 500 hPa. 552 gpdam is specifically marked as a thick black line. White contours represent the mean sea level pressure, while black ones denote the horizontal wind speed at 300 hPa, cut off at 50 $m\,s^{-1}$ and lower. Low-pressure names are taken from Institut für Meteorologie -FU-Berlin (2021)

the weather regime life cycle definition. Lastly, the light grey horizontal bars above display SCC periods for each of the three latitudes.

Greenland blocking is the predominant weather regime type throughout most of the winter period 2009/2010 (Fig. 4.3 a). The first Greenland blocking life cycle begins at around the 12th December and becomes dominant two days afterwards. Another two days later a SCC period at 45°N sets in which last for about 17 days until the 31st December. Throughout this period, Greenland blocking shows a strong projection, however, with a local minimum shortly before the SCC period decay on the 28th December. The second long Greenland blocking life cycle has its onset on the 27th January and becomes dominant at the 31st January. Again, a SCC event at 45°N is recorded beginning on the 11th February and lasting at least until the 28th February. During this period SCC at 55°N also occurred alongside the SCC at 45°N, beginning on the 18th February. The biggest difference between the onsets at 45°N and 55°N is the strong projection in the Atlantic trough alongside the Greenland blocking life cycle, which is passing $I_{\mathrm{WR}} = 1$ at a similar time as the SCC onset at 55°N. The first identified SCC period at 45°N beginning before the 1st December in this winter, however, is not connected with a strong Greenland blocking projection or Greenland blocking life cycle (not shown), but with an Atlantic trough life cycle instead.

The winter period 1994/1995 is characterised by short intervals of Atlantic trough, Zonal regime or Scandinavian trough life cycles and periods when no regime fulfils the requirement for a life cycle (4.3 b). Striking is that there are also short intervals of SCC at 55°N and 65°N at similar times as the weather regime life cycles. The first SCC at 55°N and 65°N begins on the 2nd December while the European blocking regime is still the dominant one. However, there is already a Zonal regime life cycle ongoing and an Atlantic trough life cycle onset two days after. The SCC period at 55°N decays two days before the end of both life cycle, while the SCC period at 65°N decays two days after the end of both life cycles. Another two short SCC periods have there onset on the 23rd December and decay around a similar time as the Atlantic trough life cycle that emerges three to four days after the SCC onset. An interesting connection between SCC occurrence and weather regimes can be seen in the later SCC periods, especially from 30th January onwards. There, SCC at 65°N occurs mostly in conjunction with a Scandinavian trough or Zonal regime life cycle, whereas SCC at 55°N seems to be connected to the Atlantic trough life cycles. Onset and decays of the SCC periods are similar to those of the respective weather regime life cycles, sometimes with a small time lag or time lead.

The observed behaviour can also be seen in some of the other winters, however, not as clear and not as consistent. Overlapping of SCC periods at 45°N and 55°N or 55°N and 65°N, which happens in both cases, is also likely due to the overlap in the area used for determining SCC (cf. Fig. 3.2). From the case study several possible links can be concluded, but still need further evidence. Firstly, SCC tends to occur more often together with certain weather regime types. These preferred regime types depend on the latitude for which SCC is determined. SCC at 45°N tends to favour Greenland blocking, SCC at 55°N seems to favour the Atlantic trough regime and SCC at 65°N occurs mostly in conjunction with the Zonal regime and Scandinavian trough. This result also agrees well with the observed cyclone frequency anomalies during SCC and the respective weather regime type frequency fields. Secondly, SCC onsets often occur shortly before or after the preferred weather regime type onset or when the weather regime becomes the dominant one. Therefore, not just

the weather regime type but also the transition towards the weather regime might influence the occurrence of SCC.

While 4.3 is helpful for understanding the interaction between SCC and weather regimes, we also look into the synoptic situation throughout the SCC period in the case studies. An excerpt of the period where SCC at 45°N and 55°N occurs simultaneously during a Greenland blocking life cycle is shown in Figure 4.4. Noticeable for the period from the 19th to 24th February is a strong stable zonally oriented southward shifted jet at around 40°N, with maximums of $60\,\mathrm{m\,s^{-1}}$ to $80\,\mathrm{m\,s^{-1}}$, which is in good agreement with a strong projection on to Greenland blocking. On the 19th and 20th February, cyclones Ruby and Tinka already passed into Europe while Undine and Vija form slightly north of the jet maximum in quick succession and travel towards Europe in the subsequent days. Cyclone Wera can be seen first as enclosed pressure contours over Newfoundland on the 21st February, again north of the jet, being stationary until the 22nd and moving towards Europe on the 23rd. Following Wera, a thin but strong ridge emerges near Newfoundland, while the polar front is still rather zonally oriented over large parts of the North Atlantic and near the European coast. Still, contrary to the previous cyclones, Xynthia is forming closer to the European coast near a small jet maximum on the 25th / 26th February. Due to the strengthening of the ridge over Newfoundland, the mostly zonal flow gets a stronger meridional component and Xynthia is steered south-eastwards towards Spain on the 27th February. The other synoptic situations of the SCC periods in these case studies show similarities (not shown), cyclones forming near a strong and stable jet that, depending on the latitude where SCC occurs, is shifted more to the south or north.

Generally the synoptic situation matches well with results from previous studies on the dynamics of SCC (Pinto et al., 2014; Priestley et al., 2017). A strong jet is present for a prolonged time period, cyclones form near the jet streaks and some cyclones form in group (i.e. Undine and Vija) hinting at secondary cyclogenesis.

4.1.3 Modulation of weather regimes during SCC - climatological analysis

The case studies are already hinting at specific links between weather regimes and the occurrence of SCC. The Greenland blocking regime seems to go along with SCC at 45°N, Atlantic trough with SCC at 55°N and Scandinavian blocking or Zonal regime with SCC at 65°N. Furthermore, SCC appears to be connected to weather regime transitions, since it mostly occurs shortly after a new regime onset or when the regime becomes dominant. These, however, are only possible links so far and need to be verified by a climatological analysis which includes all winter seasons. Therefore, we perform a lagged frequency analysis of the dominant weather regime at SCC onset for all three latitudes. The data is resampled using the bootstrap with 1000 iterations and a random climatology is derived to test for statistical significance. Instead of taking only SCC onset dates to resample from, the climatology uses all winter dates from 1979 to 2015 for resampling. The results are shown in figures 4.5 to 4.7 for the respective latitudes. Measured is the relative frequency of a certain weather regime life cycle type being the dominant one at SCC onset or up to 60 days before or after the SCC onset. Dark shaded areas represent the respective 25th to 75th percentile range while light shading indicates the 5th to 95th percentile range. To increase the sample size and reduce uncertainty, a three day period extension around the SCC onsets is allowed. Statistical significance is tested by using the percentile rank (cf. chapter 3). To improve the statistical significance test of the lags further, the climatology is normalised around lag 0, which however distorts the significance at lag 0. Since weather regimes are required to be persistent, being in a certain weather regime life cycle already carries information about the days before and after and thus modulates the probability of being in the given regime again. This information is known by the true sample and addressed in the random climatology by using the normalisation. Each of the eight top panels in figures 4.5 to 4.7 show the frequency for the seven different regimes as well as when no regime has an active life cycle. The bottom left panel is a composite for the mean values of each weather regime type, including the no regime, while the bottom right one shows the anomalies of the mean values from the sampled climatology. Thick coloured lines represent statistical significance.

For SCC at 45°N (Fig. 4.5) Greenland blocking and Atlantic trough seem to be the most frequent and also show the most significant frequency increase. They reach up to about 28 % relative frequency at lag 7 in case of Atlantic trough and 35% at around lag 7 for the Greenland blocking. In contrast, Scandinavian trough, Atlantic ridge and European blocking are in good agreement with there respective climatologies or partly suppressed and therefore unimportant for the occurrence of SCC. The anomalies panel shows that the enhancement in Atlantic trough up to 15 days and Greenland blocking up to 30 days are also statistically significant. The Zonal regime also shows an significant decrease five days after the SCC onset and an significant increase at around lag 35 after the enhanced Greenland blocking period subsides.

The results for SCC at 55°N (Fig. 4.6) are different. Most of the regimes show a significant decrease in frequency in the period after the SCC onset up to around ten days. This is due to the largely increased frequency of Atlantic trough during this period with a maximum of about 55% at lag 7. To put in perspective, of all SCC onset 55% show an active dominant Atlantic trough life cycle seven days afterwards. The anomalies panel also shows that the enhanced Atlantic trough

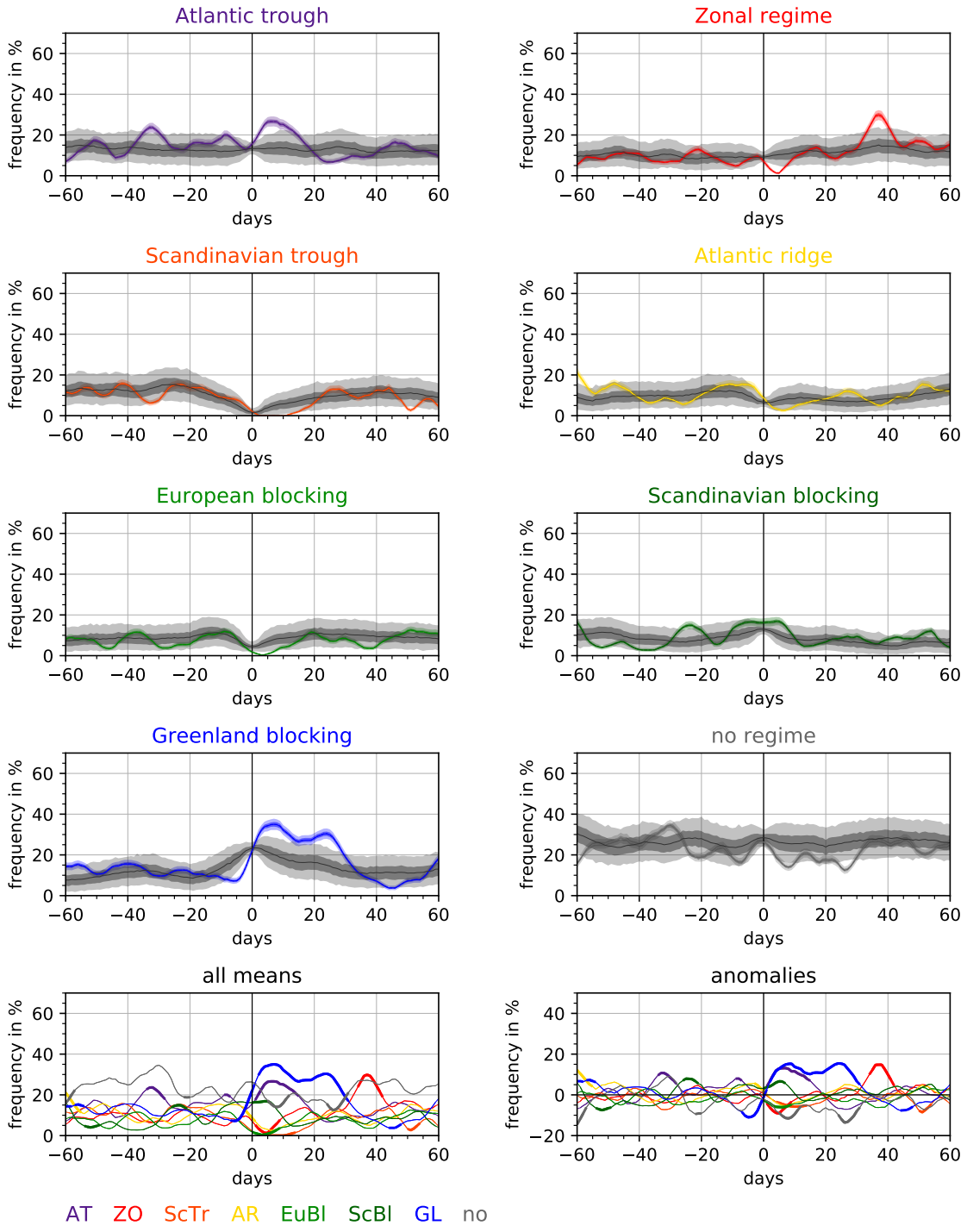

Figure 4.5: Lagged frequency analysis for SCC onsets at 45°N allowing a 72 hours interval for decreased uncertainty. Bootstrapping with 1000 iterations is used to resample the data and derive a random climatology. Coloured lines represent the frequency of each weather regime type being dominant at a certain lead/lag relative to the SCC onset (SCC onset $\pm$60 days). Dark/light shading represents the $p_{0.25}$ to $p_{0.75}$ / $p_{0.05}$ to $p_{0.95}$ range. Anomalies are calculated by subtracting the resampled mean and the random climatological mean. Thick lines represent statistical significance based on the percentile rank being lower than 5% or higher than 95%.

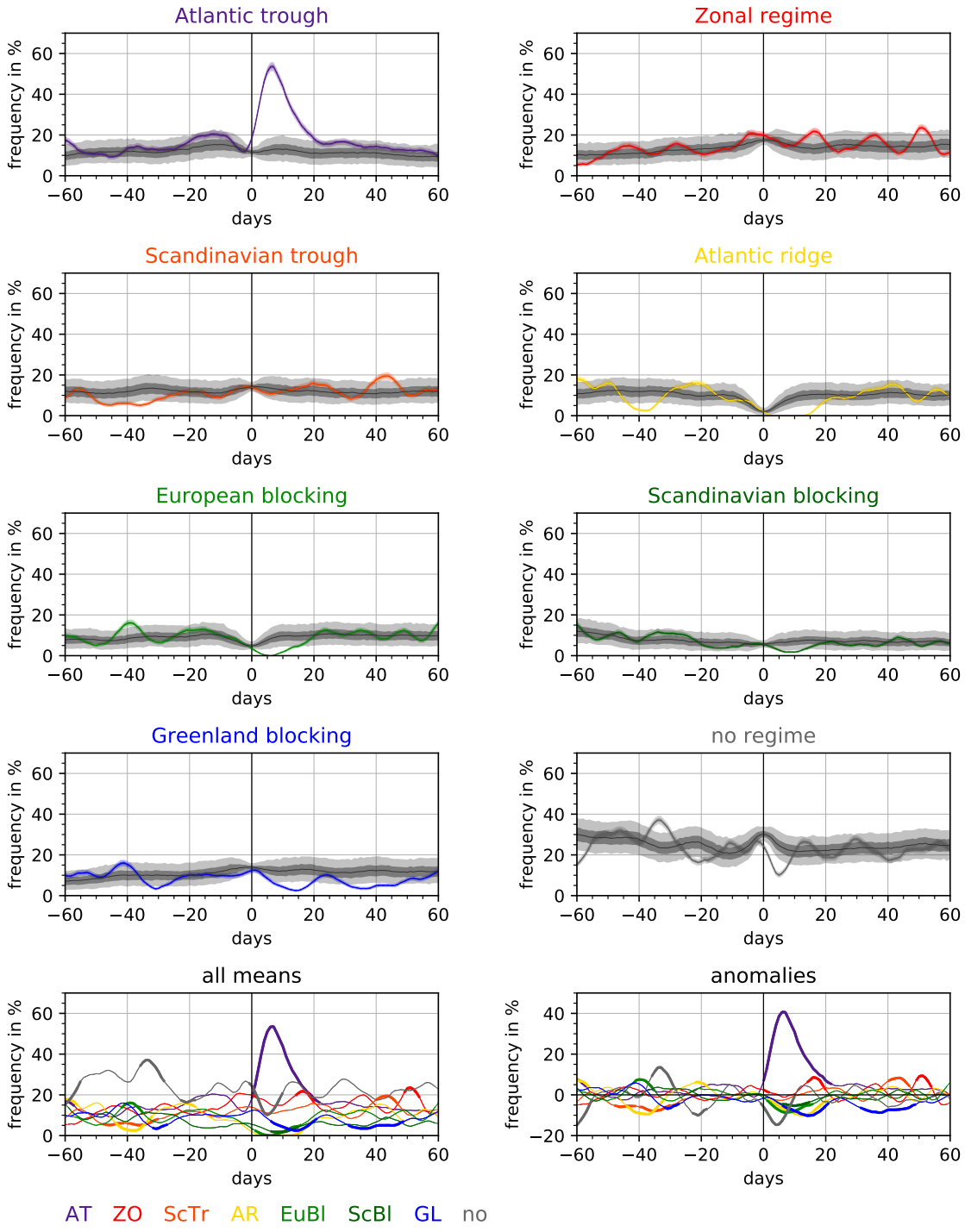

Figure 4.6: Lagged frequency analysis for SCC onsets at 55°N allowing a 72 hours interval for decreased uncertainty. Bootstrapping with 1000 iterations is used to resample the data and derive a random climatology. Coloured lines represent the frequency of each weather regime type being dominant at a certain lead/lag relative to the SCC onset (SCC onset ± 60 days). Dark/light shading represents the $p_{0.25}$ to $p_{0.75}$ / $p_{0.05}$ to $p_{0.95}$ range. Anomalies are calculated by subtracting the resampled mean and the random climatological mean. Thick lines represent statistical significance based on the percentile rank being lower than 5% or higher than 95%.

is statistically significant up to lag 20. Noticeable is also that the only other weather regime type that shows a significant increase in frequency is the Zonal regime starting at lag 15.
The lagged frequency analysis for the SCC onsets at 65°N shows yet another different picture. For a period up to 12 days after the onset the Zonal regime is the most frequent one with a maximum of 37%, followed by the Scandinavian trough with 27% and Atlantic trough with 22% at lag 7. Blocking regimes, including Atlantic ridge, European blocking, Scandinavian blocking and Greenland blocking are all suppressed. Especially Greenland blocking shows a significantly decreased frequency for a long period up to 45 days.
The comparison of all three figures shows that SCC seems to precede transitions in the dominant weather regime slightly. While depending on the latitude, a different regime type is favoured, the frequency at lag 0 is mostly comparatively low and still rising for five to seven days after. Only Greenland blocking for SCC at 45°N shows a distinct increase in frequency with 23% at lag 0, already. The comparison also reveals that the period of significant frequency increase tends to be about 15 to 20 days long in general. This is the case for the Atlantic trough regime in Figure 4.5 and 4.6 as well as the Zonal regime and Scandinavian trough in Figure 4.7. However, the Greenland blocking regime for SCC at 45°N is affected on a longer time scale up to 30 days but interestingly enough, there is a local minimum at 15 days. Some cases might respond similar to the general tendency to decay at around 15 to 20 days after the SCC onset and some might live considerably longer due to stratospheric influence.
In conclusion, the climatological analysis not only confirms most of the possible links derived from the case study analysis, but also provides a quantitative impression about the importancy. For SCC at 45°N, Greenland blocking and Atlantic trough are the two important weather regime types, with Greenland blocking occurring more often and on longer time scales. The clearest link shows SCC at 55°N and the Atlantic trough regime which has a large increase in frequency while other regime types are suppressed. Lastly, for SCC at 65°N, the Zonal regime and the Scandinavian trough show the largest increase in frequency, while Greenland blocking is being suppressed for a longer time period. A lead-lag relationship between SCC and dominant regime transitions is also discovered, since the regime frequencies of the preferred regimes are increasing after the SCC onset for all three latitudes.

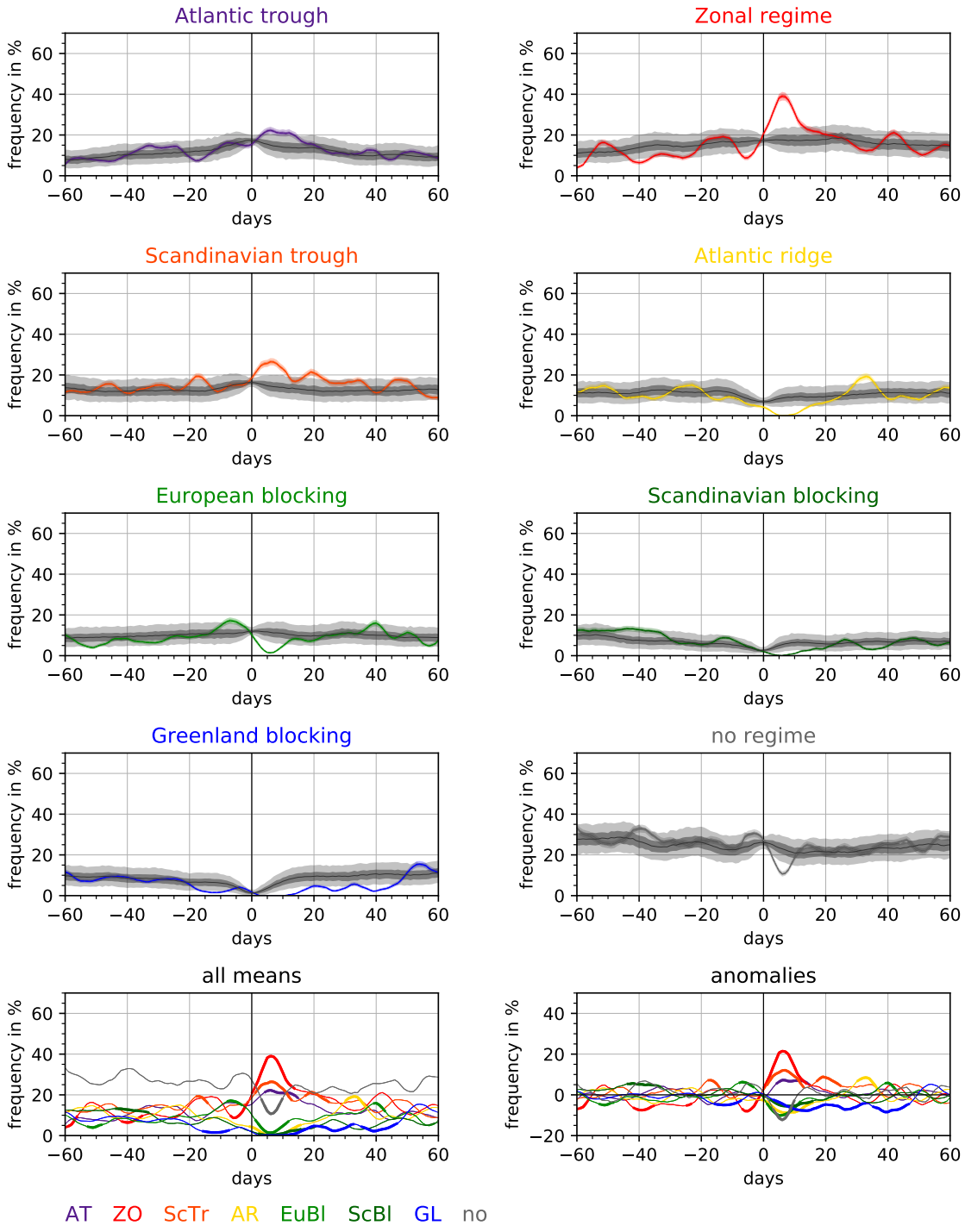

Figure 4.7: Lagged frequency analysis for SCC onsets at 65°N allowing a 72 hours interval for decreased uncertainty. Bootstrapping with 1000 iterations is used to resample the data and derive a random climatology. Coloured lines represent the frequency of each weather regime type being dominant at a certain lead/lag relative to the SCC onset (SCC onset $\pm$60 days). Dark/light shading represents the $p_{0.25}$ to $p_{0.75}$ / $p_{0.05}$ to $p_{0.95}$ range. Anomalies are calculated by subtracting the resampled mean and the random climatological mean. Thick lines represent statistical significance based on the percentile rank being lower than 5% or higher than 95%.

Table 4.1: Relative frequency of dominant regime transitions calculated by using bootstrapping with 1000 iterations. The climatology is determined by choosing random time periods during the winters from 1979 to 2015 of similar average length as the SCC periods at the respective latitudes.

	resample (45°N/55°N/65°N)	**climatology (45°N/55°N/65°N)**	**anomalies (45°N/55°N/65°N)**
no transition	0.25 / 0.21 / 0.13	0.20 / 0.18 / 0.20	0.05 / 0.03 / -0.07
one transition	0.47 / 0.47 / 0.44	0.46 / 0.46 / 0.39	0.01 / 0.01 / 0.05
mult. transition	0.28 / 0.32 / 0.43	0.34 / 0.36 / 0.41	-0.06 / -0.04 / 0.02

4.1.4 Interaction between weather regime transitions, life cycle stage and the occurrence of SCC

The climatological analysis shows that shortly after SCC onsets the frequency of certain regimes being the dominant ones is quickly rising. Therefore, a lot dominant regime transitions have to take place in that time period. It is, however, unclear if this is due to a general increase in dominant regime transitions during SCC or because transitions are mainly occurring in the earlier stages of a SCC period. Unknown is also if the dominant regime transitions are true transitions or life cycle onsets. A true dominant transition is a transition from an already ongoing regime instead of the no regime. Since the climatological analysis only gives results for the dominant regime type, the relationship between weather regime life cycle stages and SCC occurrence has not been analysed yet. This section tries to address these issues.

Dominant weather regime transitions and SCC

To verify if the total amount of dominant weather regime transitions increases during SCC, bootstrapping with 1000 iterations is used again to resample and build a random climatology. The random climatology is calculated by building randomly selected periods of similar length as the SCC periods at each latitude. Measured is the number of dominant regime transitions during SCC periods. The results are then categorised into three cases and the relative frequency of belonging to each case is determined. These cases are SCC periods with no transition, with exactly one transition and with multiple transitions. Table 4.1 shows the resampled and climatological monte-carlo mean for each category as well as the difference between them. Statistical significance is tested by comparing the probability density distributions of the resample and climatology (cf. Figures A.2 to A.4 in the appendix). Since the climatology is sampled from all winter days, differences between the climatologies for each latitudes are mainly due to SCC periods having a slightly different average length depending on the latitude. While there are differences between the resample frequencies at each latitude and their respective climatology, none are of statistical significance. Therefore, an overall increasing amount of dominant regime transitions can be eliminated as reasoning for the high number of dominant regime transitions found in the climatological analysis.
To investigate the other possibility of transitions occurring at a similar stage of an SCC period, scatter plots are made. They show the time difference between transition date and the SCC on-

set as the x-coordinate and time difference between the transition date and SCC decay as the y-coordinate. Figures 4.8 to 4.10 show the results for SCC at all three latitudes. Negative values mean that the SCC onset/decay is later in time than the dominant transition date. The coloured symbols represent dominant transitions towards the respective weather regime type. Transitions dates are only included if the targeted weather regime life cycle overlaps at least for a day with one SCC period. A grey symbol shows that a dominant regime transition occurred but from no-regime, meaning it is equivalent to a life cycle onset. The scatter plots can be divided into four quadrants beginning at top right going counter clockwise. Quadrant one includes both positive x- and y-values. This means that the transitions date is after the SCC period. Therefore it includes those weather regime life cycles that begin within the SCC period but become dominant only after the SCC period has decayed already. Quadrant two should always be empty because it includes negative x-values and positive y-values. This would mean that the transitions occurs earlier than the SCC onset but later than the SCC decay, which of course is not possible, because the SCC decay is always later in time than the SCC onset. Quadrant three features both negative x- an y-values, and therefore includes life cycles that become dominant before the SCC period begins. This, however, does not require the life cycle to be dominant throughout most of the SCC period. It is possible that another dominant transition occurs during or even before the SCC period, but the weather regime life cycle overlaps at least partly with the SCC period. Lastly, quadrant four covers all transitions that occur within a SCC period. The black dashed line represents the middle of the SCC period, because it is equally distant from the SCC onset and the SCC decay. The further afar from the line, the closer the transition is to the SCC onset/decay. In all three cases, there are a lot of transitions that fall into either quadrant three or four. Therefore, only a few weather regime life cycles begin within the SCC period and become dominant only after the SCC period decayed. This means that the SCC period either ends within the preferred life cycle or a new life cycle becomes already dominant while the SCC is still ongoing (far right side of the dashed line in quadrant four).

In case of SCC at 45°N (cf. Fig. 4.8), there are a lot of blue crosses representing transitions towards the Greenland blocking, which agrees well with the high frequency of dominant Greenland blocking regimes during SCC at 45°N. While they are quite spread out between quadrant three and four, more than half of them gather on the left side of the dashed line in quadrant four. This means that Greenland blocking becomes dominant more often in the early to mid stage of an SCC period. Noteworthy is also that dots representing the Atlantic trough are gathered mostly in this area, too, which is also quite sensible due to the frequency of Atlantic trough being significantly higher shortly after the SCC onset as well (cf. Fig. 4.5). Dots in quadrant three show regime transitions to a variety of weather regimes including Atlantic ridge, Scandinavian blocking besides Greenland blocking and Atlantic trough. However, as mentioned, these life cycles are not required to be dominant throughout the whole SCC period and may or may not be in their decay phases when SCC sets in.

Figure 4.9 shows the situation for SCC at 55°N. Here, the signal is much clearer. A lot of dominant transitions towards the Atlantic trough around one to six days after the SCC onset can be observed, which again matches well with the results from the climatological analysis. Interestingly, before the SCC onset and after the SCC reached its mid stage, there are only very few transitions towards the Atlantic trough. Instead, towards the end of the SCC period a lot of transitions to the Zonal

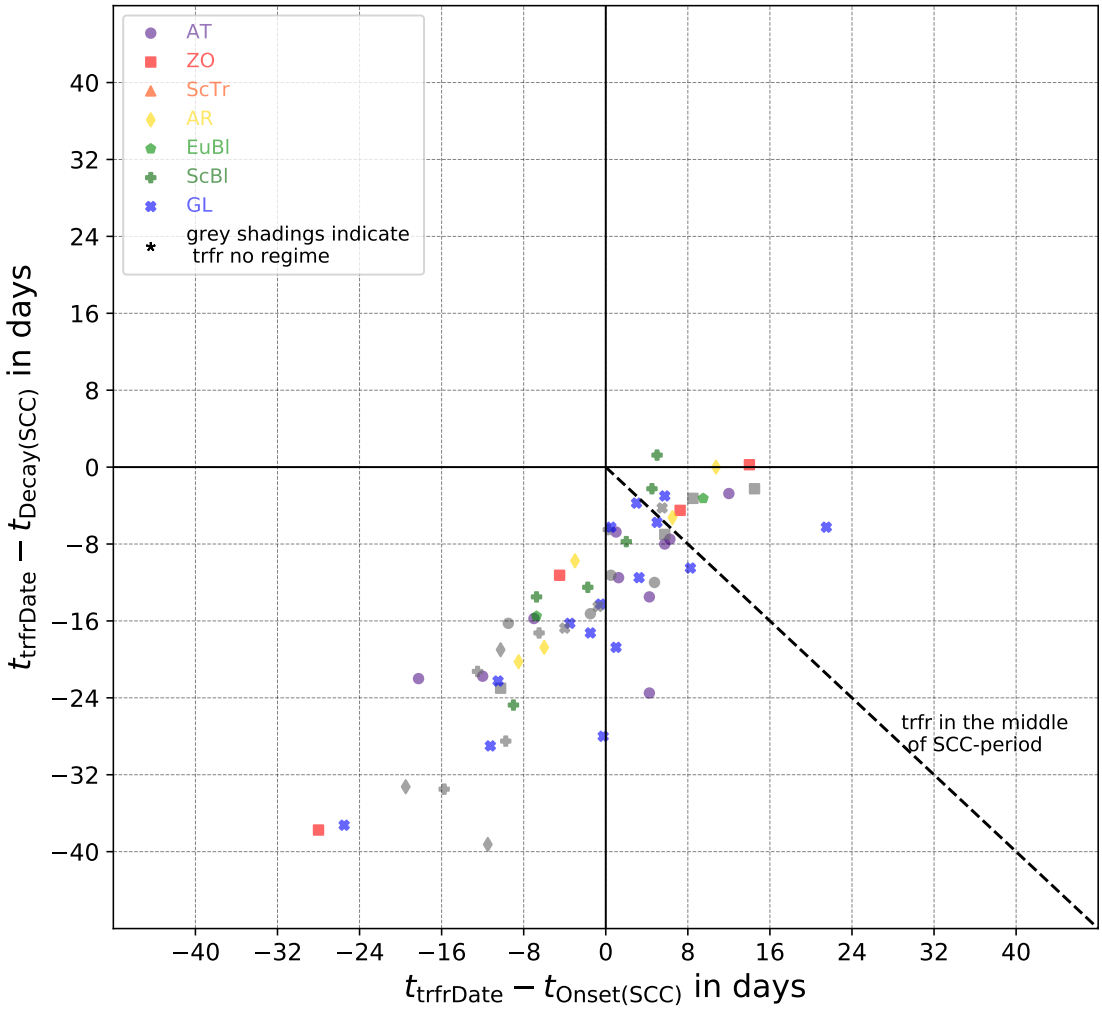

Figure 4.8: Scatter plot showing the positions of dominant weather regime transitions compared to the SCC periods at 45°N. t_{trfrDate} is the date at which the new regime becomes dominant, $t_{\text{Onset(SCC)}}$ is the onset and $t_{\text{Decay(SCC)}}$ the decay date of the SCC period. The x-coordinate denotes the time difference between the transition date and SCC onset and the y-coordinate the time difference between the transition date and SCC decay. Shape and colour of symbol displays which regime is dominant after the transition. Grey shading means the transition is coming from no-regime and is equal to the life cycle onset. The dashed line represents the mid stage of an SCC period.

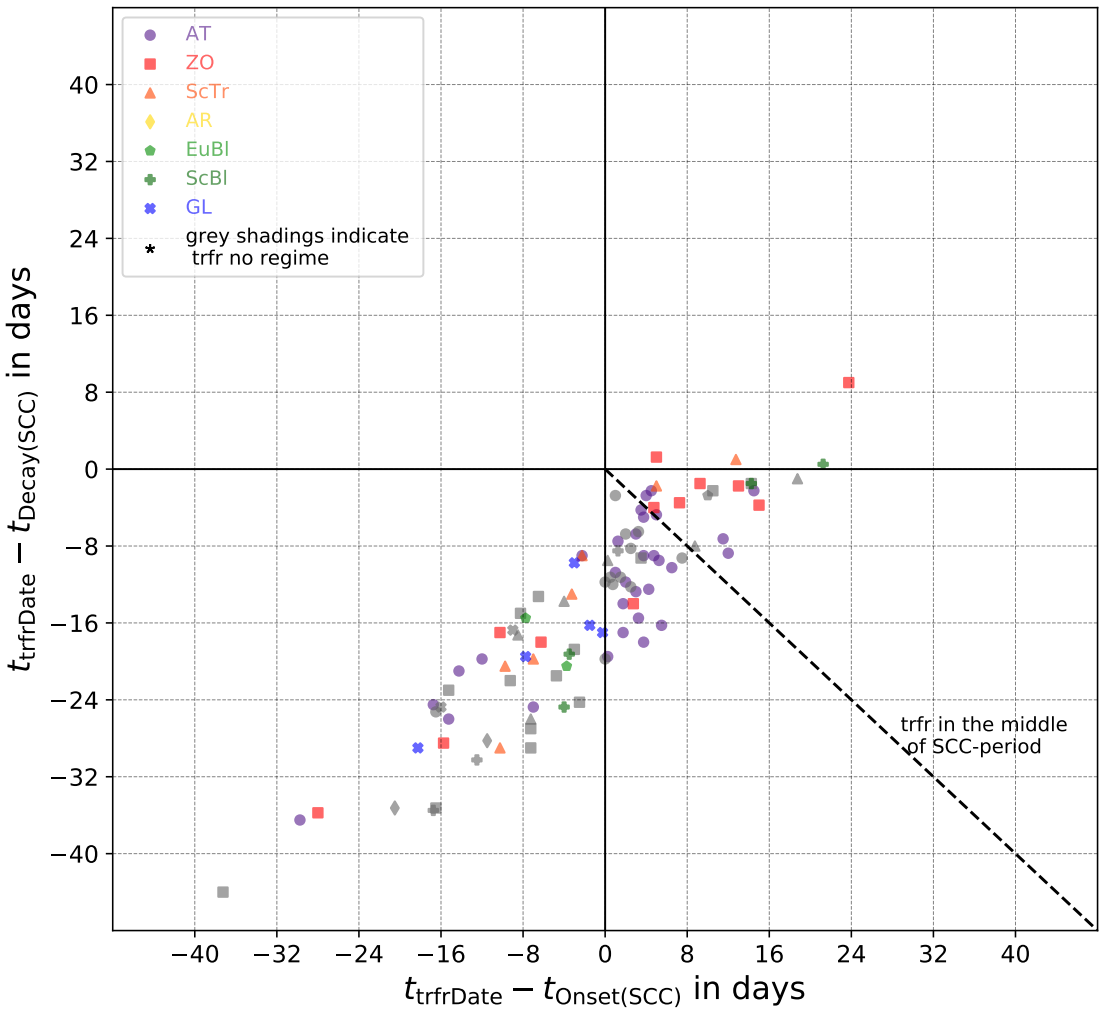

Figure 4.9: Scatter plot showing the positions of dominant weather regime transitions compared to the SCC periods at 55°N. t_{trfrDate} is the date at which the new regime becomes dominant, $t_{\text{Onset(SCC)}}$ is the onset and $t_{\text{Decay(SCC)}}$ the decay date of the SCC period. The x-coordinate denotes the time difference between the transition date and SCC onset and the y-coordinate the time difference between the transition date and SCC decay. Shape and colour of symbol displays which regime is dominant after the transition. Grey shading means the transition is coming from no-regime and is equal to the life cycle onset. The dashed line represents the mid stage of an SCC period.

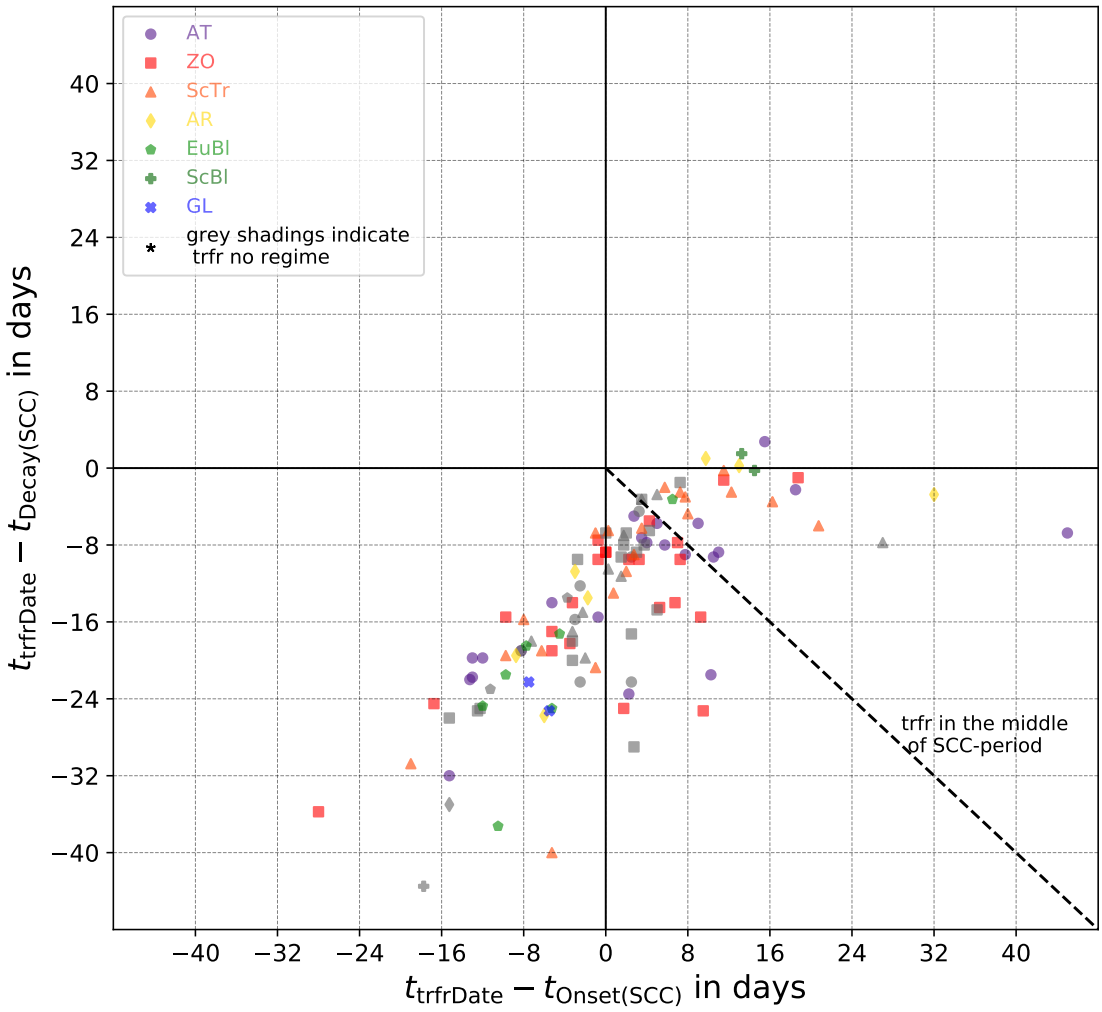

Figure 4.10: Scatter plot showing the positions of dominant weather regime transitions compared to the SCC periods at 65°N. t_{trfrDate} is the date at which the new regime becomes dominant, $t_{\text{Onset(SCC)}}$ is the onset and $t_{\text{Decay(SCC)}}$ the decay date of the SCC period. The x-coordinate denotes the time difference between the transition date and SCC onset and the y-coordinate the time difference between the transition date and SCC decay. Shape and colour of symbol displays which regime is dominant after the transition. Grey shading means the transition is coming from no-regime and is equal to the life cycle onset. The dashed line represents the mid stage of an SCC period.

regime occur. Similar to the results from SCC at 45°N, there are a variety of dots in quadrant three, though this time mainly consisting of cyclonic regime types.

Lastly, Figure 4.10 displays the result in case of SCC occurring at 65°N. In this case, there are a lot of Scandinavian trough and Zonal regime transitions on left side of the dashed line in quadrant four. However, compared to the Atlantic trough regime for SCC at 55°N, there are also a lot of Zonal regime and Scandinavian trough transitions in quadrant three up to about seven days prior to the SCC onset. Noteworthy is also the amount of Atlantic trough transitions close to the mid stage of the SCC events. These may or may not be connected to situations where SCC occurs at both 55°N and 65°N as seen in the winter 1994/1995 (cf. Fig. 4.3).

All in all dominant regime transitions are closely connected to SCC periods. They often occur with a time lag up to six days after the SCC onset while still being in an earlier stage of the SCC period. This is especially prominent for the transitions to the Atlantic trough regime in case of SCC at 55°N and explains the rapid increase in dominant regime frequency seen in the climatological analysis. For 45°N and 65°N their respective preferred regimes might also become dominant slightly before SCC sets in with a time lead up to about six days. For SCC at 45°N, this is also sensible considering Greenland blocking is already quite frequent at SCC onset and has a shallow frequency increase compared to the steep rise of Atlantic trough for SCC at 55°N.

SCC occurrence compared to the stage of a weather regime life cycle

SCC at different latitudes shows a strong connection with transitions in the dominant weather regime to the respective preferred regime type. Most often the SCC onset precedes the transitions slightly by up to six days. True transitions, however do not carry information about the lead/lag relationship between the life cycle onsets and SCC onsets. Thus, life cycles might already begin around the SCC onsets or even earlier. Only the grey dots in Figures 4.8 to 4.10 are equivalent to actual life cycle onsets. Therefore, a dedicated analysis is carried out to acquire information about link between the stage of a weather regime life cycle and the occurrence of SCC. Similarly to the transitions analysis, scatter plots are made based on life cycles that overlap at least once with an SCC period. Figures 4.12 to 4.14 show the results of the analysis. The coordinates changed slightly, so that the x-coordinate describes the time difference between weather regime life cycle onset and SCC onset, while the y-coordinate represents the time difference between the life cycle decay and the SCC decay. Again, the plot can be divided into four quadrants starting from the top right going counter clockwise. Quadrant one includes positive x- and y-values and thereby life cycles that decay after the SCC decays and begin after the SCC onset. The second quadrant consists of life cycles that begin before SCC onsets and decay after the SCC decays. Quadrant three features life cycles that have their onsets before the SCC onsets and their decays before the SCC decays and lastly, the four quadrant includes life cycles that begin after the SCC onset but decay before the SCC decays. Fictional life cycles generic for each quadrant are shown in Figure 4.11. In summary, life cycles in quadrant one begin within SCC periods but also outlast them, life cycles in quadrant two have embedded SCC periods, life cycles in quadrant three begin prior to the SCC period but also decay within the SCC period and lastly, life cycles in quadrant four are embedded into SCC periods. Another conclusion is that dots close to the center are life cycles that begin and decay around the same times as the SCC period.

For SCC at 45°N (cf. Fig. 4.12), there are some Greenland blocking life cycles in each quadrant, however, they mostly fall within the the -7 to 7 square and thus are considerably close to the center. Scandinavian blocking and Atlantic ridge life cycles farther from the center can be found mainly in the third quadrant. Since they begin mostly about eight to 24 days prior to the SCC onset and also decay eight to sixteen days prior, they are likely to be in their decay stage when SCC sets in, while different life cycles begin and become dominant shortly after. Of all the Greenland blocking life cycles more than half show positive y-values. Therefore, SCC periods decay more often within Greenland blocking life cycles than afterwards. This might be the case due to the lessening impact of the decaying regime, which might not be strong enough to uphold the SCC

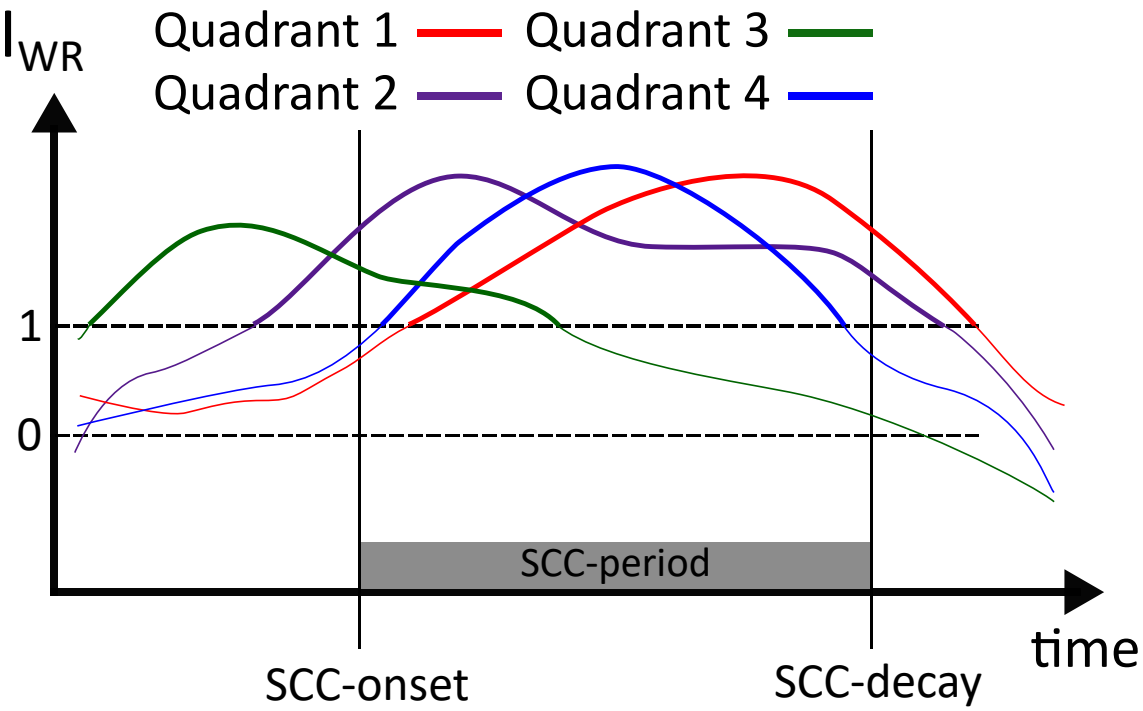

Figure 4.11: Sketch of fictional life cycles in a weather regime index plot, generic for each quadrant in Figures 4.12 to 4.14.

period. It is, however also possible that this behaviour is due to randomness, since the sample size is small.

Similar to the dominant transition analysis, SCC at 55°N shows a clearer signal in the SCC-weather regime life cycle link than SCC at 45°N (cf. Fig. 4.13). A lot of Atlantic trough life cycles are clustered at around two to four days after the SCC onset which all decay within about ±4 days around the SCC decay. It is also notable that overall there are in general a lot of cyclonic regime life cycles, besides the Atlantic trough, compared to the blocking ones. These are, however, more spread out compared to the Atlantic trough regime life cycles. Atlantic ridge, Scandinavian blocking and European blocking life cycles are mainly gathered within the third quadrant far from the center and therefore are likely to be in their decaying stage when SCC occurs.

Lastly, in case of SCC at 65°N, there are many life Zonal regime and Scandinavian trough life cycles as well as some Atlantic trough life cycles close to center. Especially, the Zonal regime life cycles tend to decay up to four days prior to the end of the SCC period. Noticeable is also that there are many Scandinavian trough life cycles that have their onsets up to four days after the beginning of a SCC period, but outlast the SCC period by up to 20 days. Blocking regime life cycles can mostly be found in the third quadrant, especially prominent are the European blocking and Atlantic ridge. They usually decay eight to 20 days prior to the SCC decay and begin 16 to four days prior to the SCC onset. Similar to SCC at 55°N, this means that these life cycles are in their decay stage when SCC occurs.

All in all, not only dominant weather regime transitions, but also the weather regime life cycles themselves are closely connected to the SCC period. The favoured weather regime types for each latitude are those which begin and decay roughly around the same time ±4 days as the SCC period. While in case of SCC at 45°N a similar amount of Greenland blocking life cycles can

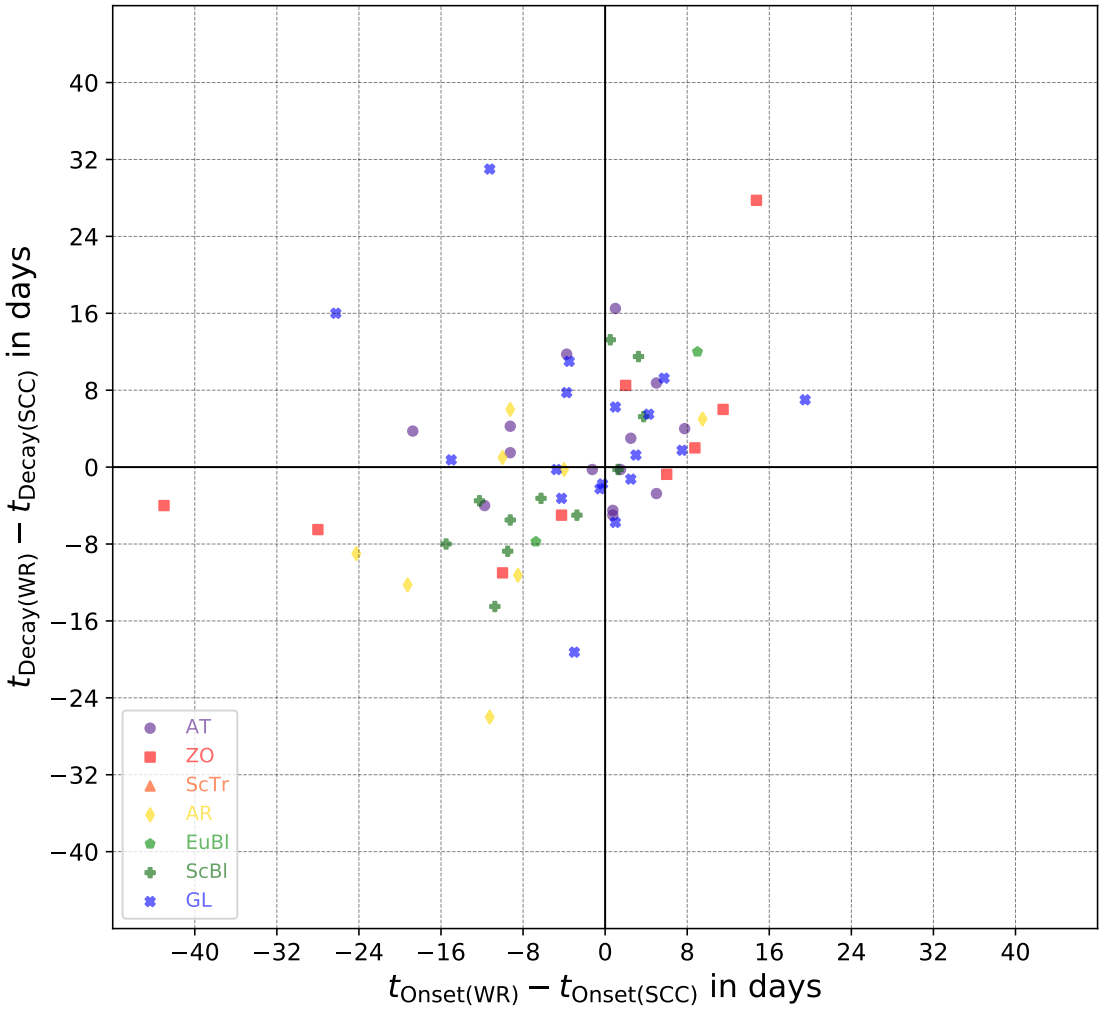

Figure 4.12: Scatter plot showing the relative position in time of SCC periods at 45°N to weather regime life cycles. $t_{\mathrm{Onset(SCC)}}$ and $t_{\mathrm{Decay(SCC)}}$ are the onset/decay dates of the SCC period and $t_{\mathrm{Onset(WR)}}$ and $t_{\mathrm{Decay(WR)}}$ are the onset/decay dates of the WR-LC. The x-coordinate denotes the time difference between weather regime life cycle onsets and SCC onsets and the y-coordinate the time difference between the life cycle decay and SCC decay. Different coloured and shaped symbols represent individual weather regime life cycles sharing at least one time step with a SCC period.

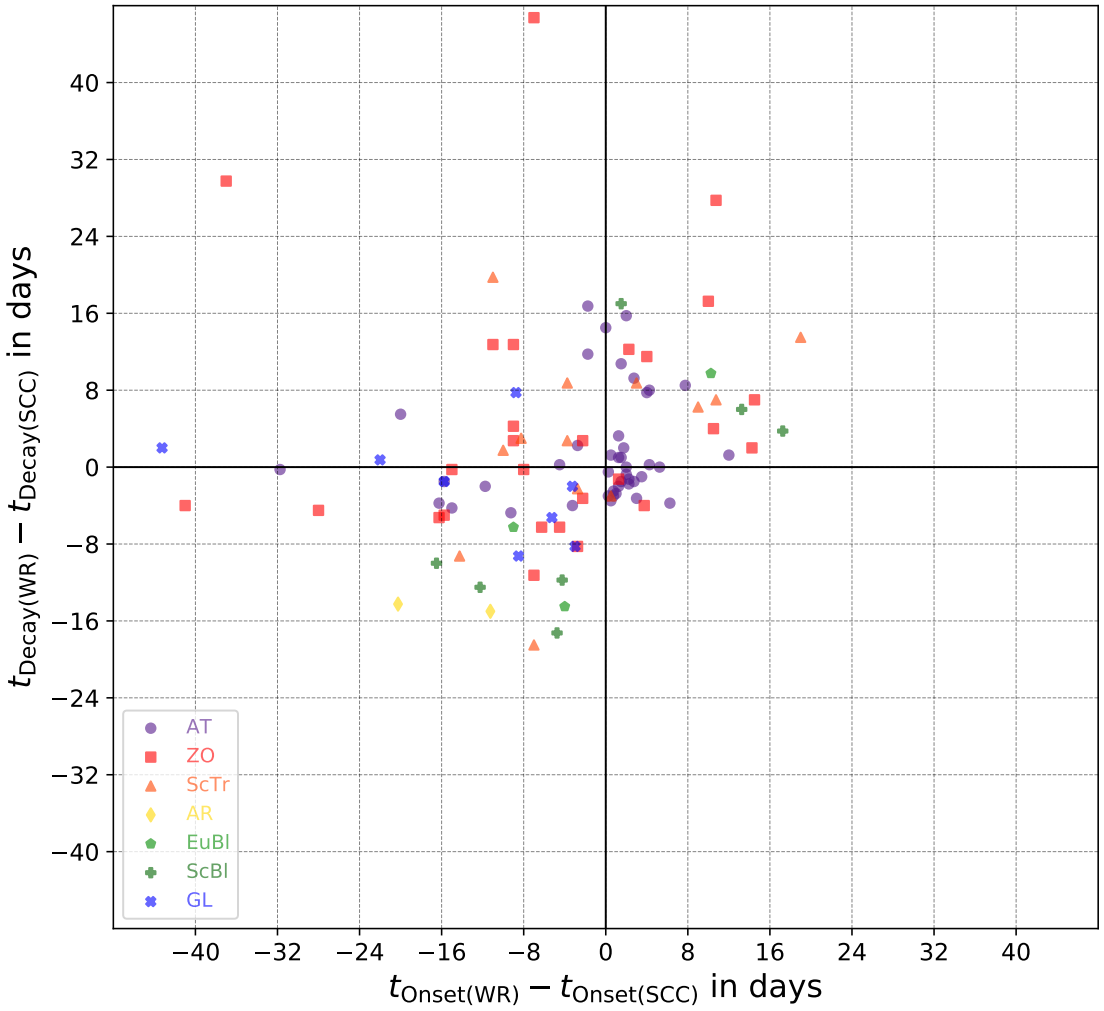

Figure 4.13: Scatter plot showing the relative position in time of SCC periods at 55°N to weather regime life cycles. $t_{\mathrm{Onset(SCC)}}$ and $t_{\mathrm{Decay(SCC)}}$ are the onset/decay dates of the SCC period and $t_{\mathrm{Onset(WR)}}$ and $t_{\mathrm{Decay(WR)}}$ are the onset/decay dates of the WR-LC. The x-coordinate denotes the time difference between weather regime life cycle onsets and SCC onsets and the y-coordinate the time difference between the life cycle decay and SCC decay. Different coloured and shaped symbols represent individual weather regime life cycles sharing at least one time step with a SCC period.

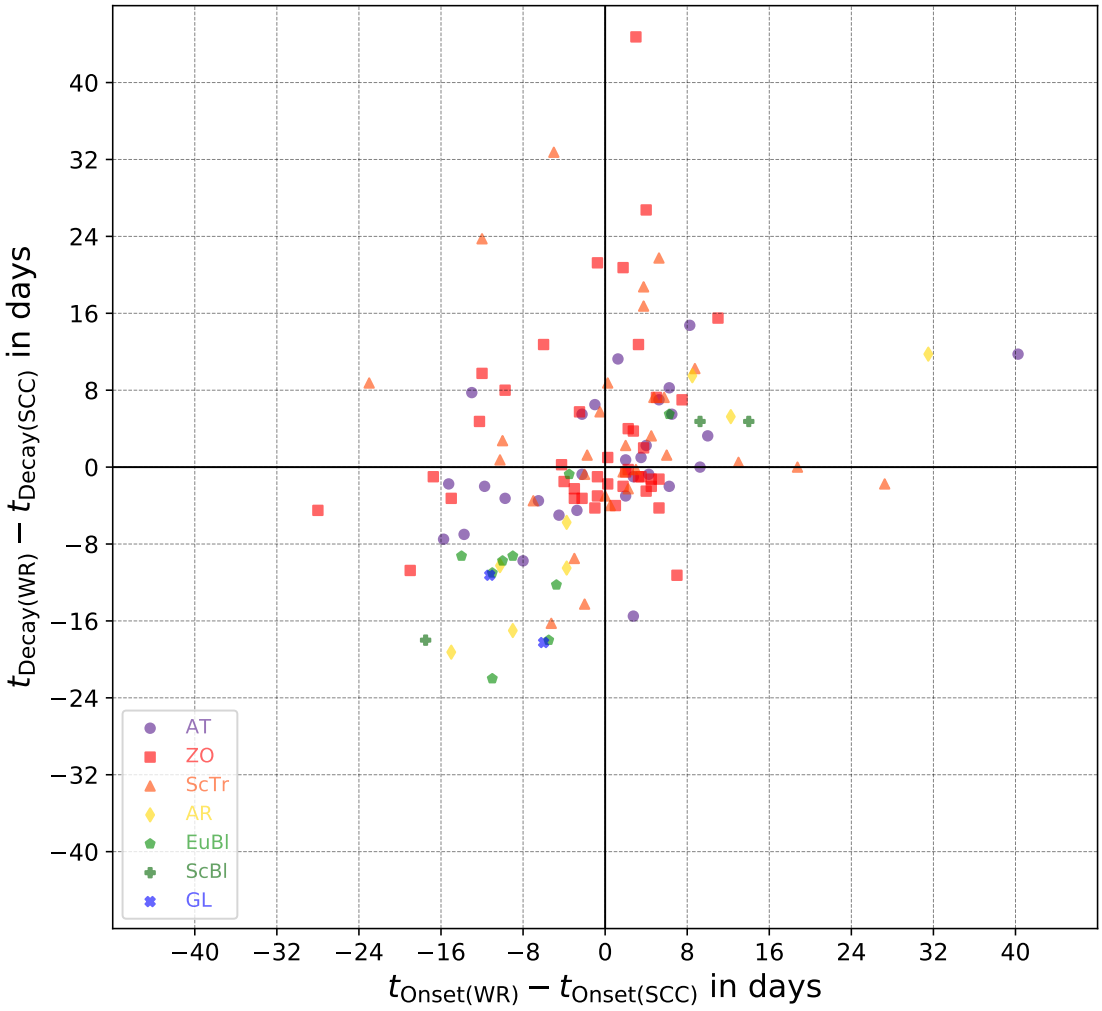

Figure 4.14: Scatter plot showing the relative position in time of SCC periods at 65°N to weather regime life cycles. $t_{\mathrm{Onset(SCC)}}$ and $t_{\mathrm{Decay(SCC)}}$ are the onset/decay dates of the SCC period and $t_{\mathrm{Onset(WR)}}$ and $t_{\mathrm{Decay(WR)}}$ are the onset/decay dates of the WR-LC. The x-coordinate denotes the time difference between weather regime life cycle onsets and SCC onsets and the y-coordinate the time difference between the life cycle decay and SCC decay. Different coloured and shaped symbols represent individual weather regime life cycles sharing at least one time step with a SCC period.

be found in each of the four quadrants, Atlantic trough life cycles for SCC at 55°N and Zonal regime life cycles for SCC at 65°N show a different behaviour. A lot of Atlantic trough life cycles begin shortly after the SCC onset and have to become dominant quickly due to the large amount of dominant transitions towards the Atlantic trough (cf. Fig. 4.9). For SCC at 65°N, the Zonal regimes tend ends prior to the SCC period while the Scandinavian trough tend outlast the SCC period. Atlantic ridge, European blocking and Scandinavian blocking life cycles that reach into a SCC period at 55°N or 65°N are usually in their decaying stage since they begin earlier but also decay about eight to 16 days before the SCC decay which is about the length of most SCC periods (cf. Fig. A.5 in the appendix).

4.2 Link to the stratosphere

The stratospheric polar vortex (SPV) is on average the strongest during winter, however its variability is also largest during this time. Anomalous states, such as an exceptionally strong or an exceptionally weak SPV, can influence the jet position, surface weather or occurrence frequency of different weather regimes due to stratosphere-troposphere coupling (Beerli and Grams, 2019; Domeisen et al., 2020). This leads to the question if and how stratospheric extremes affect serial cyclone clustering and if connections to weather regimes exist. Taking this question into account, the following sections provide a more detailed analysis of a possible link between serial cyclone clustering and the strength of the stratospheric polar vortex.

4.2.1 Strength of the stratospheric polar vortex and its influence on serial cyclone clustering

To analyse how the strength of the stratospheric polar vortex might influence the occurrence of serial cyclone clustering, a 56 day time-lead-lag analysis of the SPV strength is done for SCC onsets. As a proxy for the strength of the stratospheric polar vortex, the zonally averaged zonal wind at 10 hPa and 60°N is used. Since the SPV is significantly weaker in Autumn and Spring and the lead-lag period comprises two months, which might reach into the middle of Spring/Autumn, zonal wind anomalies $u10_{\text{ano}}$ are calculated to remove possible distortions. The results for the lead-lag analysis is shown in Figures 4.15 and 4.16. The figures show violins which are depictions of the frequency distributions of $u10_{\text{ano}}$ estimated with a kernel density estimation. Blue violins represent the distributions based on the $u10_{\text{ano}}$ values at SCC onsets and their respective leads/lags. Orange violins, however, represent climatological values based on bootstrapping with 1000 iterations. The thick dashed line within the violin depicts the median, while the thin dashed lines represent the 75th and 25th percentile.

For leads -56 to -28, the climatological values and the ones based on the SCC onset are quite similar for each latitude (cf. Fig. 4.15). They all share approximately a normal distribution with a median of $0\,\mathrm{m\,s^{-1}}$. Slight differences like the small local maxima at e.g. -35 or -28 days at 65°N are most likely due to the small sample size and the increased influence of outliers. However 0 to 14 days prior to the SCC onsets at 45°N, a strong systematic bi-modality is noticeable. At -14 days, the one maximum at about $0\,\mathrm{m\,s^{-1}}$ which was prominent for the bigger leads splits into two maxima, a smaller one at about $-30\,\mathrm{m\,s^{-1}}$ to $-20\,\mathrm{m\,s^{-1}}$ and a larger one at $10\,\mathrm{m\,s^{-1}}$ to $20\,\mathrm{m\,s^{-1}}$. However, the median and 25th percentile are still similar to the random climatology, since the

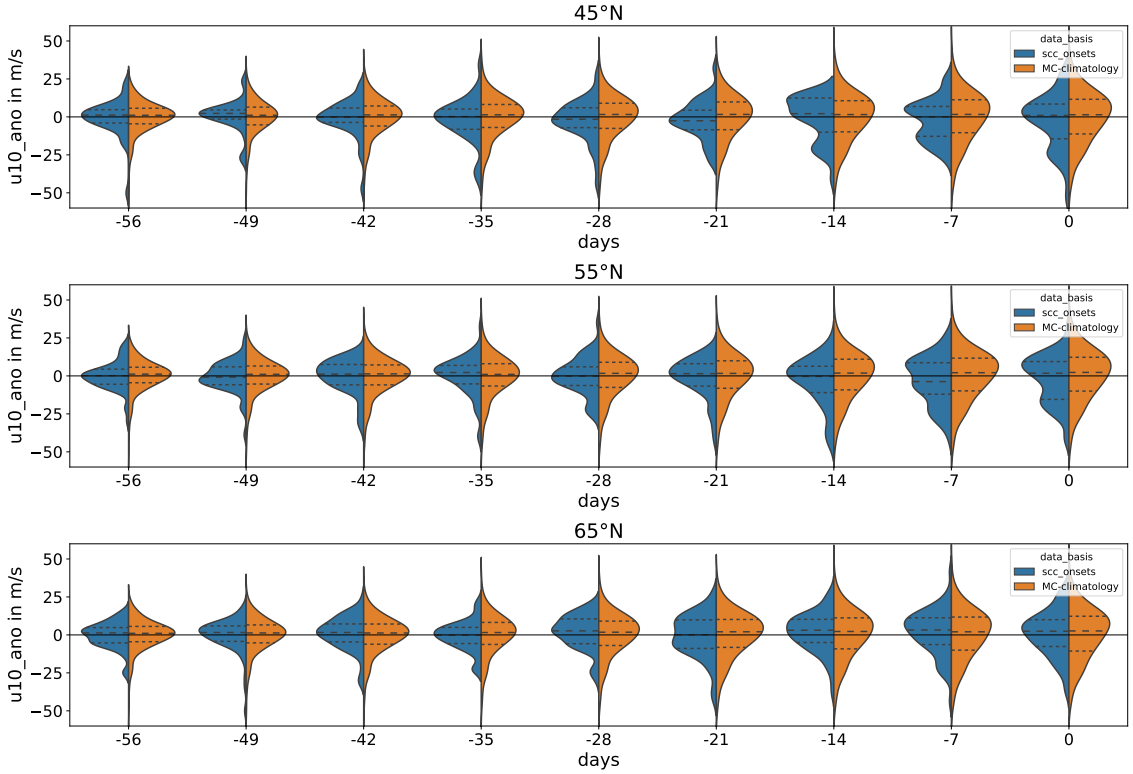

Figure 4.15: Lead-lag analysis of zonally averaged zonal wind anomalies at 10 hPa and 60°N at SCC onsets for -56 to 0 days. Violins for each lead-lag timestep show the frequency distributions of zonal wind anomalies approximated via kernel density estimation, based on the SCC-periods (blue violins) and a random winter climatology calculated via the bootstrap method with 1000 iterations (orange violins).

maximum is at about $5\,\mathrm{m\,s^{-1}}$, so in between the two maxima in case of SCC at 45°N. At lag -7 the bi-modality is more striking, since both maxima are similar in size, yet the gap between them also closed. The lower local maximum is at about $-20\,\mathrm{m\,s^{-1}}$ to $-15\,\mathrm{m\,s^{-1}}$ and the upper one at about $5\,\mathrm{m\,s^{-1}}$ to $10\,\mathrm{m\,s^{-1}}$. Finally, at lag 0, the bi-modal behaviour is still present but also fading, since the local minimum is rather weak. The larger maximum is already similar to the climatological one at about $0\,\mathrm{m\,s^{-1}}$ to $5\,\mathrm{m\,s^{-1}}$.

In case of SCC at 55°N there is only a slight bi-modality at the SCC onset. Up to seven days prior to the SCC onset, the $u10_{\mathrm{ano}}$ distribution matches well with the climatology, however at -7 days the distribution lost some of its smoothness.

Lastly, SCC at 65°N does not seem to affect or be affected by the strength of the stratospheric polar vortex prior to the SCC onset, since the general distribution roughly resembles the climatology.

While Figure 4.15 shows the strength of the SPV before the SCC onsets, Figure 4.16 depicts how the SPV develops after the SCC onsets. The most prominent feature in the period before is the bi-modality in case of SCC at 45°N. The subsiding tendency shown in lag 0 compared to -7 and -14 is further continuing in the later lags. Until 14 days after the SCC onset, the bi-modality seen before vanished completely, yet the distribution shifted slightly to higher $u10_{\mathrm{ano}}$ values compared to the climatology. While the median and 25th and 75th percentile are still similar up to 14 days after the SCC onset. For a prolonged period, from lag 21 to 42, the 25th percentile is about $-5\,\mathrm{m\,s^{-1}}$ to $0\,\mathrm{m\,s^{-1}}$, which is higher than the respective climatology at about $-15\,\mathrm{m\,s^{-1}}$.

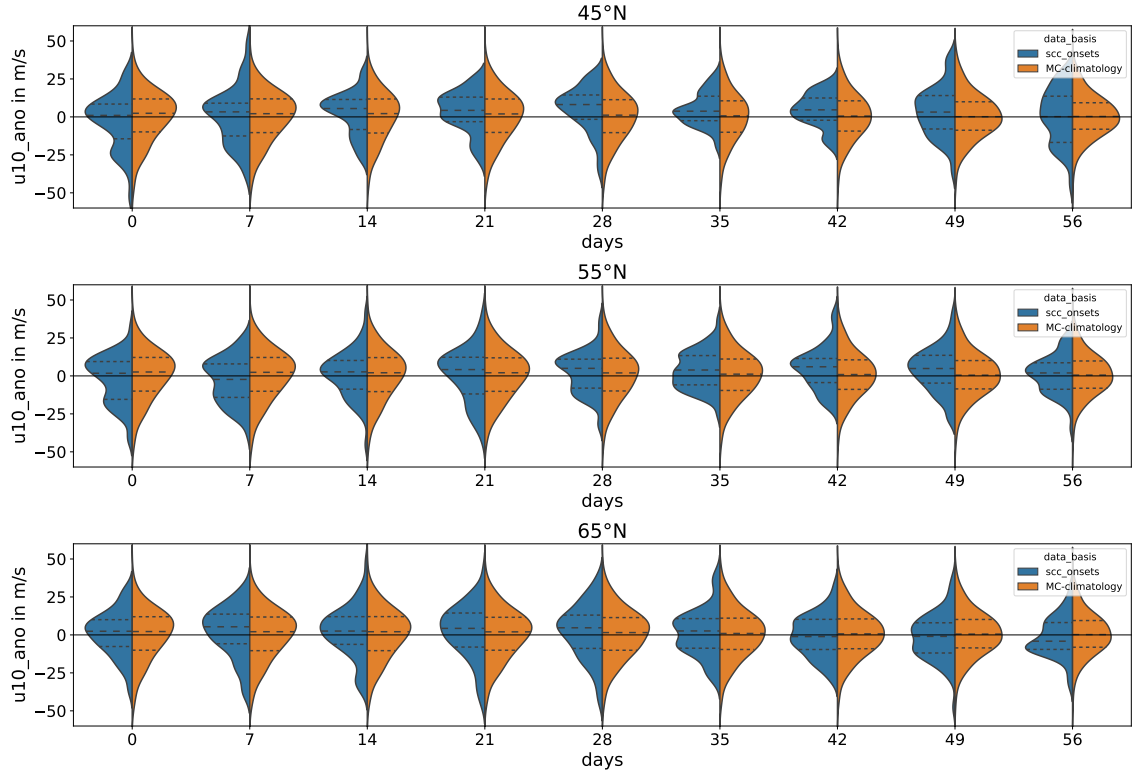

Figure 4.16: Lead-lag analysis of zonally averaged zonal wind anomalies at 10 hPa and 60°N at SCC onsets for 0 to +56 days. Violins for each lead-lag timestep show the frequency distributions of zonal wind anomalies approximated via kernel density estimation, based on the SCC-periods (blue violins) and a random winter climatology calculated via the bootstrap method with 1000 iterations (orange violins).

For SCC at 55°N the $u10$ anomalies are generally in a good agreement with their respective climatology. The slight bi-modality at lag 0 is quickly subsiding and already indistinct at lag seven. Also noticeable is that at lag 42 and 49 the distribution is slightly shifted towards positive values. The median and 25th percentile is about 5 $\mathrm{m\,s^{-1}}$ above their climatological counter parts.

In case of SCC at 65°N, the results are in very good agreement with the respective climatological values nearly throughout the whole 56 day period. Only at lag 56 there is a slight shift of the median to about $-5\,\mathrm{m\,s^{-1}}$.

All in all, the strongest link between SCC and the strength of the stratospheric polar vortex can be seen in case of SCC at 45°N. There is a distinct bi-modality in the period between -14 to zero days prior to the SCC onset. Some SCC periods at 45°N follow a period of weaker states of the SPV while some follow climatological conditions. Therefore knowledge of the SPV strength could possibly improve the predictability of SCC in the 14 days afterwards. In the days after the SCC onsets, the strongest response is also noticeable in case of SCC at 45°N. For a prolonged time period from lag 21 on, the SPV is in a slightly stronger state, which might be the recovery of the SPV after the SCC period ends.

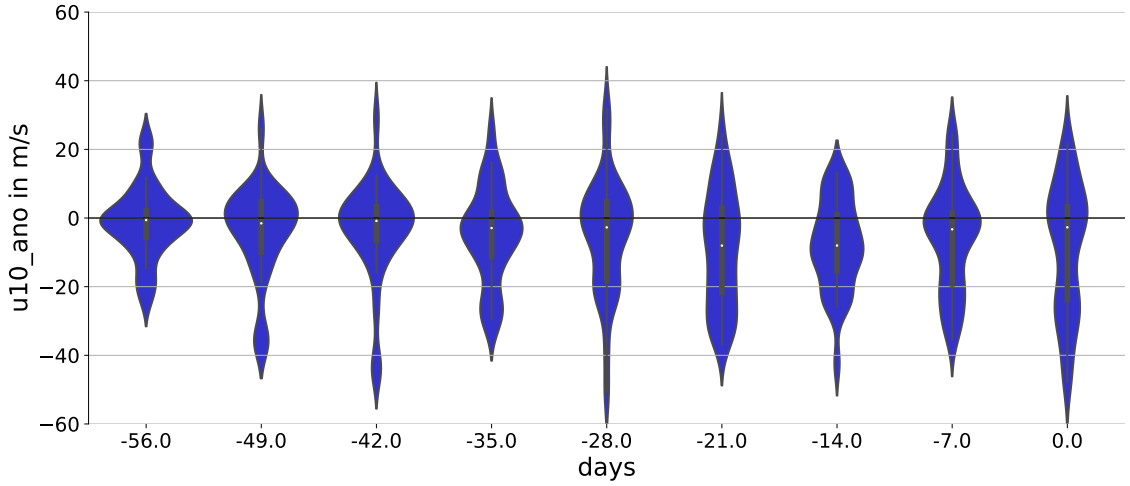

Figure 4.17: Lead-lag analysis of zonal mean zonal wind anomalies at 10 hPa and 60°N for Greenland blocking onsets in winter from 1979 to 2015 for -56 to 0 days.

4.2.2 Strength of the stratospheric polar vortex and its connection to the weather regimes

As the previous results have shown, the occurrence of SCC at 45°N is partly connected to weaker states of the stratospheric polar vortex around the SCC onset. However, also the occurrence of certain weather regimes is influenced by sudden stratospheric warmings (Domeisen et al., 2020). Therefore, before analysing the connection between SSW, SCC and weather regimes, the strength of the stratospheric polar vortex during the three most important weather regimes for SCC at each latitude are examined, encompassing Greenland blocking for 45°N, Atlantic trough for 55°N and Zonal regime for 65°N. Since Greenland blocking and Zonal regime show the strongest signal, the order is changed in the following analysis to GB, ZO and AT.

Since the previous results are all in respect to the onset date of the SCC, we also use only life cycle onsets for the lead-lag analysis between the strength of the SPV and the weather regimes for better comparability. To remove distortions due to the strong seasonality of the stratospheric polar vortex, zonal wind anomalies are observed. Figures 4.17 to 4.21 show the results of the lead-lag analysis of the three different regime types for a -56 to 56 day period around the life cycle onsets. In the -56 to 0 days period of all three weather regime life cycles (Fig. 4.17 to 4.19) the variability increases the closer to the regime onsets. While the violins at lag -56 are still rather short but curvy, at e.g. lag -28 they are more shallow and longer. The same behaviour can be seen for all other weather regime types (not shown), therefore we can preclude regime specific characteristics. Since the lag period is up to two months, zonal wind values are from October and November if the regime life cycle onsets are in December or January. In October or November, however, the variability in the strength of the stratospheric polar vortex is comparatively small to the winter months (Shi et al., 2020), which is reflected in the short and curvy violins throughout the -56 to 0 days lead-lag analysis of all regime types.

The lead-lag analysis of the Greenland blocking onsets from the -56 to 0 days period (Fig. 4.17) shows a declining tendency of $u10_{\text{ano}}$ from lag -35 to lag -14. Before, the median of zonal wind anomalies is still around $0\,\mathrm{m\,s^{-1}}$, however at lag -35 the median gets slightly negative with about $-3\,\mathrm{m\,s^{-1}}$. This increasing negative anomaly of the median peaks at lag -14 with about $-10\,\mathrm{m\,s^{-1}}$.

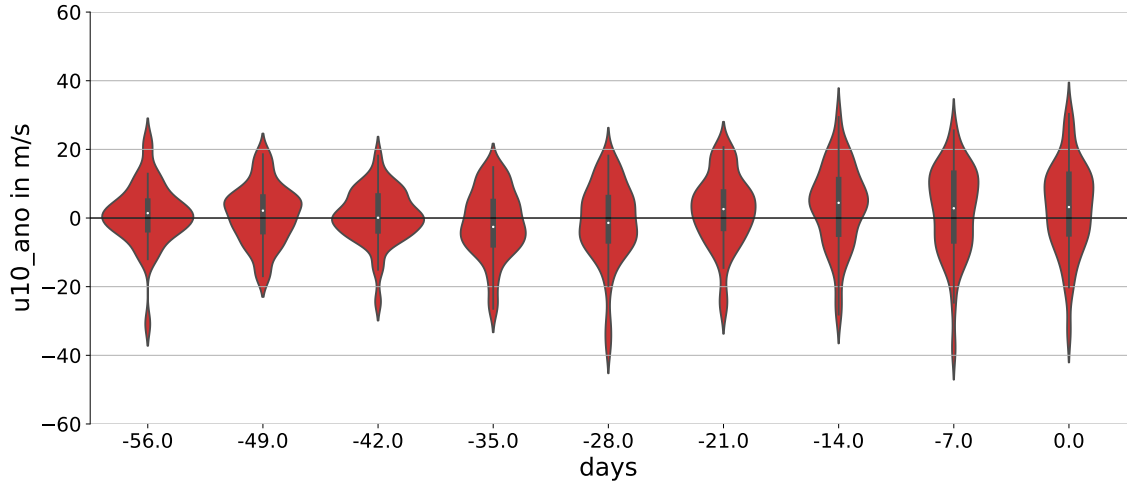

Figure 4.18: Lead-lag analysis of zonal mean zonal wind anomalies at 10 hPa and 60°N for Zonal regime onsets in winter from 1979 to 2015 for -56 to 0 days.

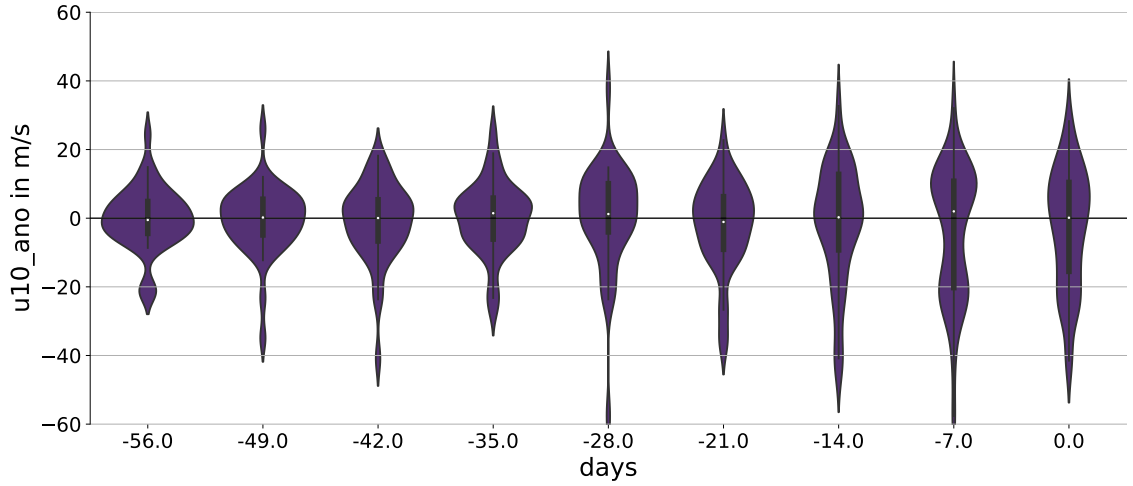

Figure 4.19: Lead-lag analysis of zonal mean zonal wind anomalies at 10 hPa and 60°N for Atlantic trough onsets in winter from 1979 to 2015 for -56 to 0 days.

Afterwards, the median increases again and therefore the SPV recovers in at least 50% of the cases. However, at the Greenland blocking onsets, the violin shows a shallow bi-modality with maxima at around $u10_{\text{ano}} = 0\,\text{m}\,\text{s}^{-1}$ and $-25\,\text{m}\,\text{s}^{-1}$.

In case of Zonal regime onsets for the period -56 to 0 days (Fig. 4.18), on average, there is also a slight weakening of the SPV of about $-3\,\text{m}\,\text{s}^{-1}$ at lag -35 and -28. However this changes to a general strengthening of the SPV for the period from -21 days to the onsets themselves, with a maximum increase of about $5\,\text{m}\,\text{s}^{-1}$ at lag -14. Compared to the lead-lag analysis of the Greenland blocking, the variability of the SPV is smaller, the violins, especially the ones close to the regime life cycle onsets, are shorter and curvier, so in better agreement with each other.

Lastly, in Figure 4.19, the results for the Atlantic trough analysis are shown. The medians of the zonal wind anomalies stay close to $0\,\text{m}\,\text{s}^{-1}$ for most of the 60 day period. However, the variability increases greatly, similar to the results for the Greenland blocking analysis, but contrary to the Zonal regime analysis. Besides the strong increase in variability from lag -21 to the regime onsets, the only other striking result is the bi-modality at lag -7 with maxima at $-20\,\text{m}\,\text{s}^{-1}$ and $10\,\text{m}\,\text{s}^{-1}$.

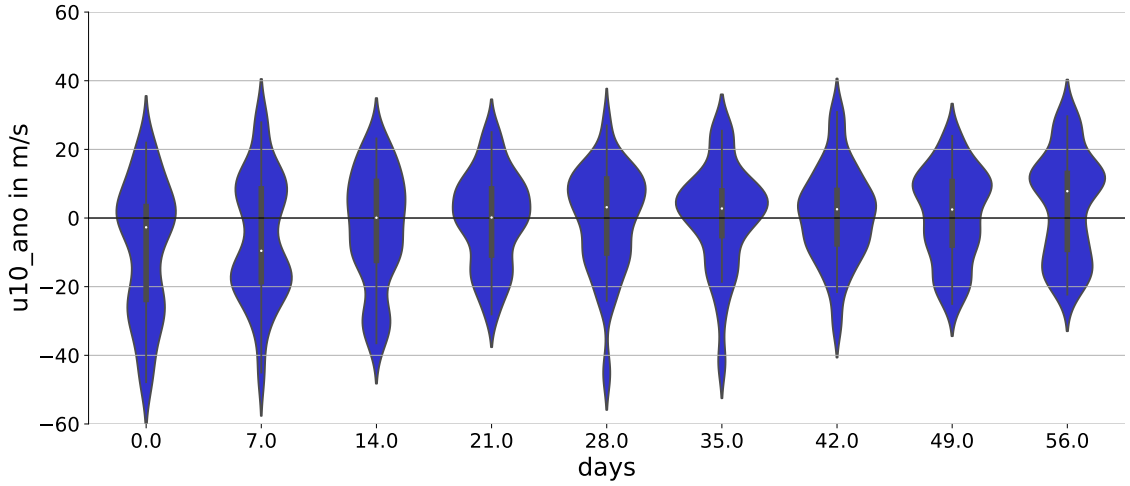

Figure 4.20: Lead-lag analysis of zonal mean zonal wind anomalies at 10 hPa and 60°N for Greenland blocking onsets in winter from 1979 to 2015 for 0 to +56 days.

However, at the regime onset, the bi-modality has already declined for the most part and the result is a very shallow unimodal distribution.

Before the detailed discussion of the period from 0 to 56 days, it is important to note that the violin size is automatically adjusted depending on the properties of the remaining distributions within each figure. This means that if there are large differences in variability (cf. lag -56 and lag 0 in Fig. 4.17 to 4.19), the size gets adjusted so that the violin with larger variability is thinner. However, if the violins have similar variability, each violin has a similar comparably large size for better visibility of differences in shape. This is the case for Figures 4.20 to 4.22 and the reason for the visible size difference at regime onsets (e.g. cf. lag 0 of Fig. 4.17 and 4.20) even though the data basis is the same. Therefore, the general SPV variability at regime onsets in the winter months are similar to those in March/April and much larger than in October/November.

For Greenland blocking onsets (Fig. 4.20), there is a large drop in SPV strength at lag 7. The median is at about $u10_{\text{ano}} = -10\,\text{m}\,\text{s}^{-1}$. The bi-modality, seen at the regime onset, also becomes more apparent. The maxima are slightly higher with about $-20\,\text{m}\,\text{s}^{-1}$ and $10\,\text{m}\,\text{s}^{-1}$. At lag 14 the median is around $0\,\text{m}\,\text{s}^{-1}$, therefore the SPV recovered on average to climatological strength. Also, the bi-modality mostly vanished. From lag 28 to 48, the median is slightly positive with about $3\,\text{m}\,\text{s}^{-1}$. However, at lag 56 there is a sudden increase up to about $10\,\text{m}\,\text{s}^{-1}$.

In contrast to the weakening of the stratospheric polar vortex from -21 to 7 days around Greenland blocking onsets, Zonal regime onsets seem to be connected with a strengthened SPV (cf. Fig. 4.21). The positive tendency from lag -21 extends further until about lag 42. Before and at the Zonal regime onsets, the positive anomaly of the median is still rather small with $3\,\text{m}\,\text{s}^{-1}$ to $5\,\text{m}\,\text{s}^{-1}$. However, 14 to 28 days after the regime onset, the median is about $10\,\text{m}\,\text{s}^{-1}$ above climatological conditions. At lag 49, the period of generally enhanced SPV strength ends with the median returning to about $0\,\text{m}\,\text{s}^{-1}$, lastly 56 days after the regime onset the SPV is slightly weakened with a median of about $-3\,\text{m}\,\text{s}^{-1}$.

Lastly, the analysis of the Atlantic trough onsets for the period from 0 to 60 days, that the median only slightly differentiates from climatological conditions throughout most of the period. Compared to the Greenland blocking or the Zonal regime, no periods of prolonged positive or negative

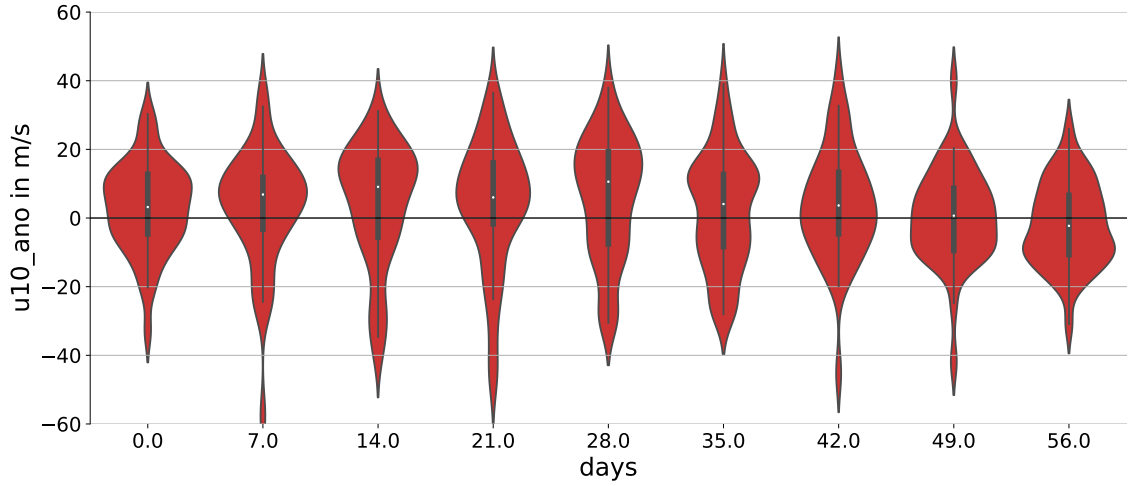

Figure 4.21: Lead-lag analysis of zonal mean zonal wind anomalies at 10 hPa and 60°N for Zonal regime onsets in winter from 1979 to 2015 for 0 to +56 days.

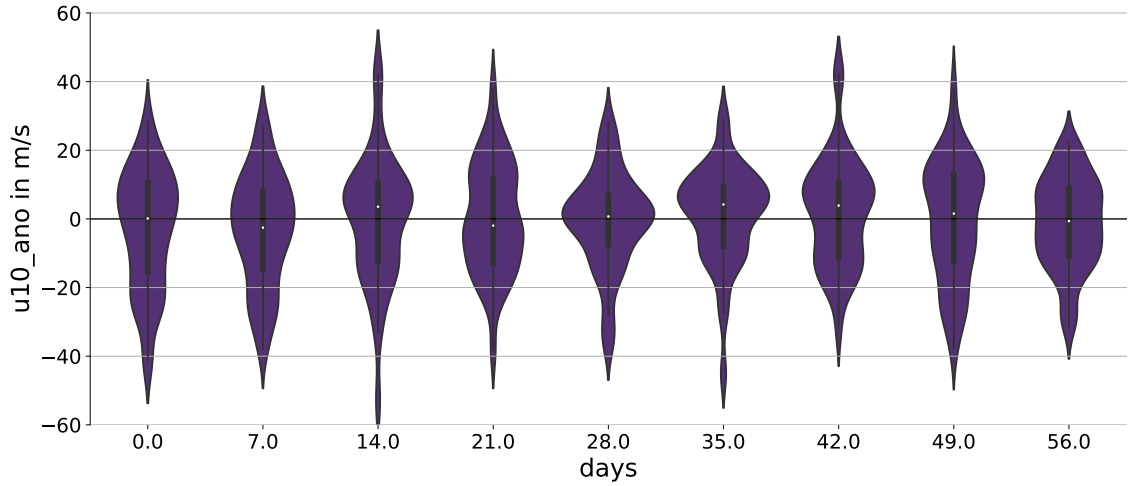

Figure 4.22: Lead-lag analysis of zonal mean zonal wind anomalies at 10 hPa and 60°N for Atlantic trough onsets in winter from 1979 to 2015 for 0 to +56 days.

median values can be identified, with the exception of the short period from lag 35 to 49 when the median shows consistently positive anomalies up to 5 $\mathrm{m\,s^{-1}}$. Noticeable, however, is that the median is alternating between slightly negative and slightly positive values at e.g. lag 7, 14 and 21.

In summary, the three weather regime types that are most import for SCC at 45°N/55°N/65°N respectively, show differences in their relationship with the strength of the stratospheric polar vortex. Greenland blocking regimes follow a period when the SPV is weakened with a time lag of about 7 to 21 days. Zonal regimes, however, show only a weak link with the SPV before their onsets, but tend to result in a prolonged period of a strong SPV 7 to 28 days afterwards. Lastly, Atlantic trough regime onsets are mostly indifferent to the strength of the stratospheric polar vortex. On average the SPV only slightly differentiates from climatological conditions. In general, Greenland blocking onsets seem to be connected with a weaker SPV, Zonal regime onsets with a stronger SPV and Atlantic trough onsets with normal SPV conditions (cf. Fig. A.6).

A comparison with the results of the SCC analysis (Fig. 4.15, 4.16), shows intersections especially between the lead-lag relationship of the Greenland blocking and the lead-lag relationship of SCC at 45°N. While 7 to 21 days prior to the Greenland blocking onset, the SPV is considerably weaker, SCC at 45°N shows a bi-modal connection. This hints at a possible connection between SCC at 45°N, Greenland blocking and weakened SPV. Comparing the results from SCC onsets at 65°N and Zonal regime onsets, the intersection is rather small, since at lags -14, 21 and 28, the SPV is also slightly strengthened but on a smaller scale. Lastly, comparing the wind anomalies for SCC onsets at 55°N and those for the Atlantic trough onset, shows both slight similarities and differences. In the period from -56 to -14 the median is in both cases close to $0\,\mathrm{m\,s^{-1}}$ and during the period from 35 to 49 both cases show on average slight positive anomalies. However, the clear bi-modality at lag 0 for SCC at 55°N is not well represented in the results for the Atlantic trough analysis.

4.2.3 Connection between SCC, weather regimes and weak/strong states of the stratospheric polar vortex

The previous results have shown that there are some connections between the occurrence of SCC at different latitudes and the strength of the stratospheric polar vortex. In addition, different weather regimes also show differences in the SPV strength which partly overlap with the results of the SCC analysis. Especially prominent in the SCC analysis is the period from -14 to 7 days which shows a bi-modal distribution in case of SCC at 45°N, where many SCC cases are connected to normal or slightly stronger SPV conditions, while there are also cases which are linked to weaker SPV conditions. Interestingly, Greenland blocking, which is found to be dominant the most after the SCC onset at 45°N, shows a weakened SPV prior to its onset too. Therefore the question arises if the cases are linked with each other.

To answer this questions, we once again conduct a lagged frequency analysis of the dominant weather regime type at SCC onsets, similar to those in section 4.1.3. To also incorporate the dependency on the SPV strength, the SCC onsets are clustered into cases with similar SPV strength. Since the bi-modality in the SPV strength can be seen in the period from -14 to 7 days, the clustering algorithm uses a -20 to 10 day period around the SCC onsets to categorize the different SCC onsets based on similar $u10$ values.

The results of the analysis for SCC at 45°N can be seen in Figure 4.23. Part (a) shows the wind speed for the period from -60 to 60 days around each SCC onset. Blue coloured lines are members of cluster 1, which includes SCC onsets with a normal or strengthened SPV in the period -20 to 10 days around the SCC onset. Contrary, red colours denote the attribution to cluster 2 and therefore consists of SCC onsets with a comparably weaker SPV. The thick solid lines represent the cluster means and the thick dashed lines the cluster medians. As by definition of the clustering method, the distance between the cluster 1 and cluster 2 mean is largest for the period from -20 to 10 days. However, before and after this period, the lines intertwine with each other. Noticeable is also, that the cluster 2 mean is decreasing until lag 0, with a minimum of about $5\,\mathrm{m\,s^{-1}}$. Part (b) shows the lagged frequency anomalies of the dominant weather regime types at SCC onset depending on the cluster. The calculations follow the same method as the lagged frequency analysis in chapter 4.1.3 (cf. Fig. 4.5 to 4.7), but only the last panel (anomalies) is shown. The results greatly differ

(a)

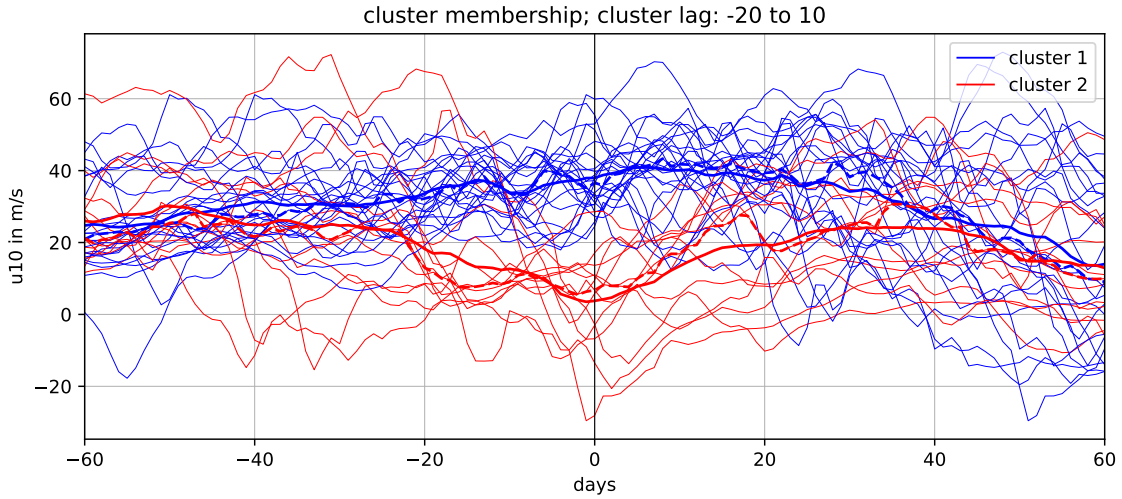

(b)

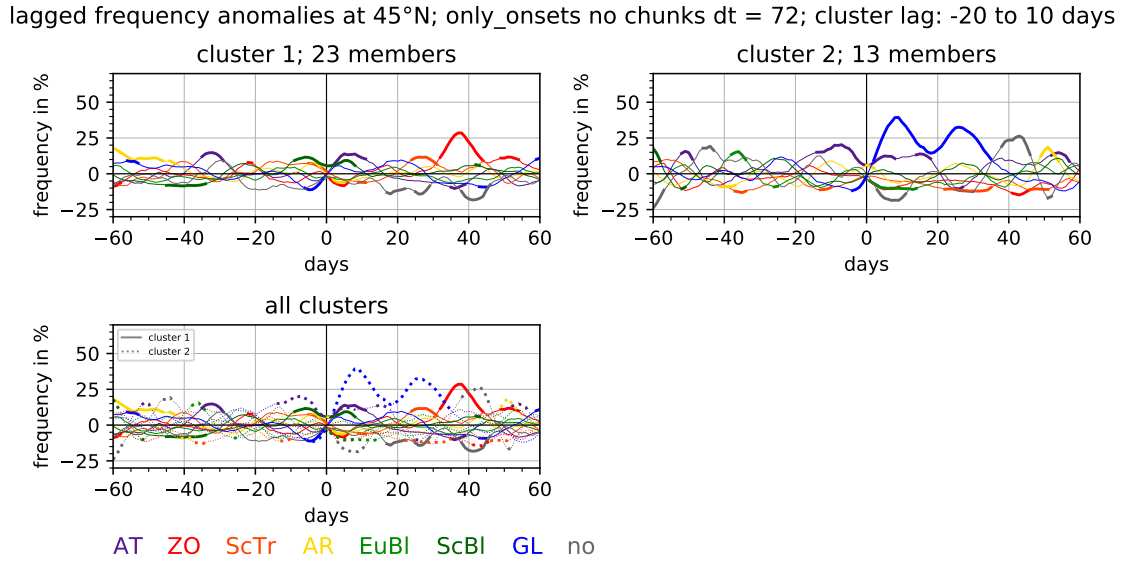

Figure 4.23: Clustered lagged frequency analysis of SCC at 45°N. Part (a) represents the SPV strength in terms of $u10$ values for the -60 to 60 day period around each SCC onset and which onsets are attributed to each cluster. Part (b) shows the lagged frequency anomalies of each cluster as well as its statistical significance (thick lines) based on bootstrapping with 1000 iterations. Cluster 1 consists of SCC onsets connected to a weak SPV in the period -20 to 10 days around the SCC onset, while cluster 2 encompasses those with normal or strong SPV conditions.

between cluster 1 (top left) and cluster 2 (top right). In case of cluster 1, embodying SCC onsets with normal/strong SPV conditions, Atlantic trough shows the largest significant anomaly in a 20 period after the SCC onsets with a maximum of about 15% at day 5. From 30 to 45 days there is also a significant increase in the Zonal regime with a maximum of about 30% 38 days after the SCC onsets. Greenland blocking, however, shows only a small increase without being statistically significant, even though it has been found to be the one, being dominant most frequently after SCC onsets at 45°N (cf. Fig. 4.5). In contrast, Greenland blocking frequency is significantly increased in the period from 0 to 35 days with two local maxima at about 10 and 27 and a local minima at 18 days. Anomalies reach up to 40% at the first local maxima, 15% at the local minima and 30% at the second local maxima. Even though overshadowed by the large increase in Greenland blocking in the period from the onset to 20 days afterwards, noticeable is also the slight significant increase in the Atlantic trough regime, which reaches about 10%. However, Atlantic trough is dominant even more frequently in the period from -15 days to the SCC onset with up to 20% at -10 days. In actuality, the frequency anomaly is declining towards a local minimum at the SCC onset. While the period of enhanced Greenland blocking activity is declining, there is a large increase in cases where no regime is being dominant. This increase becomes significant at about 37 days after the SCC onset and reaches a maximum of 25% at 42 before declining rapidly. Therefore, it is likely that this increase comes from decaying Greenland blocking regimes without transitioning into another regime type.

Comparing the results of both clusters, SCC at 45°N is connected to the SPV, so that it occurs often together with Greenland blocking in cases where the SPV is weakened. However, a weak SPV is by no means a mandatory condition. As denoted cluster 1 consist of 23 members while cluster 2 only amounts for 13 members. So there are still more cases of SCC at 45°N that do not have a connection to a weakened SPV, but those are also not connected to a longer lasting period of Greenland blocking but rather occur preferably in conjunction with a short Atlantic trough period. Interesting is also that even though the clustering is done for the period from -20 to 10 days, it still influences which transitions occur at around 30 to 35 days after the SCC onset. Cases with a weak SPV tend to have no transitions and end in a period where no regime is dominant, but if the SPV is slightly strengthened or in normal conditions, transitions towards the Zonal regime seem occur more frequently. This results still needs to be treated with caution since on average cluster 1 includes SCC cases with a slightly stronger SPV even 20 days after SCC onset.

For comparison, the same analysis is also carried out for SCC at 55°N and 65°N. For 55°N there is also a slight bi-modality visible from -7 to 7 days, yet not as strong as for SCC at 45°N (cf. Fig. 4.15, 4.16), while SCC at 65°N has not shown a similar behaviour in this time period.

As for SCC at 45°N, the clustering algorithm divides the SCC onsets at 55°N into two clusters, the first with on average stronger or normal SPV conditions and the second with a slightly weaker SPV. Immediately noticeable is that the mean of cluster 2 is generally larger than in case of SCC at 45°N (Fig. 4.23, 4.24). During the -20 to 10 day period it is at about $20\,\mathrm{m\,s^{-1}}$ while for SCC at 45°N, the cluster 2 mean is at about $5\,\mathrm{m\,s^{-1}}$ to $10\,\mathrm{m\,s^{-1}}$. Similarly the mean of cluster 1 in case of SCC at 55°N is also slightly above the one for SCC at 45°N.

The influence on the lagged frequency analysis is however small. In both cases Atlantic trough is significantly enhanced with maxima of about 42% at around 7 days after the onset, while most other regimes show negative anomalies. The major difference is visible in the period from 10 to 20

(a)

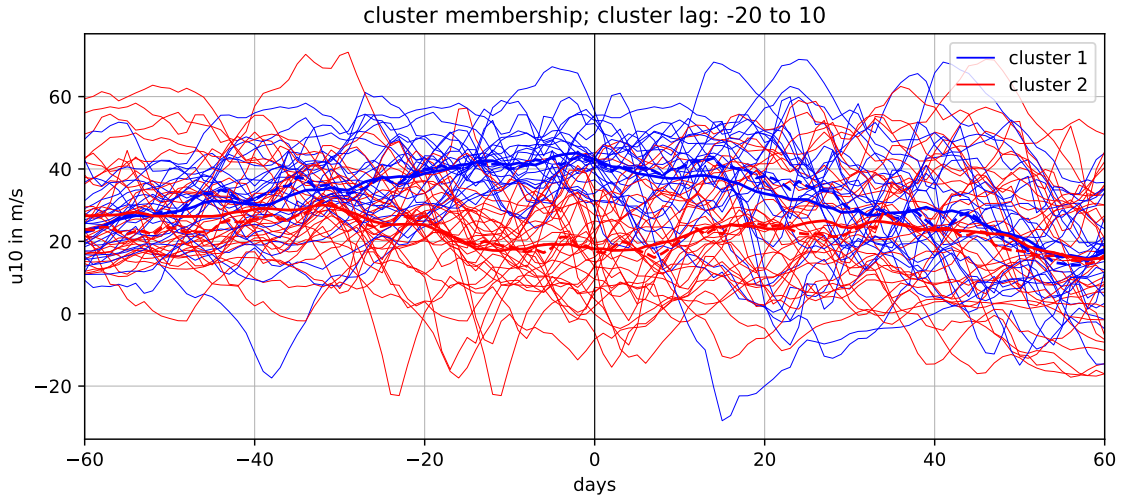

(b)

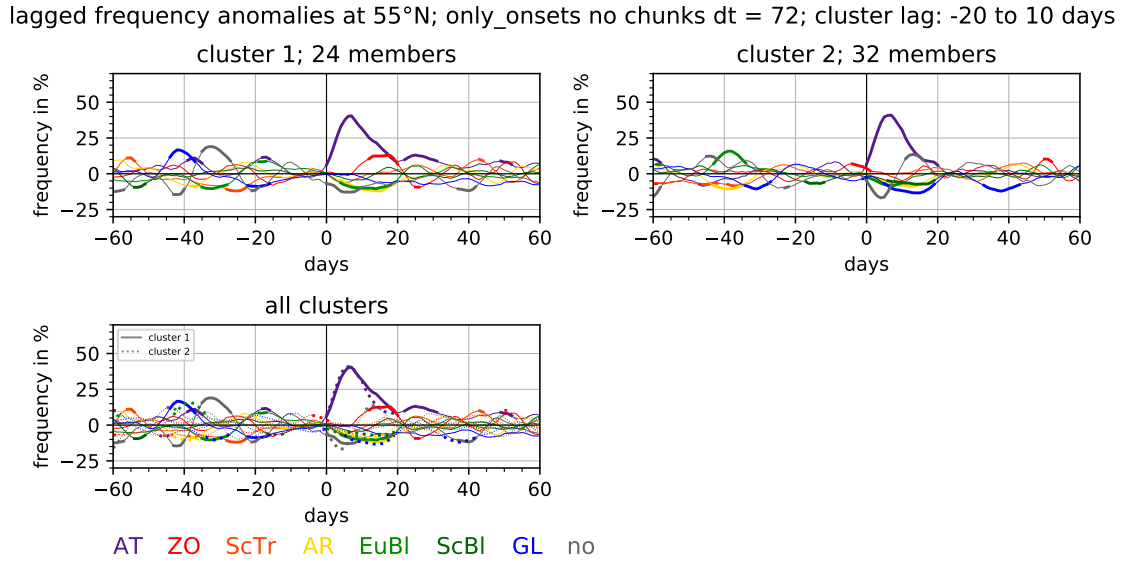

Figure 4.24: Clustered lagged frequency analysis of SCC at 55°N. Part (a) represents the SPV strength in terms of $u10$ values for the -60 to 60 day period around each SCC onset and which onsets are attributed to each cluster. Part (b) shows the lagged frequency anomalies of each cluster as well as its statistical significance (thick lines) based on bootstrapping with 1000 iterations. Cluster 1 consists of SCC onsets connected to a weak SPV in the period -20 to 10 days around the SCC onset, while cluster 2 encompasses those with normal or strong SPV conditions.

(a)

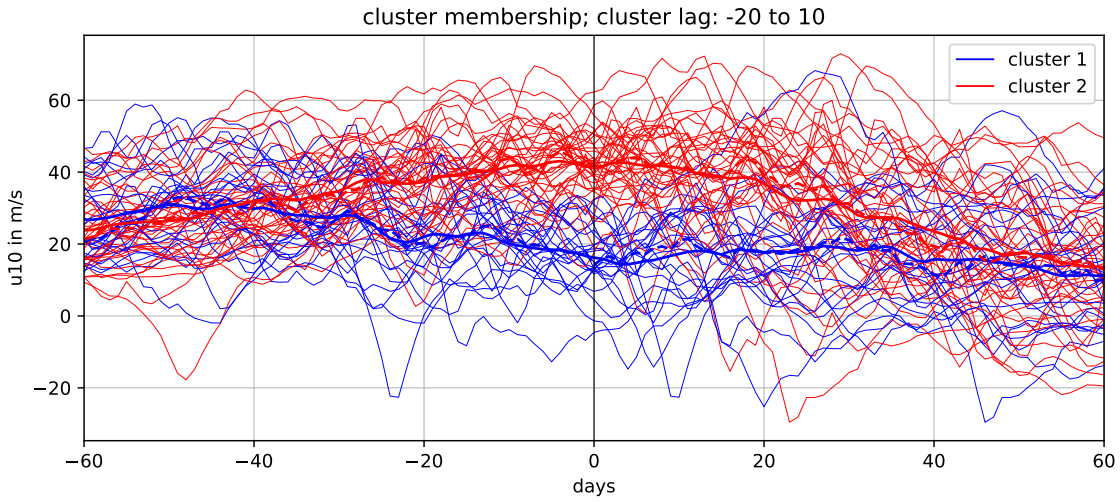

(b)

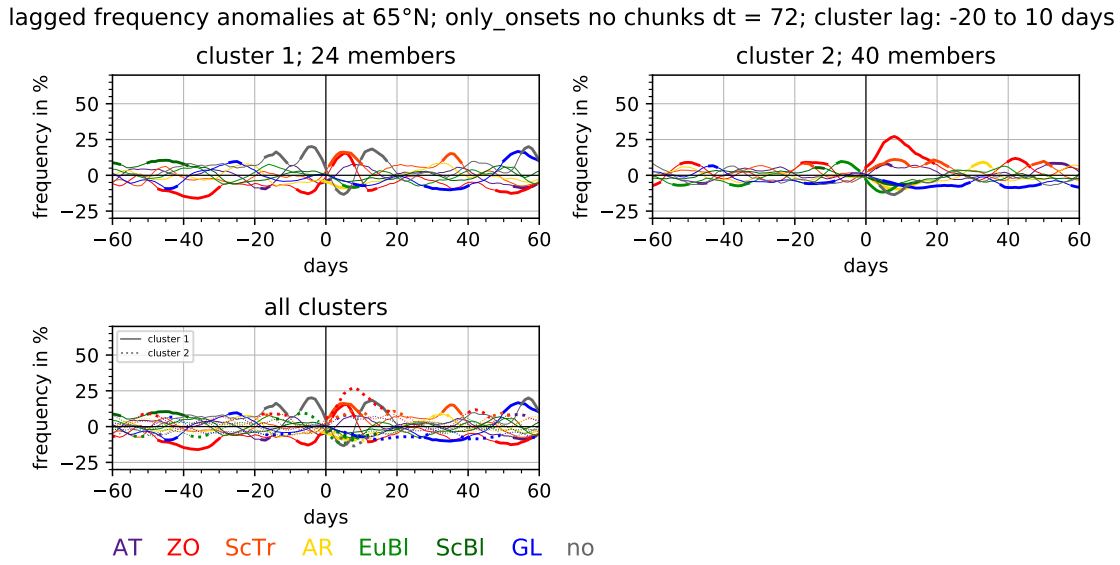

Figure 4.25: Clustered lagged frequency analysis of SCC at 65°N. Part (a) represents the SPV strength in terms of $u10$ values for the -60 to 60 day period around each SCC onset and which onsets are attributed to each cluster. Part (b) shows the lagged frequency anomalies of each cluster as well as its statistical significance (thick lines) based on bootstrapping with 1000 iterations. Cluster 2 consists of SCC onsets connected to a weak SPV in the period -20 to 10 days around the SCC onset, while cluster 1 encompasses those with normal or strong SPV conditions.

days when the frequency of Atlantic trough is declining and transitions into other regimes occur. For cluster 1, therefore cases with a stronger SPV, the Zonal regime is significantly enhanced in this period with anomalies up to 10%. Cases with a slightly weakened SPV, however show an increase of the no regime type. Similar to the behaviour for SCC at 45°N in the 35 to 45 days period, a stronger SPV favours transitions towards the Zonal regime, while a slightly weaker SPV is linked to decays without new regimes becoming dominant. Also noteworthy in case of cluster 1, is that even though frequency of Atlantic trough is declining, it still maintains a significant positive anomaly of about 10% until 30 days after the SCC onset.

Lastly, the results of the analysis for SCC at 65°N are shown in Figure 4.25. It is important to note that contrary to the analysis for SCC at 45°N and 55°N, cluster 1 encompasses SCC onsets with a weakened instead of a strengthened SPV state. Likewise cluster 2 covers all cases with a strong SPV. Similar to the analysis for SCC at 55°N both cluster means show higher values with about $20\,\mathrm{m\,s^{-1}}$ and $40\,\mathrm{m\,s^{-1}}$ respectively, as for SCC at 45°N. The larger number of members in cluster 2 suggests that during SCC at 65°N, the SPV is more often in a stronger than weaker state.
The lagged frequency analysis shows a different picture than in case of SCC at 45°N and 55°N, but at the same time a similar behaviour. For both cluster, Zonal regime and Scandinavian trough are the two regimes that show the largest positive frequency anomaly in the 20 days period after the SCC onset. However, in case of cluster 1 with a weakened SPV, the anomaly is rather small with up to 10% and only last for up to 10 days after the SCC onset. The period from 10 to 20 days shows a significant increase, also up to 10%, of no regime being dominant. In contrast, SCC at 65°N that is accompanied by a stronger SPV, represented by cluster 2, shows a much stronger increase in the Zonal regime. The period of significantly increased Zonal regime activity is extended to the whole 20 days after the SCC onset and the maximum at about 8 days after the onset, rises up to 25%. Therefore, similar to the previous results, with a strong SPV, the Zonal regime becomes dominant more often, while in case of a slightly weaker SPV, periods where no regime is dominant are more likely.
All in all, the analysis between SCC and the occurrence of different weather regimes with consideration for the state of the SPV, yield interesting results, yet logical results. SCC at 45°N occurring in conjunction with a weak SPV or SSW is very likely to be connected with a prolonged period of Greenland blocking. This is sensible considering that Greenland blocking is more frequent after sudden stratospheric warmings (Domeisen et al., 2020) and that the SPV is on average slightly weaker at Greenland blocking onsets (Fig. A.6). Furthermore, in cases of SCC at 45°N, the strength of the SPV seems to be also important for the time period 35 to 45 days after the SCC onset. A strong SPV shows an increased likelihood of the Zonal regime being dominant throughout this time period. This is also quite sensible because the SPV is on average slightly higher at Zonal regime onsets (Fig. A.6). In cases with a weak SPV, the Zonal regime is suppressed during this time period, thus leading to a period when no regime is dominant. The interchanging behaviour between an enhanced Zonal regime or no regime activity depending on whether the SPV is strong or weak can also be observed for SCC at 55°N and 65°N. For SCC at 55°N the influence by the SPV is rather small, since the Atlantic trough regime is by far most frequently dominant independent of the SPV strength. However, the transition type after the Atlantic trough regime decays seems to be influenced. A strong SPV leads to an increased amount of transitions towards the Zonal regimes, while cases with a weak SPV end up with no regime being dominant. Lastly, for SCC at 65°N, the Zonal regime and Scandinavian trough show the largest increase in frequency out of all regime types regardless of the SPV strength. Nevertheless, strong SPV conditions favour the Zonal regime and thereby lead to a more distinct and prolonged increase in the Zonal regime frequency, while a weakened SPV results in more shorter periods of enhanced Zonal regime activity which are superseded by a period when no regime being dominant is more likely.

5 Summary and outlook

Strong extra-tropical cyclones in the North-Atlantic European region during winter are a major cause for economic losses in Europe. However, over small time periods the largest cumulative losses occur when multiple cyclones cross the same area in quick succession - a so-called serial cyclone clustering. On time scales from a few days to several weeks, different patterns in the large-scale circulation, known as weather regimes, strongly influence the prevailing weather conditions and the cyclonic behaviour which leads to the question if they have also an impact on SCC.
Therefore, this study aims to find possible links between the occurrence of serial cyclone clustering and weather regimes, especially under the premise of SCC at three different locations, 45°N 5°W, 55°N 5°W and 65°N 5°W. A key objective was to find the manner that links SCC and weather regimes. Based on this idea, a few case studies are conducted which, combined with further results of the analysis, lead to a set of major questions (see 1) which we briefly answer in the following.

1. **Do specific weather regimes modulate the cyclone occurrence in the North-Atlantic European region in a similar matter as serial cyclone clustering?**

   Three of the seven regime types show similar regions of increased or decreased cyclonic behaviour as for SCC at the three different latitudes. Greenland blocking generally captures the cyclone occurrence during SCC at 45°N quite well, however it does not fully capture the enhanced cyclonic activity over the Mediterranean. The cyclone frequency during the Atlantic trough regime is very similar to SCC at 55°N . Lastly, Zonal regime is in good agreement with the result from SCC at 65°N.

2. **What are the predominant weather regimes during serial cyclone clustering and is there a lead-lag interaction between the occurrence?**

   In accordance to the modulation in cyclone occurrence, the same three weather regimes seem to be predominant during serial cyclone clustering at the three latitudes. Greenland blocking for 45°N, Atlantic trough for 55°N and Zonal regime for 65°N. SCC generally precedes the time when the weather regime becomes dominant by up to six days and lasts for a similar time as the associated weather regime life cycle. After the SCC onset, weather regime frequency is significantly modulated for a period of about 15 days to 20 days, however in case of Greenland blocking after SCC onsets at 45°N, the frequency is significantly modulated by up to 30 days.

3. **When does serial cyclone clustering occur in respect to the stage of a regime life cycle and do regime transitions play a vital role for the occurrence of serial cyclone clustering?**

SCC mainly occurs in the early stage of the weather regime life cycles or slightly before depending on the latitude for SCC. Dominant regime transitions are very important and mostly occur in the early stage of a SCC period between zero and four days after the SCC onset.

4. **In what manner does the stratospheric polar vortex influence serial cyclone clustering and what is the role of the weather regimes?**

   Weak stratospheric polar vortex events seem to especially affect the occurrence of SCC at 45°N with a time lead of -14 to -7 days before the SCC onset. In a similar manner, Greenland blocking shows also a connection to weak SPV events and is especially likely to be dominant during SCC which is preceded by a weak SPV.

The brief answers mainly consists of the key results of this study, however they are also simplified. In the following, the results are again summarized more extensively.

Depending on the latitude at which SCC occurs, results differ greatly. For SCC at 45°N the cyclone tracks are shifted southwards and the cyclone activity near Greenland is suppressed. In contrast, SCC at 55°N modulates the cyclone tracks by condensing cyclones in the North-Atlantic Ocean near the Norwegian Sea between Great Britain and Iceland. Lastly, for SCC at 65°N cyclones condense mainly in the Norwegian sea east of Iceland. Similar patterns are also shown by some of the weather regimes. Cyclone occurrence during Greenland blocking resembles SCC at 45°N, while Atlantic trough is similar to SCC at 55°N. Lastly the cyclone occurrence during Zonal regime and to an extent also during the Scandinavian trough corresponds to SCC at 65°N.

The results of the climatological study are in agreement with the modulation of the cyclone occurrence, the weather regimes with enhanced activity match those of similar cyclone occurrence. During SCC at 45°N, Greenland blocking is enhanced for a long period up to 30 days after the SCC onset. Less, but still significant is also a shorter period up to 15 days in which Atlantic trough is more likely to be dominant. In case of SCC at 55°N, Atlantic trough is by far most often the dominant regime type for a period to 20 days. At maximum more than 50% of SCC at 55°N are linked with an Atlantic trough regime being dominant. Especially the Zonal regime, but also the Scandinavian trough are more likely to be dominant during SCC at 65°N in the 15 day period after SCC occurs. For all three latitudes there is also a short ramp up period of about 5 days after the SCC onset until the frequency reaches its peak which emphasizes the importance of regime transitions.

The total amount of dominant regime transitions does however not increase, instead transitions to a similar regime type take place at similar time lags after the SCC onset. Those transitions mainly occur in the early stage of a SCC period within 6 days of the SCC onset or in fewer cases slightly precede the SCC period. For SCC at 45°N, transitions occur mostly to the Greenland blocking or Atlantic trough regime. The Atlantic trough regime also counts by far the most transitions in case of SCC at 55°N which occur nearly exclusively after the SCC onset. Lastly transitions towards the Zonal regime and Scandinavian trough are frequent for SCC at 65°N. We also found that the Greenland blocking, Atlantic trough, Zonal regime and Scandinavian trough life cycles begin and decay closely to the SCC period respective to each latitude. This is especially true for the Atlantic trough life cycles in case of SCC at 55°N. They also follow the same pattern as the dominant

transitions, they also mostly emerge shortly after the SCC onsets. In contrast, the Zonal regime life cycles for SCC at 65°N begin similarly often before and after the SCC onset. However they tend to decay already before the SCC period ends. The results for Greenland blocking in case of SCC at 45°N are not as distinct besides the general tendency to occur alongside the SCC periods. The study also showed that the stratospheric polar vortex seems to influence SCC the alongside occurring weather regimes. While the SPV is not required to be either weak or strong for SCC to occur, the weather regime types that are dominant after the SCC onset are connected to the SPV strength. Especially for SCC at 45°N, periods of prolonged enhanced Greenland blocking activity are mostly coupled with a weak SPV or even SSWs. Contrary, in cases with a normal or slightly stronger SPV, Greenland blocking activity is hardly enhanced at all, instead the Atlantic trough shows a slight increase in frequency. This completely different behaviour found for SCC at 45°N is not replicated in case of SCC at 55°N or 65°N. Nonetheless, the strength of the SPV still influences the weather regime activity by modulating the transition after the for each latitude favoured regime type decays. In cases where the SCC period is coupled with a weak SPV, the weather regime decays more often without a new regime becoming dominant ending up in a period where no regime is dominant. However, if the SCC period is coupled with a slightly stronger SPV, transitions towards the Zonal regime are more likely.

While we found multiple links between SCC and weather regimes as well as an influence by the SPV, further research is still required. This study is focussed on a statistical approach to find connections between SCC and weather regimes, however, neglecting a verification of the physical reasoning behind the results. Furthermore, even though the analysis were mostly conducted in respect to the SCC period/onset, cause and effect cannot be fully differentiated. Therefore it is not clear if for example transitions to certain weather regimes trigger SCC or if SCC forces a transitions to a certain regime type. The lead-lag relationship already gives an idea, assuming preceding events are the cause while the effect is the one following the event. This however still needs to be verified and also suits a more physically oriented analysis. Lastly, research can also be conducted about how the results might be able to affect predictability on a sub-seasonal time scale, since for example the weather regime types are influenced on a longer time scale.

References

Baldwin, M. P. and T. J. Dunkerton, 2001: Stratospheric Harbingers of Anomalous Weather Regimes. *Science*, **294 (5542)**, 581–584, doi: 10.1126/science.1063315, publisher: American Association for the Advancement of Science Section: Report.

Beerli, R. and C. M. Grams, 2019: Stratospheric modulation of the large-scale circulation in the Atlantic–European region and its implications for surface weather events. *Quarterly Journal of the Royal Meteorological Society*, **145 (725)**, 3732–3750, doi: 10.1002/qj.3653, _eprint: https://rmets.onlinelibrary.wiley.com/doi/pdf/10.1002/qj.3653.

Büeler, D., R. Beerli, H. Wernli, and C. M. Grams, 2020: Stratospheric influence on ECMWF sub-seasonal forecast skill for energy-industry-relevant surface weather in European countries. *Quarterly Journal of the Royal Meteorological Society*, **146 (733)**, 3675–3694, doi: https://doi.org/10.1002/qj.3866, _eprint: https://rmets.onlinelibrary.wiley.com/doi/pdf/10.1002/qj.3866.

Berrisford, P., et al., 2011: The ERA-Interim archive Version 2.0. **(1)**, 23, URL: https://www.ecmwf.int/node/8174, place: Shinfield Park, Reading Publisher: ECMWF.

Björnsson, H. and S. A. Venegas, 1997: A manual for EOF and SVD analyses of climate data. Tech. Rep. 97-1, McGill University, 52 pp., Montréal, Québec.

Booth, J. F., Y.-O. Kwon, S. Ko, R. J. Small, and R. Msadek, 2017: Spatial Patterns and Intensity of the Surface Storm Tracks in CMIP5 Models. *Journal of Climate*, **30 (13)**, 4965–4981, doi: 10.1175/JCLI-D-16-0228.1, publisher: American Meteorological Society Section: Journal of Climate.

Brown, E., 2016: 9.07 Statistics for Brain and Cognitive Science. *Massachusetts Institute of Technology: MIT OpenCourseWare*, URL: https://ocw.mit.edu.

Cassou, C., L. Terray, and A. S. Phillips, 2005: Tropical Atlantic Influence on European Heat Waves. *Journal of Climate*, **18 (15)**, 2805–2811, doi: 10.1175/JCLI3506.1, publisher: American Meteorological Society Section: Journal of Climate.

Cattell, R. B., 1943: The description of personality: basic traits resolved into clusters. *The Journal of Abnormal and Social Psychology*, **38 (4)**, 476–506, doi: 10.1037/h0054116.

Cattiaux, J., R. Vautard, C. Cassou, P. Yiou, V. Masson-Delmotte, and F. Codron, 2010: Winter 2010 in Europe: A cold extreme in a warming climate. *Geophysical Research Letters*, **37 (20)**, doi: 10.1029/2010GL044613, _eprint: https://agupubs.onlinelibrary.wiley.com/doi/pdf/10.1029/2010GL044613.

Catto, J. L., 2016: Extratropical cyclone classification and its use in climate studies. *Reviews of Geophysics*, **54 (2)**, 486–520, doi: 10.1002/2016RG000519, _eprint: https://agupubs.onlinelibrary.wiley.com/doi/pdf/10.1002/2016RG000519.

Charlton-Perez, A. J., R. W. Aldridge, C. M. Grams, and R. Lee, 2019: Winter pressures on the UK health system dominated by the Greenland Blocking weather regime. *Weather and Climate Extremes*, **25**, 100 218, doi: 10.1016/j.wace.2019.100218.

Chen, G., S. A. Jaradat, N. Banerjee, T. S. Tanaka, M. S. H. Ko, and M. Q. Zhang, 2002: Evaluation and comparison of clustering algorithms in analyzing ES cell gene expression data. *Statistica Sinica*, **12 (1)**, 241–262, URL: https://keio.pure.elsevier.com/en/publications/evaluation-and-comparison-of-clustering-algorithms-in-analyzing-e, publisher: Institute of Statistical Science.

Chen, Y.-C., 2017: Monte Carlo Simultions and Bootstrap. URL: http://faculty.washington.edu/yenchic/17Sp_302/R11.pdf.

Compo, G. P., et al., 2011: The Twentieth Century Reanalysis Project. *Quarterly Journal of the Royal Meteorological Society*, **137 (654)**, 1–28, doi: https://doi.org/10.1002/qj.776, _eprint: https://rmets.onlinelibrary.wiley.com/doi/pdf/10.1002/qj.776.

Dacre, H. F. and J. G. Pinto, 2020: Serial clustering of extratropical cyclones: a review of where, when and why it occurs. *npj Climate and Atmospheric Science*, **3 (1)**, 1–10, doi: 10.1038/s41612-020-00152-9, number: 1 Publisher: Nature Publishing Group.

Dee, D. P., et al., 2011: The ERA-Interim reanalysis: configuration and performance of the data assimilation system. *Quarterly Journal of the Royal Meteorological Society*, **137 (656)**, 553–597, doi: https://doi.org/10.1002/qj.828, _eprint: https://rmets.onlinelibrary.wiley.com/doi/pdf/10.1002/qj.828.

Domeisen, D. I. V., C. M. Grams, and L. Papritz, 2020: The role of North Atlantic–European weather regimes in the surface impact of sudden stratospheric warming events. *Weather and Climate Dynamics*, **1 (2)**, 373–388, doi: 10.5194/wcd-1-373-2020, publisher: Copernicus GmbH.

Estivill-Castro, V., 2002: Why so many clustering algorithms: a position paper. *ACM SIGKDD Explorations Newsletter*, **4 (1)**, 65–75, doi: 10.1145/568574.568575.

Ferranti, L., S. Corti, and M. Janousek, 2015: Flow-dependent verification of the ECMWF ensemble over the Euro-Atlantic sector. *Quarterly Journal of the Royal Meteorological Society*, **141 (688)**, 916–924, doi: 10.1002/qj.2411, _eprint: https://rmets.onlinelibrary.wiley.com/doi/pdf/10.1002/qj.2411.

Fink, A. H., T. Brücher, V. Ermert, A. Krüger, and J. G. Pinto, 2009: The European storm Kyrill in January 2007: synoptic evolution, meteorological impacts and some considerations with respect to climate change. *Natural Hazards and Earth System Sciences*, **9 (2)**, 405–423, doi: 10.5194/nhess-9-405-2009, publisher: Copernicus GmbH.

Furtado, J., 2005: On the balanced response of the troposphere to variability in the extratropical stratosphere. paper 775, Colorado State University - Department of Atmospheric Science, 118 pp., Fort Collins, Colorado. URL: http://hdl.handle.net/10217/69275.

Grams, C. M., R. Beerli, S. Pfenninger, I. Staffell, and H. Wernli, 2017: Balancing Europe's wind power output through spatial deployment informed by weather regimes. *Nature Climate Change*, **7 (8)**, 557–562, doi: 10.1038/nclimate3338.

Hamerly, G. and C. Elkan, 2002: Alternatives to the k-means algorithm that find better clusterings. *Proceedings of the eleventh international conference on Information and knowledge management - CIKM '02*, ACM Press, McLean, Virginia, USA, 600–607, doi: 10.1145/584792.584890.

Hansen, A. R. and A. Sutera, 1986: On the Probability Density Distribution of Planetary-Scale Atmospheric Wave Amplitude. *Journal of the Atmospheric Sciences*, **43 (24)**, 3250–3265, doi: 10.1175/1520-0469(1986)043<3250:OTPDDO>2.0.CO;2, publisher: American Meteorological Society Section: Journal of the Atmospheric Sciences.

Hart, N. C. G., S. L. Gray, and P. A. Clark, 2015: Detection of Coherent Airstreams Using Cluster Analysis: Application to an Extratropical Cyclone. *Monthly Weather Review*, **143 (9)**, 3518–3531, doi: 10.1175/MWR-D-14-00382.1, publisher: American Meteorological Society Section: Monthly Weather Review.

Hawcroft, M. K., L. C. Shaffrey, K. I. Hodges, and H. F. Dacre, 2012: How much Northern Hemisphere precipitation is associated with extratropical cyclones? *Geophysical Research Letters*, **39 (24)**, doi: 10.1029/2012GL053866, _eprint: https://agupubs.onlinelibrary.wiley.com/doi/pdf/10.1029/2012GL053866.

Hersbach, H., et al., 2020: The ERA5 global reanalysis. *Quarterly Journal of the Royal Meteorological Society*, **146 (730)**, 1999–2049, doi: 10.1002/qj.3803.

Hodges, K. I., 1994: A General Method for Tracking Analysis and Its Application to Meteorological Data. *Monthly Weather Review*, **122 (11)**, 2573–2586, doi: 10.1175/1520-0493(1994)122<2573:AGMFTA>2.0.CO;2, publisher: American Meteorological Society Section: Monthly Weather Review.

Hodges, K. I., 1995: Feature Tracking on the Unit Sphere. *Monthly Weather Review*, **123 (12)**, 3458–3465, doi: 10.1175/1520-0493(1995)123<3458:FTOTUS>2.0.CO;2, publisher: American Meteorological Society Section: Monthly Weather Review.

Hoskins, B. J. and K. I. Hodges, 2002: New Perspectives on the Northern Hemisphere Winter Storm Tracks. *Journal of the Atmospheric Sciences*, **59 (6)**, 1041–1061, doi: 10.1175/1520-0469(2002)059<1041:NPOTNH>2.0.CO;2, publisher: American Meteorological Society Section: Journal of the Atmospheric Sciences.

Institut für Meteorologie -FU-Berlin, 2021: Low Pressure Systems 2010. URL: http://www.met.fu-berlin.de/wetterpate/tief2010/, archive Location: berlin, brandenburg, europa, welt Publisher: Sebastian Bölling, Thomas Dümmel.

Jeppesen, J., 2020: Fact sheet: Reanalysis. URL: https://www.ecmwf.int/en/about/media-centre/focus/2020/fact-sheet-reanalysis.

Jerez, S. and R. M. Trigo, 2013: Time-scale and extent at which large-scale circulation modes determine the wind and solar potential in the Iberian Peninsula. *Environmental Research Letters*, **8 (4)**, 044 035, doi: 10.1088/1748-9326/8/4/044035, publisher: IOP Publishing.

Kraus, H., 2004: *Die Atmosphäre der Erde: eine Einführung in die Meteorologie*. 3d ed., Springer, Berlin, oCLC: 249135761.

Kroese, D. P., T. Brereton, T. Taimre, and Z. I. Botev, 2014: Why the Monte Carlo method is so important today. *WIREs Computational Statistics*, **6 (6)**, 386–392, doi: https://doi.org/10.1002/wics.1314, _eprint: https://onlinelibrary.wiley.com/doi/pdf/10.1002/wics.1314.

Lackmann, G., 2011: *Midlatitude synoptic meteorology: dynamics, analysis, and forecasting*. American Meteorological Society, Boston, Mass, oCLC: ocn711050643.

Mailier, P. J., D. B. Stephenson, C. A. T. Ferro, and K. I. Hodges, 2006: Serial Clustering of Extratropical Cyclones. *Monthly Weather Review*, **134 (8)**, 2224–2240, doi: 10.1175/MWR3160.1, publisher: American Meteorological Society Section: Monthly Weather Review.

Matsueda, M., 2011: Predictability of Euro-Russian blocking in summer of 2010. *Geophysical Research Letters*, **38 (6)**, doi: 10.1029/2010GL046557, _eprint: https://agupubs.onlinelibrary.wiley.com/doi/pdf/10.1029/2010GL046557.

Matsueda, M. and T. N. Palmer, 2018: Estimates of flow-dependent predictability of wintertime Euro-Atlantic weather regimes in medium-range forecasts. *Quarterly Journal of the Royal Meteorological Society*, **144 (713)**, 1012–1027, doi: 10.1002/qj.3265, _eprint: https://rmets.onlinelibrary.wiley.com/doi/pdf/10.1002/qj.3265.

Michel, C. and G. Rivière, 2011: The Link between Rossby Wave Breakings and Weather Regime Transitions. *Journal of the Atmospheric Sciences*, **68 (8)**, 1730–1748, doi: 10.1175/2011JAS3635.1, publisher: American Meteorological Society Section: Journal of the Atmospheric Sciences.

Michelangeli, P.-A., R. Vautard, and B. Legras, 1995: Weather Regimes: Recurrence and Quasi Stationarity. *Journal of the Atmospheric Sciences*, **52 (8)**, 1237–1256, doi: 10.1175/1520-0469(1995)052<1237:WRRAQS>2.0.CO;2, publisher: American Meteorological Society Section: Journal of the Atmospheric Sciences.

Mo, K. and M. Ghil, 1988: Cluster analysis of multiple planetary flow regimes. *Journal of Geophysical Research: Atmospheres*, **93 (D9)**, 10 927–10 952, doi: 10.1029/JD093iD09p10927, _eprint: https://agupubs.onlinelibrary.wiley.com/doi/pdf/10.1029/JD093iD09p10927.

Mohr, S., et al., 2020: The role of large-scale dynamics in an exceptional sequence of severe thunderstorms in Europe May–June 2018. *Weather and Climate Dynamics*, **1 (2)**, 325–348, doi: 10.5194/wcd-1-325-2020, publisher: Copernicus GmbH.

Neiman, P. J., F. M. Ralph, P. O. G. Persson, A. B. White, D. P. Jorgensen, and D. E. Kingsmill, 2004: Modification of Fronts and Precipitation by Coastal Blocking during an Intense Landfalling Winter Storm in Southern California: Observations during CALJET. *Monthly Weather Review*, **132 (1)**, 242–273, doi: 10.1175/1520-0493(2004)132<0242:MOFAPB>2.0.CO;2, publisher: American Meteorological Society Section: Monthly Weather Review.

Pfahl, S. and H. Wernli, 2012: Quantifying the Relevance of Cyclones for Precipitation Extremes. *Journal of Climate*, **25 (19)**, 6770–6780, doi: 10.1175/JCLI-D-11-00705.1, publisher: American Meteorological Society Section: Journal of Climate.

Pinto, J. G., I. Gómara, G. Masato, H. F. Dacre, T. Woollings, and R. Caballero, 2014: Large-scale dynamics associated with clustering of extratropical cyclones affecting Western Europe. *Journal of Geophysical Research: Atmospheres*, **119 (24)**, 13,704–13,719, doi: https://doi.org/10.1002/2014JD022305, _eprint: https://agupubs.onlinelibrary.wiley.com/doi/pdf/10.1002/2014JD022305.

Pinto, J. G., S. Ulbrich, T. Economou, D. B. Stephenson, M. K. Karremann, and L. C. Shaffrey, 2016: Robustness of serial clustering of extratropical cyclones to the choice of tracking method. *Tellus A: Dynamic Meteorology and Oceanography*, **68 (1)**, 32 204, doi: 10.3402/tellusa.v68.32204, publisher: Taylor & Francis _eprint: https://doi.org/10.3402/tellusa.v68.32204.

Preisendorfer, R. W. and C. D. Mobley, 1988: *Principal component analysis in meteorology and oceanography*. No. 17 in Developments in atmospheric science, Elsevier ; Distributors for the U.S. and Canada, Elsevier Science Pub. Co, Amsterdam ; New York : New York, NY, U.S.A.

Priestley, M. D. K., H. F. Dacre, L. C. Shaffrey, S. Schemm, and J. G. Pinto, 2020: The role of secondary cyclones and cyclone families for the North Atlantic storm track and clustering over western Europe. *Quarterly Journal of the Royal Meteorological Society*, **146 (728)**, 1184–1205, doi: 10.1002/qj.3733, _eprint: https://rmets.onlinelibrary.wiley.com/doi/pdf/10.1002/qj.3733.

Priestley, M. D. K., J. G. Pinto, H. F. Dacre, and L. C. Shaffrey, 2017: Rossby wave breaking, the upper level jet, and serial clustering of extratropical cyclones in western Europe. *Geophysical Research Letters*, **44 (1)**, 514–521, doi: https://doi.org/10.1002/2016GL071277, _eprint: https://agupubs.onlinelibrary.wiley.com/doi/pdf/10.1002/2016GL071277.

Raible, C. C., P. M. Della-Marta, C. Schwierz, H. Wernli, and R. Blender, 2008: Northern Hemisphere Extratropical Cyclones: A Comparison of Detection and Tracking Methods and Different Reanalyses. *Monthly Weather Review*, **136 (3)**, 880–897, doi: 10.1175/2007MWR2143.1, publisher: American Meteorological Society Section: Monthly Weather Review.

Reiter, E., 1969: Tropospheric Circulation and Jet Streams. paper 153, Colorado State University - Department of Atmospheric Science, 121 pp., Fort Collins, Colorado. URL: http://hdl.handle.net/10217/35345.

Riehl, H., 1962: Jet Streams of the Atmosphere. Technical Report 32, Colorado State University - Department of Atmospheric Science, 125 pp., Fort Collins, Colorado. URL: http://hdl.handle.net/10217/24425.

Seman, S., 2020: Introductory Meteorology: METEO3 - Understanding processes driving the atmosphere. URL: https://www.e-education.psu.edu/meteo3/.

Shi, Y., et al., 2020: Comparison of Major Sudden Stratospheric Warming Impacts on the Mid-Latitude Mesosphere Based on Local Microwave Radiometer CO Observations in 2018 and 2019. *Remote Sensing*, **12 (23)**, 3950, doi: 10.3390/rs12233950.

Simmons, A., et al., 2020: Global stratospheric temperature bias and other stratospheric aspects of ERA5 and ERA5.1. doi: 10.21957/RCXQFMG0, publisher: ECMWF.

Spiridonov, V. and M. Ćurić, 2021: *Fundamentals of meteorology*. URL: https://doi.org/10.1007/978-3-030-52655-97135, oCLC: 1204176692.

Swiss Re, 2000: *Storm over Europe - An underestimated risk*. Swiss Reinsurance Company.

Vautard, R., 1990: Multiple Weather Regimes over the North Atlantic: Analysis of Precursors and Successors. *Monthly Weather Review*, **118 (10)**, 2056–2081, doi: 10.1175/1520-0493(1990)118<2056:MWROTN>2.0.CO;2, publisher: American Meteorological Society Section: Monthly Weather Review.

Vitolo, R., D. B. Stephenson, I. M. Cook, and K. Mitchell-Wallace, 2009: Serial clustering of intense European storms. *Meteorologische Zeitschrift*, 411–424, doi: 10.1127/0941-2948/2009/0393, publisher: Schweizerbart'sche Verlagsbuchhandlung.

Walker, E., D. Mitchell, and W. Seviour, 2020: The numerous approaches to tracking extratropical cyclones and the challenges they present. *Weather*, **75 (11)**, 336–341, doi: https://doi.org/10.1002/wea.3861, _eprint: https://rmets.onlinelibrary.wiley.com/doi/pdf/10.1002/wea.3861.

Wang, J., H.-M. Kim, and E. K. M. Chang, 2017: Changes in Northern Hemisphere Winter Storm Tracks under the Background of Arctic Amplification. *Journal of Climate*, **30 (10)**, 3705–3724, doi: 10.1175/JCLI-D-16-0650.1, publisher: American Meteorological Society Section: Journal of Climate.

Wernli, H. and C. Schwierz, 2006: Surface Cyclones in the ERA-40 Dataset (1958–2001). Part I: Novel Identification Method and Global Climatology. *Journal of the Atmospheric Sciences*, **63 (10)**, 2486–2507, doi: 10.1175/JAS3766.1, publisher: American Meteorological Society Section: Journal of the Atmospheric Sciences.

White, C. J., et al., 2017: Potential applications of subseasonal-to-seasonal (S2S) predictions. *Meteorological Applications*, **24 (3)**, 315–325, doi: 10.1002/met.1654, _eprint: https://rmets.onlinelibrary.wiley.com/doi/pdf/10.1002/met.1654.

Yiou, P. and M. Nogaj, 2004: Extreme climatic events and weather regimes over the North Atlantic: When and where? *Geophysical Research Letters*, **31 (7)**, doi: 10.1029/2003GL019119, _eprint: https://agupubs.onlinelibrary.wiley.com/doi/pdf/10.1029/2003GL019119.

Zubiate, L., F. McDermott, C. Sweeney, and M. O'Malley, 2017: Spatial variability in winter NAO–wind speed relationships in western Europe linked to concomitant states of the East Atlantic and Scandinavian patterns. *Quarterly Journal of the Royal Meteorological Society*, **143 (702)**, 552–562, doi: 10.1002/qj.2943, _eprint: https://rmets.onlinelibrary.wiley.com/doi/pdf/10.1002/qj.2943.

A Supplementary figures

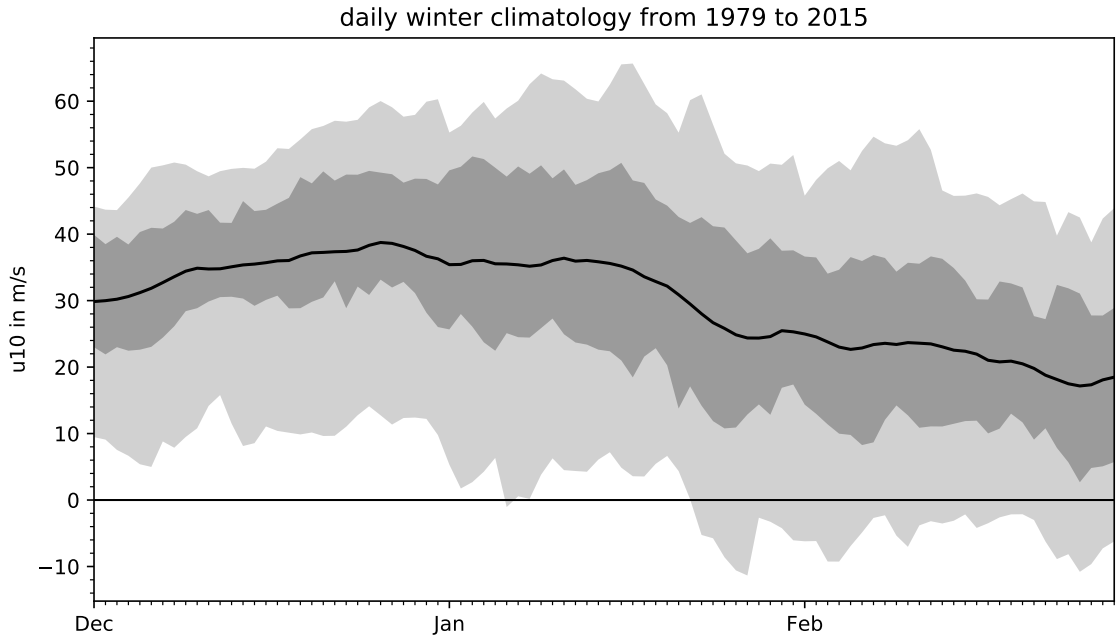

Figure A.1: Daily winter climatology of the zonally averaged zonal wind at 10 hPa and 60°N. The thick black line represents the mean value, while the dark grey and light grey shading is indicative for the 25th to 75th and 5th to 95th percentile range.

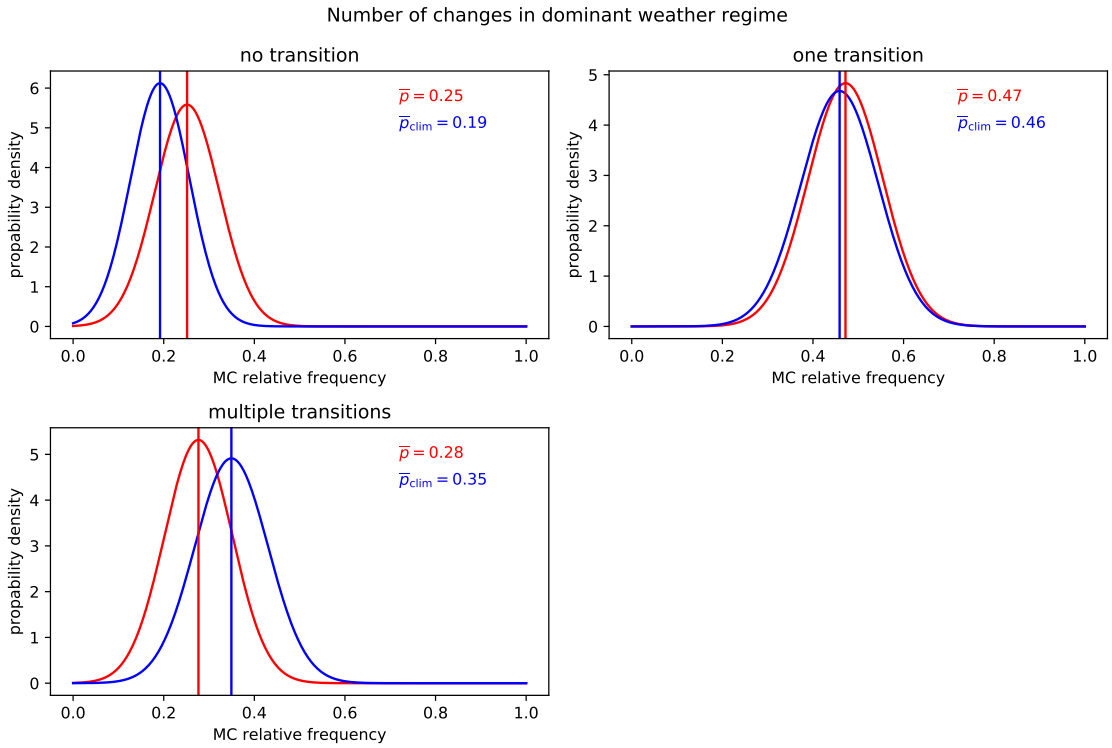

Figure A.2: Probability density distribution for different number of transitions (red) together with their respective climatological distributions (blue) to determine the statistical significance of the anomalies in case of SCC at 45°N.

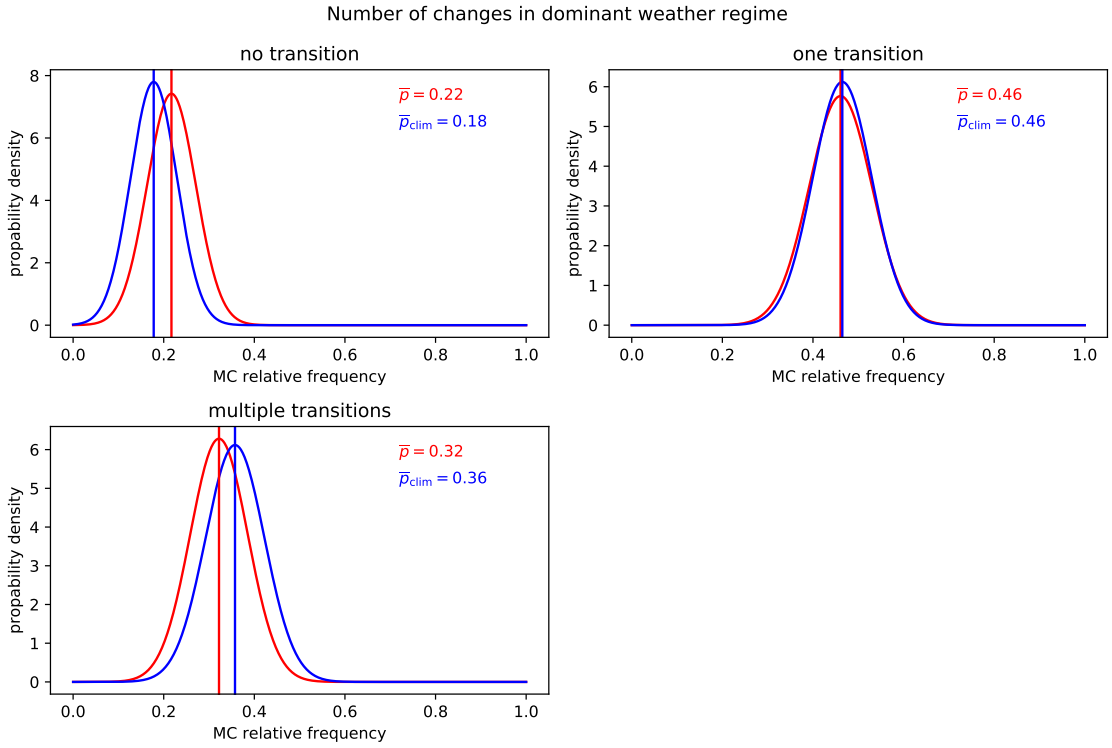

Figure A.3: Probability density distribution for different number of transitions (red) together with their respective climatological distributions (blue) to determine the statistical significance of the anomalies in case of SCC at 55°N.

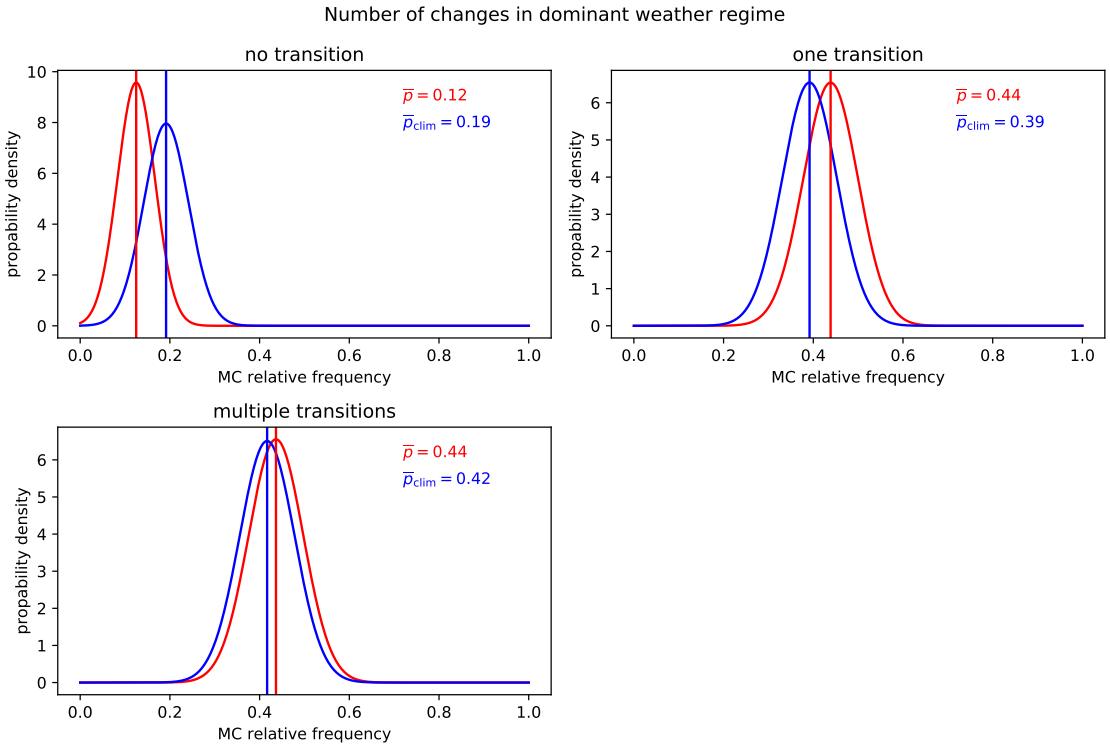

Figure A.4: Probability density distribution for different number of transitions (red) together with their respective climatological distributions (blue) to determine the statistical significance of the anomalies in case of SCC at 65°N.

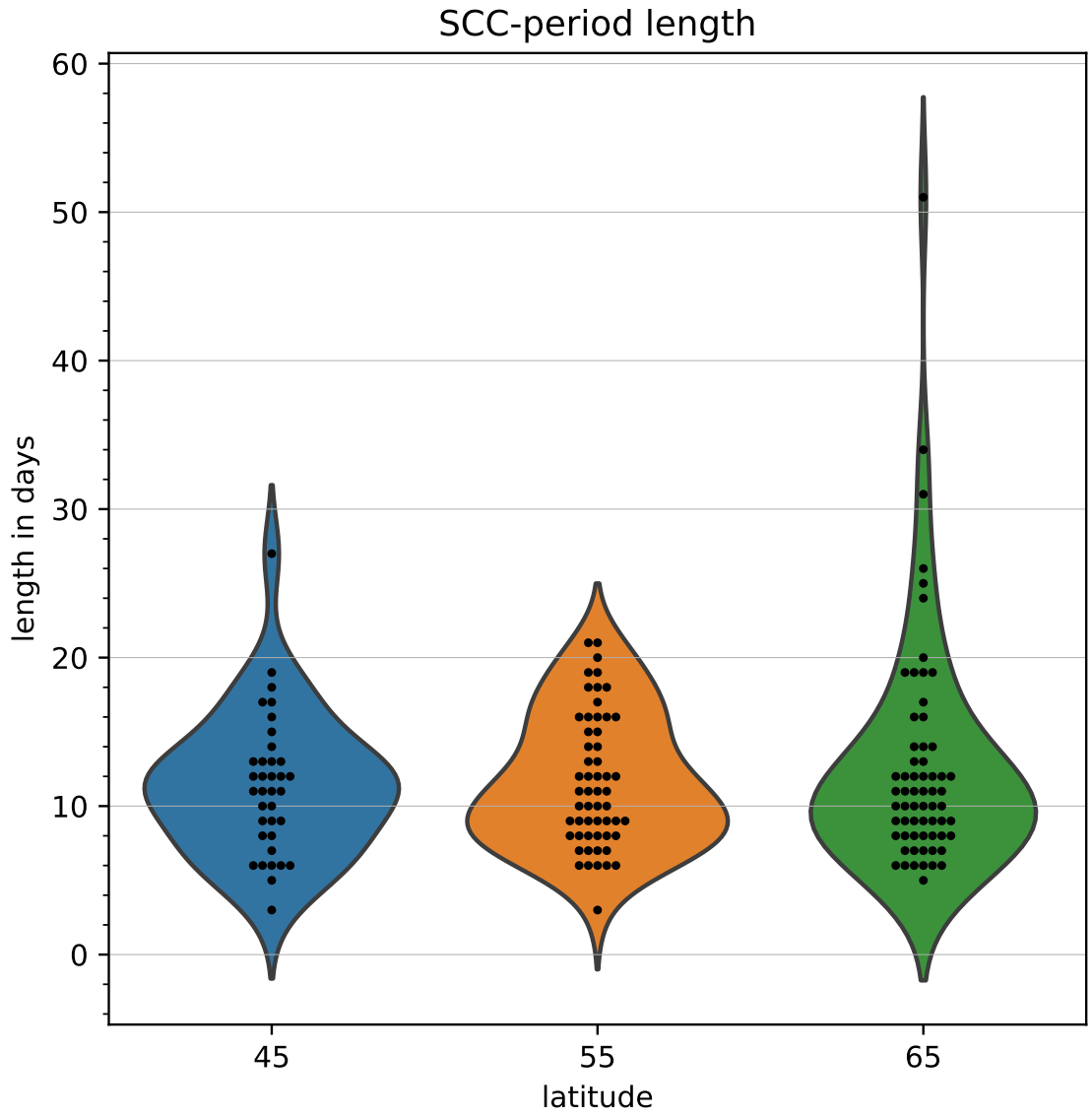

Figure A.5: Length of all SCC periods classified by latitude (45°N/55°N/65°N). Violins represent the frequency distribution depending on the period length. Black dots mark individual SCC periods.

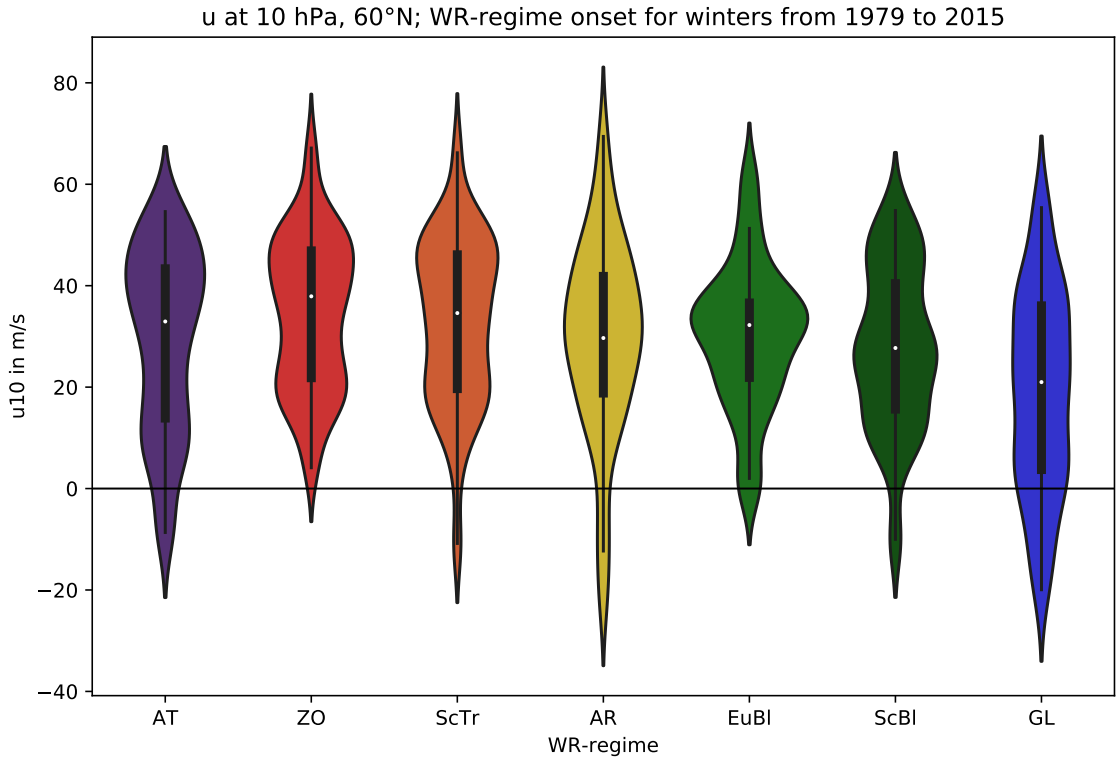

Figure A.6: Zonally averaged zonal wind values at 10 hPa and 60°N for different weather regime life cycle onsets during the winters from 1979 to 2015.

Acknowledgement

Throughout the whole master's thesis time, I received much help from many people in various ways, be it for example by general guidance or scientific discussions. I hereby want them to be acknowledged for their work and also express my gratitude.
Firstly, I want to thank Dr. Christian Grams for advising me and being always open for questions regarding research results and guidance for further steps. Together with Prof. Dr. Joaquim Pinto, they enabled me to do constructive research and allowed the master's thesis to go smoothly through the quarantine time even though regulations changed frequently.
I'm deeply grateful to M.Sc. Seraphine Hauser and M.Sc. Xiaoyang Chen who lent me close support throughout the whole time period. They invested much work and time by regularly analysing and discussing my results with me. I was always offered the possibility to meet them online on short notice even though quarantine forced working from home. They also gave me many ideas to work on, based on the general guidance I received from Christian and Joaquim. I also want to thank them for their feedback during the writing phase of the master's thesis.
I also want to thank everyone else from the young investigator group "Large-scale Dynamics and Predictability" for their constructive feedback in the early phase of the thesis on the specialization phase presentation. Last but not least, I also want to thank our administrator Gabi Klink for providing technical support and making continued home office possible without problems.
Lastly, I want to thank everyone in my family for always supporting and encouraging me throughout my studies.

Declaration of Authorship

I hereby declare that the thesis submitted is my own unaided work. All direct or indirect sources used are acknowledged as references. I am aware that the thesis in digital form can be examined for the use of unauthorized aid and to determine whether the thesis as a whole or parts incorporated in it may be deemed as plagiarism.
For the comparison of my work with existing sources I agree that it shall be entered in a database where it shall also remain after examination, to enable comparison with future theses submitted. Further rights of reproduction and usage, however, are not granted here. This paper was not previously presented to another examination board and has not been published.

Karlsruhe, 14.06.2021

Sebastian Müller